

DISSERTATION

submitted to the
Combined Faculties for the Natural Sciences and for Mathematics
of the Ruperto-Carola University of Heidelberg, Germany
for the degree of
Doctor in Natural Sciences

presented by

Master of Molecular and Cell Biology

Nikolaus Obholzer

born in Mannheim, Germany

Oral Examination: November 23rd, 2007

INAUGURAL-DISSERTATION

Zur
Erlangung der Doktorwürde
der
Naturwissenschaftlich-Mathematischen Gesamtfakultät
der
Ruprecht-Karls-Universität Heidelberg

vorgelegt von

Master of Molecular and Cell Biology

Nikolaus Obholzer

aus Mannheim, Deutschland

Tag der mündlichen Prüfung: 23. November 2007

Molecular Components of the Hair Cell Synaptic Vesicle Cycle

Referees: Prof. Dr. Stephan Frings
Assoc. Prof. Dr. Teresa Nicolson

Acknowledgements

The research for this thesis was conducted at the Vollum Institute in Portland, Oregon, USA under the supervision of Assoc. Prof. Dr. Teresa Nicolson.

My special thanks to my supervisor for all the support, constructive discussions and continuous encouragement - and for the money! Most of all thank you for giving me the opportunity to prepare this thesis. My gratitude goes to Prof. Dr. Frings for taking the trouble to be my thesis advisor and chair of my thesis committee, even though we had never met. I want to thank the members of the Nicolson lab, both past and present, for the wonderful time we spent in and outside the lab. In no other lab have I ever been so comfortable! Thank you to Sarah Song, Alex Hruuscha, Felipe Ramos, Sireesha Govadas and Gabe Finch for technical assistance. Thank you to Juli Zeppieri, Norm and again to Sarah Song and Alex Hruuscha for maintaining the fishroom. Thank you to my longtime colleague Qianyong Liu for the many discussions and the good work atmosphere that we could always maintain. Thank you to Sean Wolfson, for the many discussions about lab and life, which usually ended in him sharing and me nodding. Thank you for the paper alerts and for regularly shouting obscenities and generally lightening things up. Too bad I still don't care about Nick Cave! Thank you also for our Civ4 and UT sessions (this includes Joe). Thank you to Joe Trapani, Greta Glover, and Lavinia Sheets for the great team spirit, for allowing me to talk and talk and talk, for sharing their expert knowledge and skills, and for generally being the great people that they are. Thank you again to Lavinia Sheets and Joe Trapani for very helpful comments on this thesis. Thank you to Zev Einhorn, Weike Mo and Katie Kindt for being great colleagues and for occasionally asking for my advice, which made me feel knowledgeable and important. Thank you to Jackie DeGagne for her help with electron microscopy. Thank you to Dr. Stephanie Kaeck for her help with confocal microscopy. Thank you to the members of my family, who have always been supportive over the years.

And finally, my biggest thanks goes to my wife, Fei Ying Cheong, for her love, her constant support and encouragement, her technical assistance, her almost infinite patience and the long hours we either spent in the lab together, or she let me spend in the lab alone. Wo Ai Ni!

Summary

Hair cells of the zebrafish inner ear act as sensory receptors for both auditory and vestibular stimuli. Hair cells transmit information via glutamatergic ribbon synapses, which have the highest synaptic vesicle turnover of all chemical synapses. We have identified and positionally cloned two mutants that interfere with hair-cell synaptic activity from an ENU mutagenesis screen for vestibular dysfunction in zebrafish (Nicolson et al., 1998 and unpublished results).

We have identified vesicular glutamate transporter 3 (*vglut3*) in the *asteroid* mutant strain and find it to be critical for hair-cell function. *asteroid* mutant larvae are deaf and display a profound balance defect, while hair-cell bundle morphology and FM 1-43 dye uptake appear normal. This phenotype suggests a transmission failure downstream of mechanotransduction. Cloning and sequencing of the *asteroid* mutant allele IJ001 revealed a donor splice site mutation in exon 2 of *asteroid/vglut3* that results in a severe truncation of the protein product. We can replicate the *asteroid* phenotype by injecting morpholinos that either target the *vglut3* ATG/start site or the affected splice junction into wild-type eggs. *In situ* hybridization shows that *vglut3* appears to be exclusively expressed in hair cells of the ear and lateral line organ in the zebrafish, which is in contrast to data obtained from mammals. Concomitantly, antibodies against Vglut3 exclusively label the basal end of hair cells, can be blocked by antigen competition, and labeling is absent in *asteroid/vglut3* mutant larvae. Yet we find that *asteroid* mutant hair cells show only a 60% decrease (12.8 ± 1.0 SVs, WT, 5.34 ± 0.6 mutant) in the number of ribbon-associated synaptic vesicles at the ultrastructural level (ribbon diameters are comparable between *asteroid* mutants and WT). This indicates a role for Vglut3 in synaptic vesicle biogenesis and/or trafficking, but Vglut3 is not the sole component required for these processes. Using *in situ* hybridization, we also detect *vglut1* transcript in hair cells, but the presence of *vglut1* does not compensate for loss of *vglut3* under the conditions tested. In support of this notion, our qPCR data indicates that *vglut1* is not significantly upregulated in *asteroid/vglut3* mutants.

We have also isolated the *comet* mutant from the above-mentioned mutagenesis screen. We have determined that *comet* encodes the lipid phosphatase *synaptojanin 1 (synj1)*. *comet* mutant larvae display a balance defect that increases in severity upon challenge, suggesting fatigability, perhaps due to insufficient SV recycling. We are using the *comet* strain of zebrafish to help address the mechanisms underlying SV recycling in hair cells. To this end, we have sequenced three alleles of *comet/synj1*, all of which encode severe truncations that presumably lead to protein *null* phenotypes. We confirm the expression of *synj1* in the CNS and, in addition, show expression in hair cells of the ear by *in situ* hybridization. Interestingly, we can phenocopy the balance defect of the *comet* mutant using morpholino-mediated knockdown of the short splice variant of *synj1*, *synj1-145* alone. Injection of a translation-blocking morpholino against *synj1* also produces a phenocopy. At the electron microscopy level, *comet/synj1* mutants show a decrease in synaptic ribbon diameter (*mutant*: 293 ± 83.4 nm vs. WT: 408 ± 108 nm) that accompanies a reduced number of ribbon-associated synaptic vesicles (*mutant*: 21.9 ± 12.3 vs. WT: 36.2 ± 6.4). This can be interpreted as evidence for altered release kinetics and ribbon maintenance in *comet* mutants. We also describe the completely novel phenotype for loss of *synj1*, basal membrane blebbing. Basal blebbing is stimulation-dependent in *comet/synj1* mutants (26.3 ± 7.5 unstim. vs. 42.6 ± 24.4 post stim.), and the absence of synaptic exocytosis in *comet/gemini* double mutants that lack the synaptic Ca^{2+} channel *cav1.3* (Sidi et al., 2004) abolishes blebbing. In addition, interference with endocytosis by exposure of larvae to Latrunculin A phenocopies blebbing in wild-type hair cells.

In summary, we have identified, cloned and characterized two “novel” genes that are required for proper hair-cell transmission. Both *Synj1* and *Vglut3* are involved in SV generation and recycling and their investigation should aid further elucidation of this mechanism in future studies.

Zusammenfassung

Haarzellen im Innenohr von Zebrafischen fungieren als Sinnesrezeptoren für auditorische und vestibuläre Stimuli. Haarzellen kodieren Information über glutamaterge Bandsynapsen, an welchen im Vergleich mit anderen chemischen Synapsen der höchste Umschlag synaptischer Vesikel stattfindet. Wir haben zwei Mutanten aus einem ENU Mutageneseverfahren für vestibuläre dysfunction in Zebrafischen (Nicolson et al., 1998; nicht publiziert) identifiziert und positionell kloniert, die die synaptische Aktivität von Haarzellen behindern.

Wir haben zum einen den vesikulären Glutamat Transporter 3 (*vglut3*) identifiziert, der kritisch für Haarzellfunktion in *asteroid* Mutanten ist. Larven der *asteroid* Mutante sind taub und haben eine offensichtliche Störung des Gleichgewichtssinns, wobei Haarzellbündelmorphologie und die Aufnahme von FM 1-43 normal erscheinen. Dieser Phänotyp deutet auf ein Versagen der Signalweiterleitung unterhalb des Mechanotransduktionsschritts hin. Durch Klonierung und Sequenzierung des *asteroid* Mutantenallels IJ001 wurde uns eine Mutation in der Donorspleissstelle in Exon 2 von *asteroid/vglut3* offenbar, die in einem stark verkürzten Proteinprodukt resultiert. Wir können den *asteroid* Phänotyp durch die Injektion von Antisense-morpholinos gegen den Translationsstart von *vglut3* oder die in der Mutante betroffene Donorspleissstelle in Eier des Wildtyps kopieren. Im Gegensatz zu Ergebnissen, die aus Experimenten mit Säugern gewonnen wurden, zeigt *in situ* Hybridisierung für *vglut3* im Zebrafish Expression ausschliesslich in Haarzellen des Ohrs und des Seitenlinienorgans. Dementsprechend markieren Antikörper gegen Vglut3 ausschliesslich das basale Ende von Haarzellen, können durch Antigen blockiert werden, und die Markierung ist in *asteroid/vglut3* Mutanten nicht vorhanden. Dennoch finden wir, dass auf der ultrastrukturellen Stufe die Zahl Bandassoziiierter synaptischer Vesikel in *asteroid* Mutanten um lediglich 60% reduziert sind (12.8 ± 1.0 SVs, WT, 5.34 ± 0.6 Mutante). Der Banddurchmesser war zwischen *asteroid* Mutante und Wildtyp vergleichbar. Dies deutet darauf hin, dass *vglut3* an der Biogenese und/ oder dem Transport synaptischer Vesikel beteiligt ist, wenn auch Vglut3 nicht der einzige Faktor ist, der für diese Prozesse notwendig ist. In unserer *in situ* Hybridisierung detektieren wir auch *vglut1* Transkript in Haarzellen, aber die Anwesenheit von *vglut1* kompensiert unter unseren Testbedingungen nicht für den Verlust *vglut3s*. Dafür sprechen auch unsere qPCR-daten, die zeigen dass *vglut1* in *asteroid/vglut3* Mutanten nicht signifikant hochreguliert ist.

Aus dem oben genannten Mutationsverfahren haben wir auch die *comet* Mutante isoliert. Wir haben bestimmt, dass *comet* die Lipidphosphatase *synaptojanin 1* (*synj1*) codiert. Larven der *comet* Mutante haben eine Gleichgewichtsstörung, die mit der Zeit an Schwere zunimmt, was eine vielleicht auf insuffizientes SV recycling zurückführbare Ermüdbarkeit suggeriert. Wir verwenden den Zebrafisch-*comet*-Stamm um mehr über die Mechanismen, denen das recycling synaptischer Vesikel in Haarzellen unterliegt, herauszufinden. Wir haben dazu drei Allele von *comet/synj1* sequenziert, die allesamt starke Verkürzungen des Proteins kodieren, was vermutlich zu einem Protein-*null* Phänotypen in den Mutanten führt. Wir bestätigen die Expression von *synj1* im zentralen Nervensystem mittels *in situ* Hybridisierung und zeigen darüberhinaus Expression in den Haarzellen des Ohrs. Interessanterweise können den Gleichgewichtsdefekt der *comet* Mutante durch Morpholino-knockdown der kurzen Spleissvariante von *synj1*, *synj1-145* kopieren. Injektion eines translationsblockierenden Morpholinos gegen *synj1* hingegen kopiert *comet*. Auf der elektronenmikroskopischen Ebene zeigen *comet/synj1* Mutanten eine Verkleinerung des Durchmessers des synaptischen Bands (Mutante: 293 ± 83.4 nm vs. WT: 408 ± 108 nm), die von einer reduzierten Anzahl band-assoziiierter synaptischer Vesikel begleitet wird (Mutante: 21.9 ± 12.3 vs. WT: 36.2 ± 6.4). Dies kann als Hinweis auf eine Veränderung in der Ausschüttungskinetik und Bandzusammensetzung in *comet* Mutanten interpretiert werden. Wir beschreiben auch den völlig neuen Phänotyp für einen Verlust *synj1*'s, blebbing der Basalmembran. Basales blebbing tritt in *comet/synj1* Mutanten stimulationsabhängig auf (26.3 ± 7.5 unstim. vs. 42.6 ± 24.4 post stim.), und die Abwesenheit von synaptischer Exozytose in *comet/gemini* Doppelmutanten, denen der synaptische Ca^{2+} Kanal *cav1.3* (Sidi et al., 2004) fehlt, unterdrückt blebbing. Für eine Abhängigkeit des Blebbings von der Endozytose spricht auch, dass wir, wenn wir in Wildtyp-Larven mittels Latrunculin A mit der Endozytose interferieren, blebbing in Haarzellen verursachen.

Zusammenfassend haben wir zwei für normale Mechanotransmission benötigte "neue" Gene kloniert und charakterisiert. Sowohl *Synj1* als auch *Vglut3* sind in die Generation und im Recycling synaptischer Vesikel involviert und weitere Forschung über diese Moleküle sollte bei der Aufklärung dieser Prozesse hilfreich sein.

1 Abbreviations	1
2 Introduction	3
2.0: Aims of This Work	3
2.1: Hereditary Deafness and Known Deafness Genes	5
2.2: The Audiovestibular System in Mammals and Vertebrates	6
2.2.1: Anatomy of the Larval and Adult Zebrafish Ear	7
2.3: Hair Cell Molecular Anatomy and Physiology	8
2.3.1 Hair Cell Mechanotransduction	10
2.3.2 Properties of the Hair Cell Afferent Synapse	12
2.3.3 Ca ²⁺ at the Synapse	15
2.4 Synaptic Vesicle Exocytosis	16
2.5 Vesicular Glutamate Transporters	17
2.5.1 Vesicular Glutamate Transporter 3	20
2.6 Vesicle Recycling at Chemical Synapses	21
2.6.1 Vesicle Recycling at Ribbon Synapses	24
2.7 Known Endocytic Pathways	26
2.7.1 Organelle Identity and Membrane Signposts Are Defined by Phosphoinositides	27
2.7.2 Clathrin-Mediated Endocytosis	28
2.7.3 Bulk Endocytosis	30
2.7.4 Caveolae Endocytosis	32
2.7.5 Kiss-and-run endocytosis	32
2.8 The Phosphoinositide Phosphatase Synaptojanin1	33
2.8.1 The SAC-Phosphatase Domain	34
2.8.2 The Inositol Polyphosphate 5-Phosphatase Domain	34
2.8.3 Ptlns-Phosphates and Other Lipids in Endo- and Exocytosis	35
2.8.4 <i>synaptojanin1</i> as a Regulator of Endocytosis and the Cytoskeleton	38
2.8.5 Consequences of a <i>synaptojanin1</i> Loss	39

3 Results	41
3.1 Part1: Identification and Characterization of <i>synptojanin1</i> in Zebrafish	41
3.1.1 Positional Cloning of <i>synptojanin1</i>	42
3.1.2 <i>In situ</i> Expression Analysis of <i>synptojanin1</i>	43
3.1.3 Cloning of the <i>myosin6b</i> Promoter for Hair Cell Specific Expression	44
3.1.4 Cellular Localization of <i>synptojanin1-egfp</i>	45
3.1.5 Cellular Localization of Markers of the SV cycle in <i>comet</i> Mutants	46
3.1.6 Loss of <i>synptojanin1</i> Results in No Change in HC Ribbon Numbers, Which Are Indicators of Synapse Formation	47
3.1.7 Morpholino-Mediated Knockdown of <i>synj1-145</i> Generates a Fatiguability-of-Balance Phenotype	48
3.1.8 Morpholino-Mediated Knockdown of <i>synj1-145</i> Induces Compensatory Overexpression of <i>synj1</i> and Forces Overexpression of <i>synj1-170</i>	50
3.2 “Blebbing” as a Novel Phenotype in <i>comet</i> Mutant Hair Cells	51
3.2.1 Detection of Membrane Blebs in <i>comet</i> by Labeling With FM1-43, <i>plcδ- PH-egfp</i> , <i>myo6b:egfp</i> and <i>brn3c:gap43ΔC-gfp</i>	52
3.2.2 Blebbing in <i>comet</i> Mutants is Activity-Dependent	53
3.2.3 Blebs are Promoted by Latrunculin A	54
3.2.4 Blebs Contain Normal Amounts of Actin and Tubulin	55
3.2.5 Detection of Blebs Using Electron Microscopy	56
3.2.6 Conclusions of Part 1: <i>synptojanin1</i>	58
3.3 Part 2: <i>vglut3</i> is Required for Hearing and Balance in Zebrafish	59
3.3.1 Positional Cloning of <i>vglut</i> in <i>asteroid</i> Mutants	60
3.3.2 <i>In situ</i> Expression Analysis of <i>vglut3</i> and other <i>vglut</i> genes	62
3.3.3 Semiquantitative PCR Shows No Upregulation of <i>vglut1</i> in <i>asteroid</i> Mutant Larvae	64
3.3.4 Morpholino Knockdown of Vglut1 Causes Vestibular and Other Defects	65
3.3.5 Cellular Localization of Vglut3 Using Immunofluorescence	66
3.3.6 Antigen Competition Eliminates Vglut3 Immunolabel	67
3.3.7: Vglut1 Localizes to the Basal Half of the Cell	68

3.3.8: Synaptic Vesicle Numbers Are Reduced in <i>asteroid/vglut3</i> Mutants	69
3.3.9 Conclusions of Part 2: <i>vglut3</i>	71
4 Discussion	72
4.1 Vesicular glutamate transporter 3 in the Zebrafish Hair Cell	73
4.2 <i>synптоjanin 1</i> in the Zebrafish Hair Cell	78
4.3 Concluding Remarks	89
5 Materials and Methods	90
5.1: Materials	90
5.1.1: Enzymes and kits	90
5.1.2: Primers and oligonucleotides	91
5.1.3: Antisense Morpholinos	93
5.1.4: Plasmids and constructs	94
5.1.5: Fusion Protein Expression Constructs	97
5.1.6: Constructs for Antibody Generation	100
5.1.7: Peptides used for generating antibodies	101
5.1.8: Fixatives used for EM sample preparation	102
5.1.9: Antibodies	103
5.1.9.1: Primary antibodies	103
5.1.9.2: Secondary antibodies	103
5.1.10: Common buffer stocks and solutions	104
5.2: Methods	104
5.2.1: Methods in Molecular Biology	104
5.2.1.1: Ethanol precipitation of plasmid DNA	105
5.2.1.2: Agarose gel electrophoresis	105
5.2.1.3: DNA Restriction Digests	105
5.2.1.4: Alkaline phosphatase treatment	105
5.2.1.5: Ligation	106
5.2.1.6: Polymerase Chain Reaction (PCR)	106
5.2.1.7: DNA Sequencing	107
5.2.1.8: Site-directed mutagenesis (SDM): Quickchange II XL	107
5.2.1.9: Isolation of mRNA and Genomic DNA from larvae	108
5.2.1.10: Reverse Transcription of mRNA for PCR	108
5.2.1.11: Rapid Amplification of cDNA Ends (RACE)	108

5.2.1.12: Quantitative Real-time PCR (qPCR)	109
5.2.1.13: Transformation of competent cells	110
5.2.1.14: <i>In situ</i> hybridization	110
5.2.1.15: Transformation of spontaneous affective disorder	110
5.2.2: Methods in Histology	111
5.2.2.1: Generation of antibodies	111
5.2.2.2: Immunofluorescence Microscopy	111
5.2.2.3: Alternate Protocol for Immunostaining	112
5.2.2.4: Protocol for Immunostaining of Cryosections	112
5.2.2.5: Staining of Phosphoinositides Using Specific Antibodies	112
5.2.2.6: Electron Microscopy	113
5.2.3: Methods in Animal Husbandry	114
5.2.3.1: Zebrafish Maintenance and Breeding	114
5.2.3.2: Sorting of Larvae	114
5.2.3.3: Microinjection of DNA, RNA, Morpholinos	115
6 Literature	116

1 Abbreviations

α	anti/ alpha
Amp/ Carb	carbenicillin/ ampicillin
aa	amino acid
ATP	adenosine triphosphate
bp	base pair
CCV	clathrin-coated vesicle
CCP	clathrin-coated pit
DAG	diacylglycerol
Da	Dalton
ddH ₂ O	double distilled or MilliQ purified water
DMSO	dimethylsulfoxide
DNA	deoxyribonucleic acid
EDTA	ethylenediaminetetraacetic acid
EGFP	enhanced green fluorescent protein
g	gram
HC(s)	hair cell(s)
hr(s)	hour(s)
kb	kilobase(s)
kD	kilo Dalton
L	liter
LB	Luria Bertani broth
μ l/ μ L	microliter
μ g	microgram
M	molar
mM	millimolar
mA	milliampere
mg	milligram
μ M/ μ M	micromolar
min	minute
ml	milliliter
MO	morpholino (phosphorodiamidate morpholino oligo)
mRFP	monomeric red fluorescent protein
mRNA	messenger RNA
ms	millisecond
nM	nanomolar
nm	nanometer
O/N	overnight
ONC	overnight culture
PBS	phosphate buffered saline
PBST	phosphate buffered saline, 0.1% TWEEN
PCR	polymerase chain reaction
PM	plasma membrane
pmol	picomol
PtdIns	phosphatidylinositol

PI	phosphoinositides
PI(4)P	phosphatidylinositol-4-phosphate
PI(4,5)P ₂	phosphatidylinositol(4,5)bisphosphate
PtdIns(3)P	Phosphatidylinositol(3)phosphate
PtdIns(4)P	Phosphatidylinositol(4)phosphate
PtdIns(5)P	Phosphatidylinositol(5)phosphate
PtdIns(3,4)P ₂	Phosphatidylinositol(3,4)bisphosphate
PtdIns(4,5)P ₂	Phosphatidylinositol(4,5)bisphosphate
PtdIns(3,5)P ₂	Phosphatidylinositol(3,5)bisphosphate
PtdIns(3,4,5)P ₃	Phosphatidylinositol(3,4,5)trisphosphate
qPCR	quantitative PCR, "real-time PCR"
rpm	revolutions per minute
(at) RT	room temperature
RT	reverse transcription
RT-PCR	reverse transcription followed by PCR
s	second
SDM	site-directed mutagenesis
SV	synaptic vesicle
TBE	tris/borate/EDTA
tom	td-tomato (modified dsRed fluorescent protein dimer)
TX-100	triton-X-100
U, Unit	unit of enzyme activity.
UTR	untranslated region of an mRNA (5' or 3')
V	volt
WT	wildtype

Naming Conventions:

species	gene	protein
zebrafish	<i>synj1</i>	Synj1
human	<i>SYNJ1</i>	SYNJ1
mouse	<i>Synj1</i>	SYNJ1

2 Introduction

2.0: Aims of This Work

Hair cells (HCs) are a highly specialized neuroepithelial cell type that converts auditory or vestibular stimuli into impulses of the nervous system in vertebrates. Our research focuses on understanding the molecular mechanisms of auditory and vestibular signal transmission and synaptic vesicle recycling at the afferent HC synapse. HCs possess ribbon-type synapses, which enable them to indefatigably process and encode auditory information with a time resolution in the kilohertz range (Nouvian et al., 2006). To achieve high rates of synaptic vesicle (SV) flow, HCs maintain pools of readily releasable vesicles that are orders of magnitude larger than synapses in other neuronal cell types (Lenzi et al., 1999; Nouvian et al., 2006). How auditory synapses manage their high synaptic vesicle turnover, which can approach 1.4x the entire cell surface in a few seconds (Lenzi et al., 2002), is unknown at present. We will identify, clone and characterize two genes that are required for proper HC transmission: *synaptojanin-1* (*synj1*) and *vesicular glutamate transporter 3* (*vglut3*).

synj1 regulates phosphoinositide turnover, especially that of phosphatidylinositol (4,5) biphosphate (PI(4,5)P₂), in the synaptic vesicle cycle in a Ca²⁺-dependent manner. In order to determine why loss of *synj1* causes a balance defect, we use *comet/synj1* and *cav1.3* mutant zebrafish strains. We will use the *cav1.3* – the HC presynaptic Ca²⁺ channel- mutant fish strain as a genetic negative control for experiments involving activity-dependence, as the HC afferent synapse in these mutant animals is silent due to the lack of evoked Ca²⁺ transients (Sidi et al., 2004).

Based on previous studies in neurons and non-neuronal cells of other model systems, we expect a role for *synj1* in basal clathrin-mediated endocytosis and vesicle recycling. We will determine the importance of clathrin-mediated endocytosis (CME) for synaptic vesicle recycling in HCs. *synj1* has also been implicated in ribbon-synapse assembly in zebrafish photoreceptor cells (Allwardt et al., 2001; Van Epps et al., 2004), and in the control of neuromuscular junction

(NMJ)-innervation in *Drosophila* (Dickman et al., 2006). We will analyze HC ribbons in this regard.

In addition, we will positionally clone and describe the gene for *asteroid*, *vglut3*, in a candidate-gene approach. We will locate and describe the genomic lesion leading to the *asteroid* mutant phenotype, and replicate this phenotype by morpholino-mediated interference with mRNA processing. We will determine the expression pattern of *vglut3* and seek evidence for its functional relevance in HC transmission. Published data for other *vgluts* indicates that Vglut3 may act not only in glutamate transport, but also synaptic vesicle biogenesis (Wojcik et al., 2004; Smear et al., 2007). We will investigate if Vglut3 is the sole component required for these processes, or if other Vgluts are present.

In order to achieve these goals, we will employ a wide variety of molecular tools, data mining, immunohistochemical analysis, functional assays and imaging techniques in this study.

2.1: Hereditary Deafness and Known Deafness Genes

Hereditary or congenital deafness affects between 1/2000 (0.05%) and 1/1000 (0.1%) newborns (Marazita et al., 1993; Cohen, 1995). Deafness may be defined as *conductive*, affecting sound conduction through outer and/or middle ear, *sensorineural*, affecting the cochlea (HCs), *central*, affecting the auditory nerve, brainstem, or cerebral cortex; or a combination of these three. Another defining factor is the time of its onset. In more than half the cases, the cause is genetic, with the defects being mostly autosomal recessive and *nonsyndromic* (>70%; Van Camp et al., 1997).

Nonsyndromic hearing impairment has hearing loss as its only characteristic, whereas *syndromic* hearing impairment is associated with additional defects. For example, in Usher syndrome, hearing, balance and visual defects also occur. Non-syndromic deafness genes are dubbed *DFN* (for DeaFNess); more specifically *DFNA* when inherited in an autosomal dominant manner, *DFNB* for autosomal recessive genes, and *DFN* for X-linked genes. Several hundred genes are known to cause hereditary hearing loss and deafness, yet mutations of connexins 26 (GJB2) or 30 (GJB6) in the DFNB1 locus alone account for 50% of autosomal recessive nonsyndromic hearing loss. Because they mostly affect HCs, nonsyndromic deafness genes are likely to play a role in HC-specific functions, and are therefore of special interest to HC geneticists. A small selection of known deafness genes is shown below (Table 1).

Table 1. Selected Known Hereditary Deafness Genes.

Name	Locus (human)	Gene	Onset
DFNA2	1p34	KCNQ4	Postlingual
DFNA11	11q13.5	MYO7A	Postlingual
DFNA22	6q13	MYO6	Postlingual
DFNA48	12q13-q14	MYO1A	Postlingual
DFNB1	13q11-112	GJB2	Prelingual
DFNB3	17p11.2	MYO15	Prelingual
DFNB6	3p21	TMIE	Prelingual
DFNB12	10q21-q22	CDH23	Prelingual
DFNB22	16p12.2	OTOA	Prelingual

(from: <http://www.geneclinics.org/profiles/deafness-overview/index.html>)

2.2: The Audiovestibular System in Mammals and Vertebrates

Vertebrates perceive sound, gravity and head motion through their ears and inner ear sensory components. Mammals possess an outer, middle, and inner ear. The outer ear captures the sound and funnels it to the tympanum (ear drum). The middle ear, consisting of the middle ear cavity and the three ossicles, malleus, incus and stapes, transmit the sound to the oval window of the cochlea (inner ear). The cochlea is a fluid-filled tube with two dividers separating it into two large and one small chamber along almost its entire length. The chambers are named *Scala vestibuli*, *Scala media*, and *Scala tympani*. It is also rolled up in the shape of a snail, hence its name. When the stapes moves to transmit sound, it functions like a piston in the oval window of the cochlea, and, in the frequency of the perceived sound, sets the cochlear fluid, the *endolymph*, in motion. As the sound wave travels through the fluid, it displaces the dividers between *Scala vestibuli* and *Scala media*, the *Reissner's membrane*, and with it, the *basilar membrane*. Nested between the two membranes are the HCs (Figure 1), which here act as the sensory receptors for sound. As the membranes are displaced, the HCs are stimulated and in turn stimulate the innervating afferents called *spiral ganglion cells*, of the auditory nerve, the 8th cranial nerve.

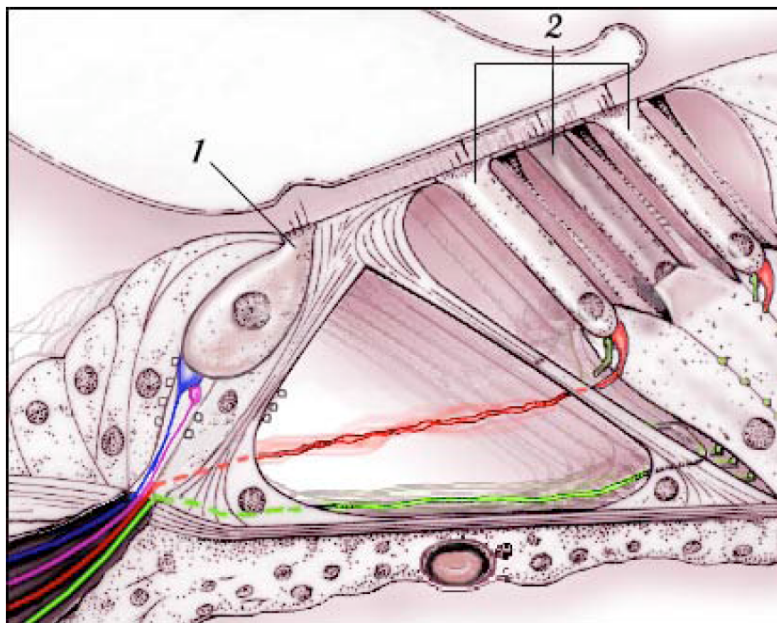


Figure 1. Crosssection through the mammalian cochlea. 1,2, HCs. Blue, Green: afferent synapses. Red: efferent synapse. (by Stephan Blatrix)

Gravity and motion are perceived via the vestibular system, which is an extension of the inner ear. The vestibular system is connected to the brain via the vestibular nerve. The vestibular system senses linear acceleration from body movement and gravity by the utricle and the saccule. Angular acceleration caused by body and/or head rotation is sensed in the three semicircular canals. Like the cochlea, the utricle, saccule and canals are filled with endolymph and utilize HCs as sensors. In the utricle and saccule, unlike in the cochlea, HCs are loosely connected to calcium carbonate stones named otoconia. The otoconia on hair bundles sense gravity like a pebble hanging on a string, and will displace the hair bundle according to gravity when the body axis changes, or when pushed back by inertia due to linear acceleration. In the semicircular canals, the endolymph pushes against HCs when driven by the inertia generated by rotary movements. These principles are conserved in all vertebrates.

2.2.1: Anatomy of the Larval and Adult Zebrafish Ear

In zebrafish, the anatomy of the ear is comparable to that of mammals, but simpler (Figure 2). Zebrafish combine the function of the mammalian outer and inner ear in the otic vesicle, with the swimbladder acting as equivalent to the tympanum. The swimbladder is also connected to the ear by ossicles. The otic vesicle has five sensory patches of HCs: three cristae (*anterior, median, posterior*) and two maculae (*anterior, posterior*). The maculae are connected to the zebrafish equivalents of the otoconia: the otoliths. While there is sensory overlap, the main function of the maculae is the sensation of sound and gravity, by virtue of the otoliths. The three semicircular canals are nestled within the otic vesicle, with their openings poised towards the cristae. Endolymph from the canals can displace the cristae by inertia. Thus, the main function of the cristae is sensing angular acceleration. Zebrafish also possess a fish-specific organ that utilizes HCs: the lateral line organ. The lateral line consists of sensory patches, called neuromasts, which are clustered on the surface of the body and centered along the sides of the fish. Neuromasts sense water movements, which assists in schooling behavior and predator evasion.

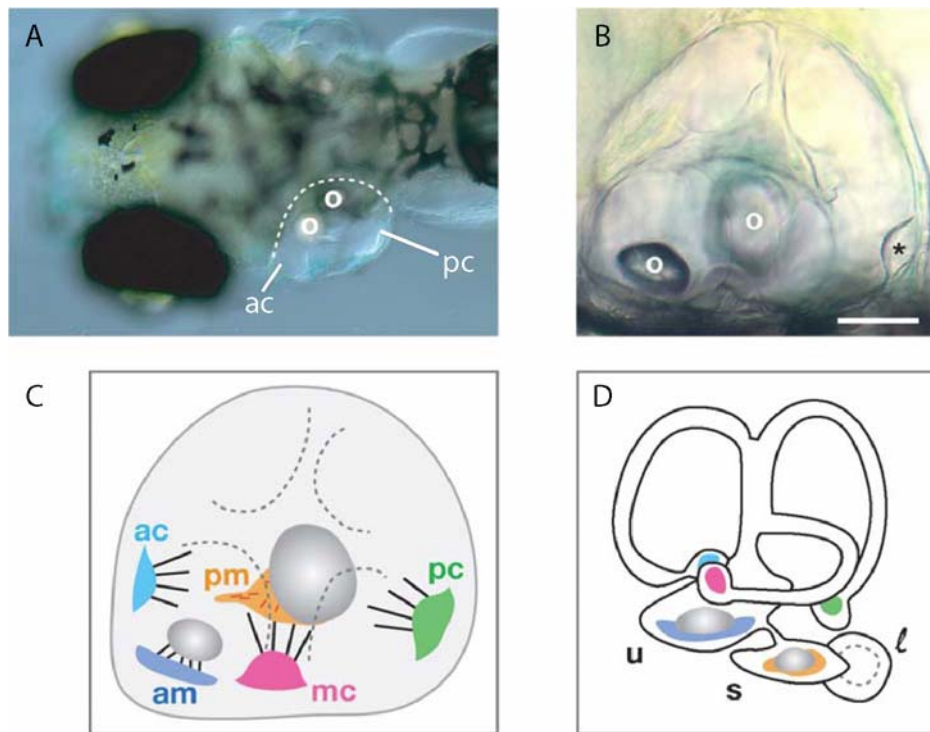


Figure 2. Zebrafish ear anatomy. **A**, top-down view of 5 day-old larval head. The right ear has been marked by the dotted line. **B**, lateral view of the same ear. **C**, schematic, indicating the sensory patches. **D**, adult ear, including semicircular canals, utricle and saccule. O, otolith. ac, anterior crista. mc, medial crista. pc, posterior crista. am, anterior macula. pm, posterior macula. u, utricle. s, saccule. from: (Nicolson, 2005).

2.3: Hair Cell Molecular Anatomy and Physiology

HCs are the sensory receptors for the auditory and vestibular systems. As such, they are highly specialized neuroepithelial cells that pose very specific demands on cellular machinery and metabolism. A large number of ion channels and pumps are present in HCs, especially for Ca^{2+} . HCs constantly depolarize and repolarize, even when “at rest”. This constant activity leads to excessive energy consumption in the form of ATP (Shin et al., 2007), and requires turnover of all active protein components. Ca^{2+} mainly enters the HC through the mechanotransduction (MET) channel, the synaptic Ca^{2+} channels, and from cisternae of the efferent postsynapse. In order to tightly regulate Ca^{2+} -levels, HCs express large quantities of Ca^{2+} pumps (Mammano et al., 2007) and the proteinacious Ca^{2+} buffers calretinin, calbindin and parvalbumin (Edmonds et al.,

2000; Heller et al., 2002; Hackney et al., 2005). For a more focused view on Ca^{2+} at the synapse, see section 2.3.3. HCs die if overstimulated, and are susceptible to a variety of drugs, especially aminoglycoside antibiotics and cisplatin (Rybak and Ramkumar, 2007). Once dead, they do not regenerate in mammals, but can do so in fish, chicken and amphibians (Kros, 2007).

HCs are highly polarized (Figure 3). At the apical end, they transduce mechanical stimuli with their bundle of stereocilia, each of which contains a MET channel, and the kinocilium. K^+ and Ca^{2+} channels, and Ca^{2+} pumps populate the basolateral membrane. Several ribbon synapses are located here, and turn the graded potentials into a graded release of glutamate. The efferent postsynapse, involved in regulatory feedback from the brain, is also located here. Because mechanotransduction and transmission at the afferent synapse are key functions of the HC as a sensory receptor, we will now discuss them in more detail.

Transduction and Synaptic Transmission at the Inner Hair Cell

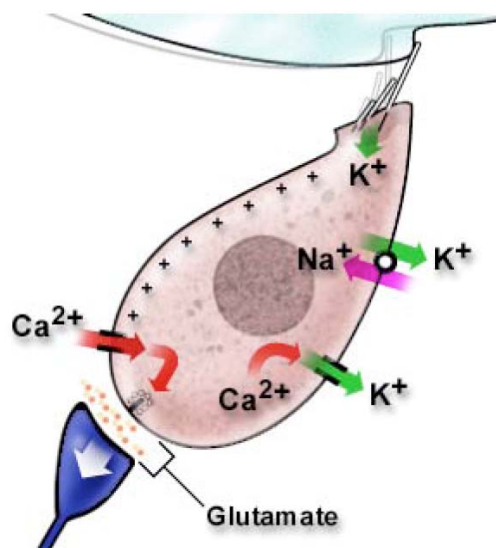


Figure 3. Prominent physiological features of HCs. HCs have two prominent anatomical features: a hair bundle, which converts mechanical stimuli into graded depolarizations of the cell membrane. Large inward K^+ currents necessitate the presence of K^+ channels and exchangers in the plasma membrane to maintain intracellular ion balance. HCs have ribbon synapses that secrete glutamate to encode the graded potentials generated by mechanotransduction. (by Stephan Blatrix)

2.3.1 Hair Cell Mechanotransduction

HCs sense mechanical stimuli with their hair bundle (Figure 4A). The Hair bundle is capable of active and passive movement, and adaptation to stimulus intensity takes place here as well. The bundle consists of an array of actin-rich stereocilia, which are arranged by their size from shortest to tallest (Figure 4C). All cilia are tapered at their base and are connected along their length with their neighbors. The tallest cilia are also connected to the kinocilium, though details vary by HC subtype, developmental stage and organism. Cilia can pivot about their base and, due to their links, deflect together. Each cilium is thought to have one MET channel (Hudspeth, 1989), which is connected to the top of next cilium by the tip link (Figure 4B, C). The tip link gates the MET channel (Corey and Hudspeth, 1983; Assad et al., 1991) (Figure 4B, D), and has recently been shown to be composed of Cdh23 and Pcdh15 (Kazmierczak et al., 2007). The MET channel has a conductance of more than 100pS and is unspecific in its cation conductance (Corey and Hudspeth, 1979; Lumpkin et al., 1997; Beurg et al., 2006). At rest, it has an opening probability >0 , and is at its highest sensitivity (Vollrath et al., 2007). The apical end of the HC is bathed in the K^+ rich endolymph, which leads to the unusual situation of a higher K^+ concentration outside of the cell than inside. When the hair bundle is deflected towards its tallest cilium by mechanical force, such as endolymph inertia in a semicircular canal or the vibrating tectorial membrane in the cochlea, the tip link opens the MET channel and the HC is depolarized by the influx of K^+ at its apex. When the MET channel opens, Ca^{2+} will also enter the bundle, and will influence MET conductance by binding to it and causing a lowering of the opening probability called “fast adaptation” (Stauffer and Holt, 2007). The MET channel is also part of a complex that can actively modulate transduction via a slower adaptation mechanism, which depends on both Ca^{2+} and myosin-1c motor function (Stauffer et al., 2005). While candidates like TRPN1 for lower vertebrates (Sidi et al., 2003), and TRPA1 in higher vertebrates (Corey, 2006), Figure 4D, have been proposed, the molecular identity of the MET channel has not yet been determined.

Transduction and adaptation also require PI(4,5)P₂ for normal kinetics, which is enriched in HC bundles and binds to myosin 1c (Hirono et al., 2004). Depletion of PI(4,5)P₂ by inhibition of phosphatidylinositol 4-kinase (PI4-K) or sequestration by aminoglycosides reduces the rates of fast and slow adaptation. Mechanotransduction creates graded electrical potentials in the HC plasma membrane. These potentials are encoded into neurotransmitter (glutamate) release at the HC afferent synapse.

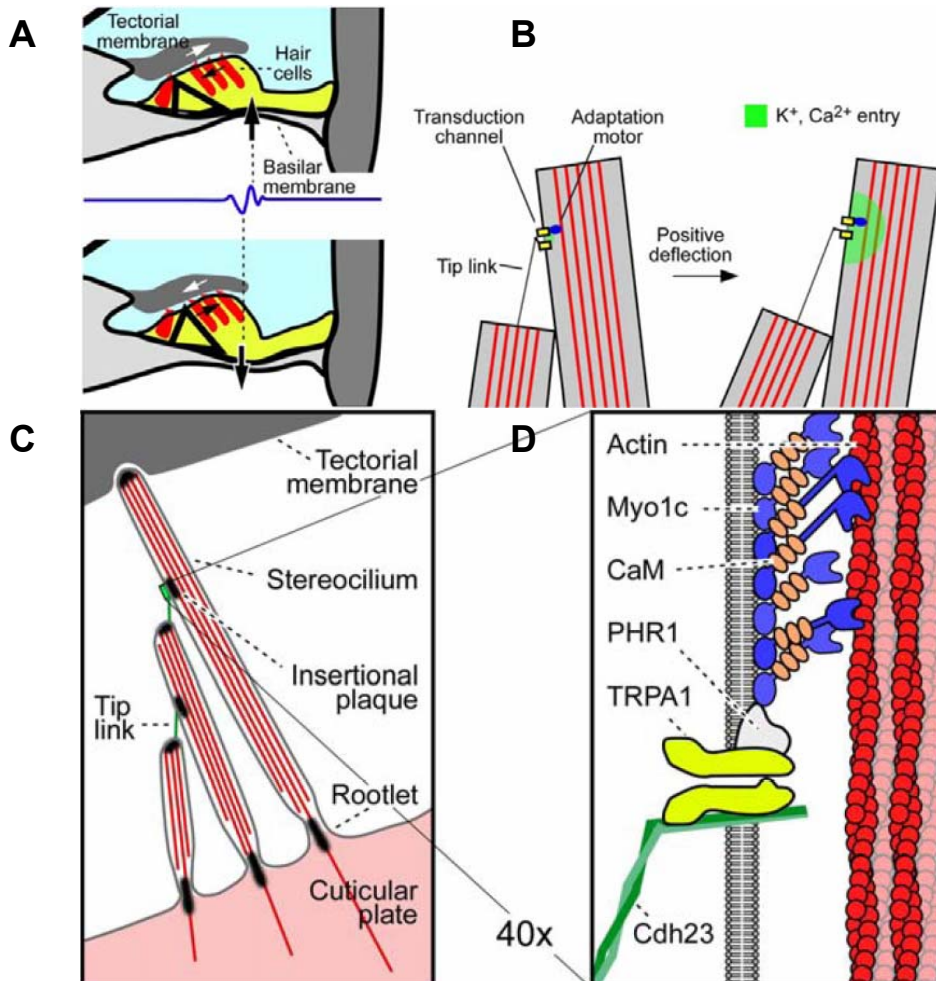


Figure 4. Hair Cell Mechanotransduction. *A*, a HC bundle consists of stereocilia, which are rooted in the cuticular plate at the apical pole of the HC, have a dense actin core and are interconnected by tip links. *B*, Enlargement schematic of the mammalian mechanotransduction apparatus, with the candidate channel TrpA1 being gated by cadherin 23, a tip-link component. Regulating the apparatus is the adaptation motor Myo1c. *C*, example of tectorial membrane movement and HC stimulation in response to a sound wave passing through the cochlea. *D*, Cation influx in response to tip-link mediated gating of the MET channel. adapted from: (LeMasurier and Gillespie, 2005).

2.3.2 Properties of the Hair Cell Afferent Synapse

The HC afferent chemical synapse determines the quality of the information that is transmitted to the auditory nerve and thus made available to the brain. Translation of graded potentials to neurotransmitter release happens with high temporal resolution and fidelity. There is some evidence that this is made possible by the synaptic ribbon. First identified as an electron-dense proteinaceous aggregate at the active zone of the HC pre-synapse, ribbons coordinate synaptic vesicles (SVs) at the active zone and allow remarkable rates of exocytosis exceeding 1000 SVs/sec (Moser and Beutner, 2000; Griesinger et al., 2005). Ribbons also appear to coordinate multivesicular release (Singer et al., 2004); vesicle release is synchronized across multiple synaptic ribbons with sub-millisecond precision (Khimich et al., 2005). Ribbons are also found in photoreceptors and rod bipolar cells (Prescott and Zenisek, 2005), as well as in the pineal gland (Karasek and Cozzi, 1990). Ribbon bodies in HCs are ovoid to spherical, whereas those of photoreceptors and rod bipolar cells are generally planar. Ribbon bodies coordinate a halo of SVs that are tethered to the body by short filaments of unknown composition in all these cases. Because of their extremely large synaptic vesicle pools in the order of $2-6 \times 10^5$ (Lenzi et al., 1999), tens of thousands of SVs can be released in HCs in response to strong stimulation (Schnee et al., 2005). How this enormous pool of SVs is generated, regulated and recycled is largely unknown. HC SVs are presumably loaded by vesicular glutamate transporter 1 (Vglut1); (Furness and Lawton, 2003), and post-synaptic receptor currents are mediated by AMPA receptors (Glowatzki and Fuchs, 2002), specifically by GluR2/3 in the mature HC (Matsubara et al., 1996; Eybalin et al., 2004). Therefore, the HC afferent synapse is glutamatergic.

The molecular composition of the ribbon synapse is not well understood, and might vary in different cell types. To date, only three major ribbon synapse components are known: Piccolo (tom Dieck et al., 2005), Bassoon (Khimich et al., 2005) and Ribeye, which may constitute the bulk of the ribbon's mass (Schmitz et al., 2000) and is the only one of the three that is specific for ribbons. To complicate things further, the ribeye gene is duplicated in teleosts (like zebrafish),

giving rise to *ribeye-a* and *ribeye-b*, the functions of which are unclear (Wan et al., 2005). Ribeye consists of an N-terminal domain that presumably mediates oligomerization, and an NAD⁺-binding C-terminus identical to the transcription factor CtBP2. The current model perceives ribbons mainly as aggregates of Ribeye molecules with their C-termini facing the center of the ribbon and their N-termini exposed to the surrounding cytosol (Schmitz et al., 2000). The role of Bassoon appears to be a specific interaction with Ribeye to anchor ribbon bodies to the active zone (tom Dieck et al., 2005).

Furthermore, Ribbon synapses show very tight control of Ca²⁺ influx at the synapse, which is partially achieved by their clustering at the active zones, and perhaps their interaction with the ribbons themselves (Khimich et al., 2005). SV release correlates linearly with Ca²⁺ (Brandt et al., 2005; Johnson et al., 2005), though Ca²⁺ does not correlate linearly with stimulus intensity (Moser et al., 2006). Voltage-gated Ca²⁺-channels respond to the graded potential changes in the plasma membrane, and differ by the cell type that employs the ribbon synapse in question. HCs express Ca_v1.3 L-type voltage-gated Ca²⁺-channels (Sidi et al., 2004), whereas Ca_v1.4 is expressed in the retina (Mansergh et al., 2005).

Synaptic vesicles (SVs) at the ribbon synapse contain many of the common SV proteins, like SNAP25, syntaxin1, or synaptobrevin/VAMP (Safieddine and Wenthold, 1999), but not synapsins, rabphilins (Von Kriegstein et al., 1999), or synaptotagmins (Safieddine and Wenthold, 1999). This presents a problem, because synaptotagmins are considered to be important Ca²⁺ sensors for SV release (Tucker and Chapman, 2002). Addressing this concern, Roux et al. have recently suggested Otoferlin as a substitute Ca²⁺-sensor (Roux et al., 2006).

Ribbon synapses are fed by three distinguishable SV pools. SVs of the readily-releasable pool (RRP) are docked at the active zone, between the ribbon proper and the presynaptic membrane. SVs tethered to the ribbon body that are not readily-releasable due to their distance from the plasma membrane, belong to the recycling pool. SVs in the cytoplasm in the vicinity of the ribbon are part of the reserve pool. The actual size of the respective pools varies by cell

type and organism (Nouvian et al., 2006). Moser et al. calculated from whole-cell capacitance measurements in mouse HCs that the RRP has a size of about 280 vesicles, and is released with a time constant of 10 ms. Mathematically speaking, the limit for the initial rate of release is 28,000 SVs/sec (Moser and Beutner, 2000)! However, Moser et al. resolved only two kinetically different components: a fast component, presumably comprising the RRP, and a slow component that accounts for the recycling and reserve pools. Of note, the slow component comprised about 6000 SVs/sec, a rate that is much higher than the release rate at conventional synapses. Griesinger et al. later reported a release rate of approximately 1400 SVs/sec and compensatory endocytosis rate of 1100 SVs/sec, as measured by 2-photon microscopy of cochlear preparations (Griesinger et al., 2005). In accordance with these data, HCs are considered to be high indefatigable (Moser and Beutner, 2000). However, strong stimulation preferentially depletes SVs tethered to the active zone-proximal half of the ribbon in bullfrog saccular HCs (Lenzi et al., 2002). The authors of this study concluded that ribbons might transport SVs to the active zone, a model for ribbon function called the “conveyor belt” model (Parsons and Sterling, 2003; Griesinger et al., 2005). This view has been challenged by the observation that to cover the short distances required, the rate of diffusion is sufficient and equal to active transport (Edmonds et al., 2004).

Moreover, ribbon bodies are not required for SV exocytosis in HCs. Bassoon knockout mice do not anchor ribbon bodies at the HC active zone (Khimich et al., 2005), yet secretion persists, albeit at a reduced rate. The authors conclude that ribbons are required for synchronizing SV fusion to ensure proper temporal coding of auditory stimuli, which is consistent with other findings suggesting that inner hair cells (IHCs) engage in multivesicular release (Glowatzki and Fuchs, 2002; Keen and Hudspeth, 2006), and that SVs away from HC active zones are still able to fuse with the PM in an activity-dependent manner (Edmonds et al., 2004).

2.3.3 Ca²⁺ at the Synapse

It appears that Ca²⁺ controls all aspects of synaptic activity and synapse formation. During synaptic development of mouse HCs, Ca²⁺ currents are the first to appear (Johnson et al., 2005). Cav1.2 (but not Cav1.3) L-type calcium channels couple neuronal excitation to CREB expression (Weick et al., 2003), which affects gene expression. At the mature ribbon synapse, the L-type channel isoform Cav1.3 is dominant and directly couples excitation to neurotransmitter secretion (Brandt et al., 2005; Platzner et al., 2000). Cav1.3 channels are tightly linked to the release machinery through anchoring to SNARE proteins- perhaps they are even attached to the ribbons directly. SNAREs bind to PI(4,5)P₂ via their C2 domains in the presence of Ca²⁺, which acts in both exo- and endocytosis.

Ca²⁺ is the pacemaker at synapses, effecting and coupling exo- and endocytosis. Influx of Ca²⁺ during synaptic activity fuels a complex control mechanism through protein phosphorylation/ dephosphorylation enforced by cdk5 and calcineurin. Ca²⁺ binds to calmodulin and activates calcineurin, which dephosphorylates a group of proteins called “dephosphins” (Cousin and Robinson, 2001). Among the dephosphins are the rank-and-file of SV cycle proteins: synapsin, dynamin 1, amphiphysin, AP180, synaptojanin, epsin, eps15 and syndapin, and perhaps others. Ca²⁺ also stimulates Phosphatidylinositol Phosphate Kinase (PIPK) via ARF6; PIPK synthesizes PI(4,5)P₂ at the plasma membrane, here acting as a signal for endocytosis via AP2 (Honing et al., 2005). PI(4,5)P₂ in turn can increase the conductance of Ca²⁺ channels, perhaps establishing a positive-feedback loop until membrane depolarization ceases. PI(4,5)P₂ also increases PMCA activity, which together with SERCA, pumps Ca²⁺ out of the cytoplasm, and a low cytoplasmic Ca²⁺ concentration inhibits calcineurin and activates cdk5. Cdk5 phosphorylates the dephosphins (Lee et al., 2004) and P/Q-type, perhaps also L-type Cav channels, which inhibits Cav channel interaction with SNAREs (Tomizawa et al., 2002), and the synapse goes back to rest.

2.4 Synaptic Vesicle Exocytosis

SVs are generally exocytosed in a Ca^{2+} -dependent manner in three steps: docking, priming, and fusion with the target membrane. Docking requires the interaction of SNARE proteins on both opposed membranes. The synaptosome-associated protein of 25 kDa (SNAP-25) interacts with syntaxin 1 and vesicle-associated membrane protein 2 (VAMP2) to form a ternary soluble N-ethylmaleimide-sensitive fusion protein attachment protein receptor (SNARE) complex that is essential for synaptic vesicle exocytosis. A 4th player, Synaptotagmin (Syt), also on the vesicle, binds to MUNC18, which stabilizes Syt in the open (docking) conformation. During docking, the association of the SNARE complex is still loose. During priming, MUNC18 is replaced by MUNC13 and Syt undergoes a conformational change that stabilizes the SNARE complex. MUNC13 also binds diacylglycerol (DAG) at the plasma membrane, a product derived from $\text{PI}(4,5)\text{P}_2$ through hydrolysis, and the active zone protein rab-interacting molecule (RIM). When Syt senses Ca^{2+} influx via its two C2 domains, it triggers the membrane fusion event by further tightening the SNARE complex, which is called “zippering”. After membrane fusion, the soluble N-ethyl maleimide sensitive factor (NSF) is recruited by accessory (SNAP) proteins to disassemble the SNARE complex. At ribbon synapses, only SVs in the readily releasable pool are primed and docked. It is unclear how SV fusion of thousands of SVs occurs at these synapses in milliseconds without Syt (see section 2.3.2).

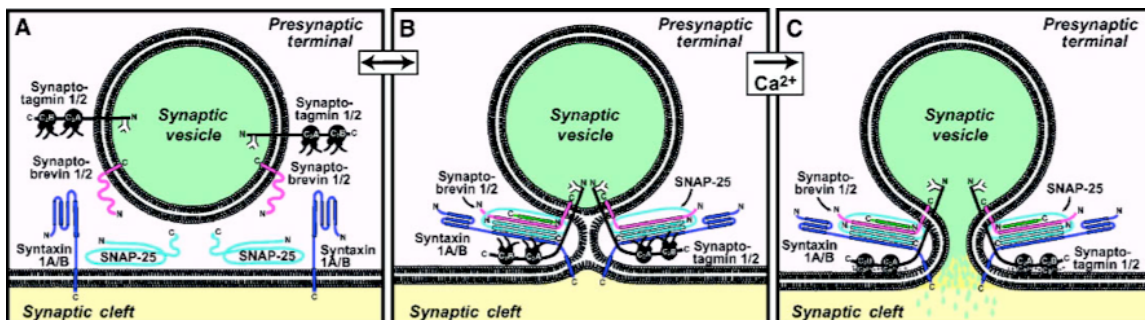


Figure 5. Model for the functions of SNARE proteins, complexins, and synaptotagmins 1 and 2 in synaptic vesicle exocytosis. In docked vesicles (*panel A*), SNAREs and synaptotagmins are not engaged in direct interactions. During priming (*panel B*), SNARE complexes form, complexins (green) are bound to fully assembled complexes, and synaptotagmins constitutively associate with the assembled SNARE complexes. The synaptic vesicle membrane and plasma membranes are forced into close proximity by SNARE complex assembly, which results in an unstable intermediate that is shown as a speculative fusion stalk. Ca^{2+} influx (*panel C*) further destabilizes the fusion intermediate by triggering the C_2 domains of synaptotagmin to partially insert into the phospholipids. This action is proposed to cause a mechanical perturbation that opens the fusion pore. Note that the nature and stability of the putative fusion intermediate is unclear and that SNARE complex assembly in panel B is suggested to be reversible, whereas Ca^{2+} triggering is not.

2.5 Vesicular Glutamate Transporters

Glutamate is the major excitatory neurotransmitter in the vertebrate brain. It is generated from L-Glutamine by phosphate-activated transaminase and in order to fulfill its role as a neurotransmitter, it is stored in SVs in concentrations reaching 60mM (Burger et al., 1989). SVs of a glutamatergic synapse are filled with L-Glutamate by the vesicular glutamate transporter (Vglut). Vglut proved surprisingly difficult to identify, until in 1994, the brain-specific Na⁺-dependent inorganic phosphate transporter (BNPI) was cloned (Ni et al., 1994). BNPI was initially found to mediate Pi uptake, but localizes to synaptic vesicles (Bellocchio et al., 1998). Then EAT-4, the *C. elegans* orthologue of BNPI, was found to be required for glutamatergic neurotransmission (Lee et al., 1999). In 2000, (Bellocchio et al., 2000) and (Takamori et al., 2000) both unambiguously identified BNPI as the vesicular glutamate transporter (Vglut1). Two more isoforms were identified in rapid succession: Vglut2 (Bai et al., 2001; Fremeau et al., 2001; Hayashi et al., 2001; Herzog et al., 2001; Takamori et al., 2001), and Vglut3 (Fremeau et al., 2002; Gras et al., 2002; Schafer et al., 2002; Takamori et al., 2002). Predicted secondary structures are shown in Figure 6.

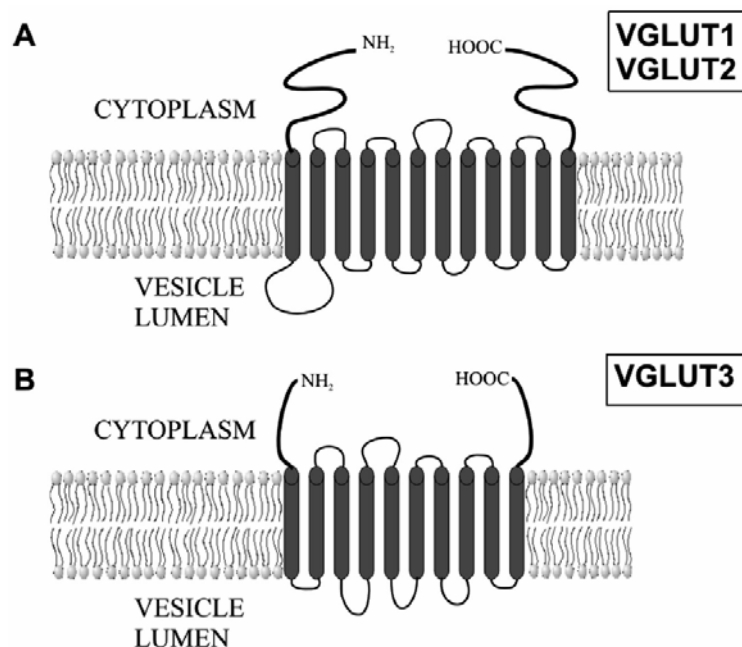
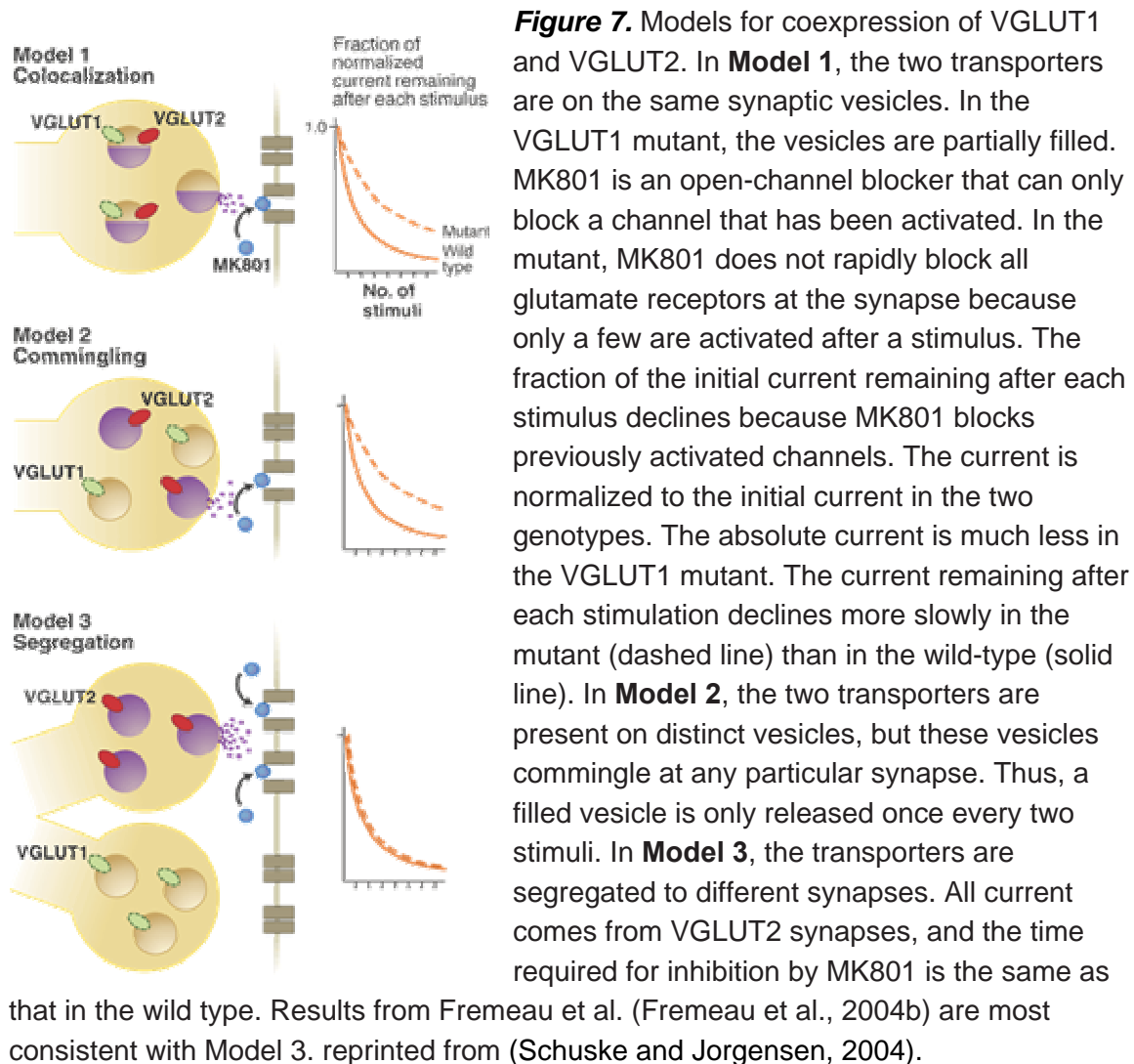


Figure 6. Predicted secondary structure of VGLUTs. VGLUT1 and 2 have 12 transmembrane segments, VGLUT3 has 10. Both termini are facing into the cytosol. from: (Liguz-Leczna and Skangiel-Kramska, 2007).

Glutamate transport is ATP-dependent and H⁺-sensitive, because it relies on an electrochemical gradient that is established by v-H⁺-ATPases. The resulting membrane potential difference acts as the driving force. However, unlike vesicular monoamine transporters or the GABA transporter, the electrical ($\Delta\psi$) component, not the pH component of this gradient is much more important for Vglut1 and -2 (Takamori et al., 2000; Herzog et al., 2001). Vglut3 function is dependent on both (Gras et al., 2002). Furthermore, Vgluts can co-transport phosphate and Na⁺ in reverse direction when in the plasma membrane (Ni et al., 1994), and requires a low concentration of Cl⁻ to function (Harteringer and Jahn, 1993).

In the mature mammalian CNS, *vglut1* and -2 appear in essentially overlapping distributions, though they are coexpressed in some neurons during development (Fremeau et al., 2004a). There has been much speculation about the physiological role of expressing two Vgluts in a single cell, which are summarized in Figure 7. When Vglut1 is knocked out, hippocampal pyramidal neurons are silenced, and a significant reduction in the number of SVs within 300 nm of the active zone in excitatory terminals in the hippocampus and cerebellum is seen. In addition, several SV-associated proteins are then underexpressed in hippocampal extracts (Fremeau et al., 2004b).

In mouse hippocampal neurons, Vglut1 and -2 proteins appear to sort to mutually exclusive vesicle populations, which are targeted to respective release sites (Fremeau et al., 2004b). It is currently estimated that vesicles possess 1-3 copies each on average (Takamori et al., 2006), even though only one copy is required to fill a vesicle (Daniels et al., 2006). Whether this excess of neurotransmitter transporter provides a safety net for SV function, or is a function of an inherent inaccuracy in SV recycling, is not known. However, it has been shown that after exocytosis, Vglut1 can interact directly with the endocytic machinery (Endophilin, AP2, AP3); (Voglmaier et al., 2006; De Gois et al., 2006) during SV recycling, which may be important for establishing SV pools that are distinguishable by their Vgluts.



Furthermore, as heterologous expression of Vglut1 (Takamori et al., 2000) or Vglut2 (Takamori et al., 2001) is sufficient to enable quantal glutamate release in autaptic cultures of GABAergic neurons, it is possible that neurons traditionally assigned to one neurotransmitter class may also release glutamate *in vivo*. This role has been especially emphasized in connection with Vglut3, perhaps because it has such an unusual expression pattern (see below).

Finally, Vglut1 and Vglut2 have been implicated in Schizophrenia (Eastwood and Harrison, 2005). Alterations in the expression of VGLUT1 and VGLUT2 have also been found in the brains of patients with Parkinson's disease (Kashani et al., 2007). Comparable data for VGLUT3 is currently sketchy at best.

2.5.1 Vesicular Glutamate Transporter 3

Vglut3 is found in scattered locations in the (rat) central nervous system, occasionally overlapping with one of the other isoforms. Interestingly, Vglut3 is also expressed in some serotonergic (Gras et al., 2005) and GABAergic neurons (Fremeau et al., 2001), and even in astrocytes and non-neuronal cells such as pancreatic islet cells, suggesting that glutamate may have novel modulatory and/or signaling roles there (Takamori, 2006). The presence of Vglut3 in nonglutamatergic neurons seems to contribute to depolarization-induced potentiation of inhibition (DPI), a new form of inhibitory synaptic plasticity in cerebellar Purkinje cells. Purkinje cells express presynaptic NMDA receptors, which increase Ca^{2+} release from intracellular stores, which in turn boosts GABA release (Duguid and Smart, 2004; Seal and Edwards, 2006a).

Glutamatergic pathways participate in the processing of vestibular signals within vestibular nucleus complex (VNC) mainly through the re-uptake of glutamate into synaptic vesicles by VGLUT1 and 2, but VGLUT3 may play a similar role in areas other than medial and inferior nuclei of the VNC (Deng et al., 2006). Another group detected intense VGLUT3 immunoreactivity in sensory epithelia cells, and weak labeling of VGLUT3-positive afferent fibers in the maculae and ampullary cristae (Wang et al., 2007) of the cochlea.

VGLUT3 is thought to play a role in the pathogenesis of Parkinson's disease (Chung et al., 2006). VGLUT3 is exclusively located in the glomerular neuropil, where it colocalizes extensively with the vesicular inhibitory amino acid transporter vesicular GABA transporter, suggesting that it is associated with a subset of inhibitory synapses. It is even suggested to play a role in GABA synthesis in GABAergic neurons (Gabellec et al., 2007).

Combining these data makes VGLUT3 easily the most versatile VGLUT family member, both in the cell types that express it, and in the functions it is proposed to fulfill. This also underlines that VGLUT3's roles are hardly understood.

2.6 Vesicle Recycling at Chemical Synapses

Timely recycling of SV protein and presynaptic membrane is crucial for the continued function of the synapse. Kinetically, SV endocytosis can be separated into two separate components, one fast, and one slow (Harata et al., 2006). It remains unclear if these different kinetics result from the action of two different endocytic pathways or the depletion of rate-limiting components of only CME. Regardless of which of these scenarios is true, CME is crucial for synaptic function. (Girard et al., 2005) have estimated that 90% of clathrin-coated vesicles (CCVs) in neurons are involved in SV recycling. As early as 1973, (Heuser and Reese, 1973) showed signs of clathrin-mediated vesicle re-uptake in the periaxial zone. CCVs may also bud off membrane infoldings and vacuoles created by bulk endocytosis (see Figure 8).

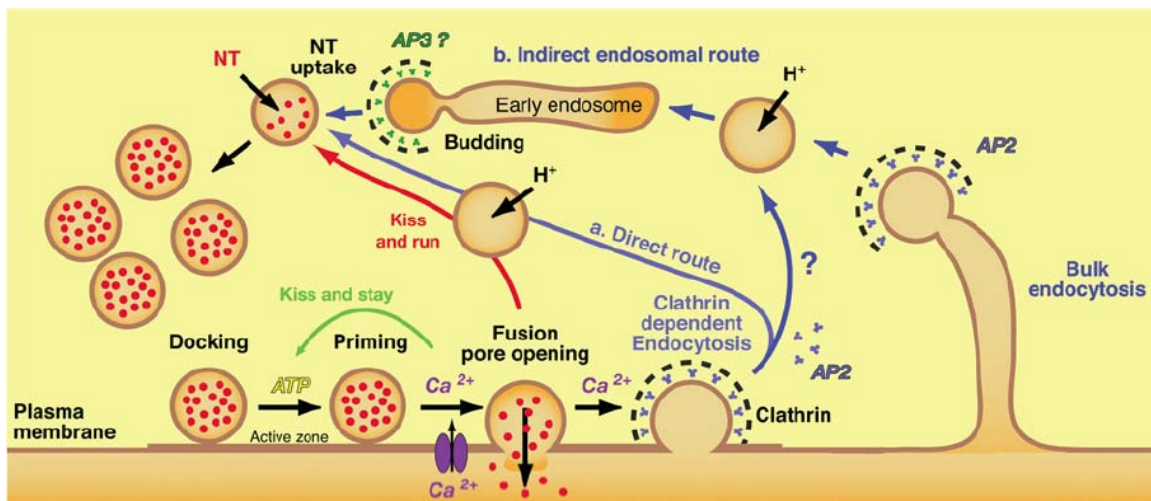


Figure 8. Vesicle recycling at chemical synapses. This comprehensive schematic by Murthy et al. depicts all known possible SV recycling routes. Kiss-and-stay and kiss-and-run are local SV recycling pathways that require exocytosis without SVs melting into the plasma membrane. Depicted are also classical CME and bulk endocytosis, which can refill SV pools directly, or indirectly via an early endosome (Murthy and De Camilli, 2003).

Since SV protein is diffusely localized in the synaptic membrane, significant amounts of SV recycling from the plasma membrane might occur away from the synapse (Fernandez-Alfonso et al., 2006). This would allow for an endocytosis rate increase by parallel events, rather than speeding up endocytosis at the same place. However, this notion may be challenged by the

observation that vesicular glutamate transporter Vglut1 and GABA transporter Vgat1 can recycle without clathrin by means of an endosomal pathway involving the unusual adaptor protein AP3B (Voglmaier et al., 2006; Nakatsu et al., 2004). Furthermore, the GTPase *dynamain* is critical for CME and SV endocytosis, and Dynamin 1 is expressed to high levels in neurons. Dynamin 1, which can function in CME and non-CME, operates faster than the other dynamins and generates smaller vesicles, is highly enriched in brain, activated by Ca^{2+} -dependent dephosphorylation by calneurin and inhibited by cdk5-dependent phosphorylation (Tomizawa et al., 2003). Two other *dynamain* isoforms exist. Dynamin 3 functionally overlaps with Dynamin 1, and can rescue a loss-of-Dynamin 1 phenotype when overexpressed. While also enriched in the brain, it is expressed at much lower levels than Dynamin 1 and presumably shows slower pinching kinetics (Ferguson et al., 2007). This is in contrast to the “slow” Dynamin 2, which is the “housekeeping” dynamin and may be responsible for the tens-of-seconds-timecourses mentioned earlier. Dynamin 2 is ubiquitously expressed to low levels, and generates clathrin-coated vesicles in receptor-mediated endocytosis. Of note, it is suppressed by high Ca^{2+} at the synapse. It generates vesicles of slightly bigger diameter than Dynamin 1 (Ferguson et al., 2007).

Currently, results point to CME as the main mechanism of SV recycling at synapses. Interference with CME at various stages leads to impairment of SV recycling in a number of organisms (Jung and Haucke, 2007). Indeed, overexpression of a dominant-negative AP180 peptide, which disrupts endocytic complex formation by competing for binding sites (Zhao et al., 2001), or RNAi-mediated knockdown of clathrin leads to a complete loss of SV recycling (Granseth et al., 2006). CME can have a time-course between <1s to >150s per event (Mueller et al., 2004; Wu, 2004), and SV recycling happens in a matter of seconds (Murthy and De Camilli, 2003). How can this large dynamic range be explained? First and foremost, there are a large number of neuron-specific splice variants for *clathrin* and *AP2 α* , but also the regulatory *synj1-145*, and isogenes like *ap180*, *endophilin1*, *amphiphysin1*, *intersectin1*, *necap1*, *auxilin1* and *dynamain 1*. There is also evidence that direct binding of SV components to

Endophilin, here by Vglut1, leads to faster processing and AP2- and D/ExxxL[LI] motif dependent sorting (Voglmaier et al., 2006). Synaptotagmin (Syt), both a SV component/ SNARE and important for both vesicle fusion and retrieval (Bai et al., 2004), also has an atypical AP2 binding site within its Ca^{2+} -sensing C2 domain, which may lead to faster CME in neurons.

The second general difference in neuronal vs. non-neuronal CME is that CME in neurons strongly depends on Ca^{2+} levels (Gad et al., 1998). During activity, Ca^{2+} passes through the synaptic, voltage-gated Ca^{2+} channels (Cav) and acts as a pacemaker at the synapse. It couples exo- and endocytosis, and is discussed in more detail in section 2.3.3. Ca^{2+} levels control the cdk5 vs. calcineurin phosphospecific regulation of the neuronal endocytosis machinery. A key player in this machinery and therefore the SV cycle is Synj1 (Cremona and De Camilli, 2001). Phosphorylation of Synj1 through Cdk5/P35 inhibits its interaction with Endophilin, prohibiting Synj1 recruitment and slowing down endocytosis (Lee et al., 2004). Finally, SVs contain an unusually high amount of cholesterol, which might act as an organizer of SV protein (Takamori et al., 2006). This would also help explain why vesicle protein can cluster at endocytic sites and remain clustered in endosomes (Jia et al., 2006). SVs thus may facilitate recycling by maintaining a defined molecular stoichiometry (Figure 9).

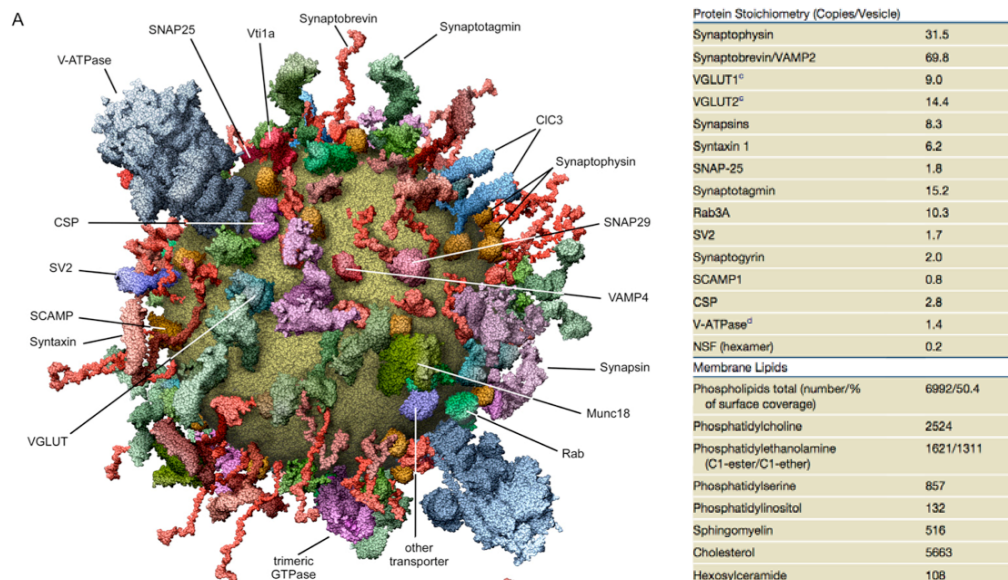


Figure 9. Molecular anatomy of a synaptic vesicle (Takamori et al., 2006).

2.6.1 Vesicle Recycling at Ribbon Synapses

It is generally assumed that there must be at least two distinct modes of endocytosis with different kinetics in HCs (Harata et al., 2006), though presumably both are dynamin- dependent (Jockusch et al., 2005; Newton et al., 2006). Between their high kinetics of exocytosis and their vast vesicle pools, HCs must have a very efficient way of replenishing SVs. Lenzi et al. estimated the rate of endocytosis to be about 1100SVs/ sec (Lenzi et al., 1999). It seems unlikely that at ribbon synapses, SVs are recycled in the same way as at conventional synapses. Local mechanisms of recycling, such as kiss-and-run and kiss-and-stay (see section 2.6), while attractive, also lack evidence. There is evidence, however, for CME and bulk endocytosis at ribbon synapses (Paillart et al., 2003), and endocytic profiles and cisternae have been observed close to ribbons in HCs following sustained depolarizations (Lenzi et al., 2002, and personal observation). Mostly due to lack of specific data, it is not clear if bulk endocytosis suffices as an explanation for the kinetics observed. We consider it as circumstantial evidence for the importance of bulk endocytosis that Voglmaier et al. report that in cultured neurons the AP3-endosomal pathway (Sudhof, 2004), even though slower than “direct” SV recycling through AP2, plays a role in compensatory endocytosis (Voglmaier et al., 2006). Whether this is also true for HCs however, remains to be investigated.

Perhaps counter-intuitively, capacitance measurements from frog saccular HCs seem to indicate that a “slow” ($\tau=6s$) mode of endocytosis, perhaps clathrin-mediated endocytosis, is the major mode of membrane recycling employed by HCs (Schnee et al., 2005). However, the fastest known CME takes place at central synapses and is in the range of $\sim 30s$. How this difference in kinetics is achieved, remains unclear (Mueller et al., 2004). Perhaps a HC-specific, yet-to-be-determined protein complement is involved. HCs lack Synaptophysin, Synapsin and Syts I and II. The latter play major roles in neurotransmitter release and recycling at central synapses (Safieddine and Wenthold, 1999). Roux et al. have shown that a previously undescribed factor, *otoferlin*, is crucial for transmission at the HC ribbon synapse. Otoferlin, which has partial similarity to

Syt in its C2 domain, may be the Ca^{2+} sensor in SV fusion and/or recycling at the HC ribbon synapse (Roux et al., 2006).

The lack of data has given rise to some more speculative ideas, in one of which the ribbon complex itself may aid SV recycling (Khimich et al., 2005). Supporting this idea, the mature synaptic Ca^{2+} channel Cav1.3 localizes to the ribbon and was found to interact with Endophilin (Chen et al., 2003), perhaps promoting vesicle endocytosis by acting as a buffer for this factor.

Yet another creative model for SV recycling has been proposed: transcytosis of membrane retrieved from the apical HC plasma membrane and trafficked through the Golgi apparatus back to the ribbon synapse (Griesinger et al., 2002; Griesinger et al., 2004; Griesinger et al., 2005). Unfortunately, the experiments supporting the transcytosis model (Griesinger et al., 2005) were performed using FM 1-43 in the absence of a MET channel blocker (Farris et al., 2004). FM 1-43 is known to pass through the MET channel pore (Gale et al., 2001; Meyers et al., 2003), so it is still unclear if the reported results are valid.

While there are some favorites, like CME and bulk endocytosis, the mechanisms underlying the rapid SV recycling observed at HC ribbon synapses are still unclear. To complicate things further, we can safely assume the concurrent presence of a number of different endocytic pathways, and it appears that the real challenge lies in the elucidation of the respective contributions of these pathways to the overall SV turnover.

2.7 Known Endocytic Pathways

A number of endocytic pathways exist in mammalian cells. The best understood mode of endocytosis is clathrin-dependent, and there is no doubt it is present at all chemical synapses. A detailed look at clathrin-mediated endocytosis (CME) is presented below, in section 2.7.2. It has often been suggested that in order to reach the fast recycling rates observed at some synapses, some mechanism other than classical CME must be present. Kiss-and-run vesicle recycling is one candidate that has been brought forward to fill the gap. Kiss-and-run relies on an intact clathrin coat around the vesicle and tight control of the fusion pore to prevent the vesicle from melting into the membrane, and allow for speedy re-uptake (He and Wu, 2007). We will take a quick look at this controversial mechanism in section 2.7.5.

Other endocytic pathways are clathrin-independent, and little understood. Certain receptors utilize parts of the endocytosis machinery, but bypass clathrin (Sauvonnet et al., 2005; Johannes and Lamaze, 2002). Phagocytosis (“cell eating”) and pinocytosis (“cell drinking”) are clathrin-independent, but are presumably also too slow for vesicle recycling. Other coat proteins, like caveolin, may be utilized in clathrin-independent endocytosis of lipid rafts (Kirkham and Parton, 2005), but again do not seem to approach the rates necessary (see section 2.7.4). Finally, there is the mysterious bulk endocytosis, in which larger “bites” of membrane are rapidly internalized, perhaps as part of an “emergency” mechanism to balance membrane flow (LoGiudice and Matthews, 2007). Bulk endocytosis will be treated in more detail in section 2.7.3.

2.7.1 Organelle Identity and Membrane Signposts Are Defined by Phosphoinositides

Phosphoinositides (PIs) contribute about 10% of total membrane lipids, and mark the membrane identity of distinct cellular organelles (Cockcroft and De Matteis, 2001; De Matteis and Godi, 2004). In addition, they function as regulatory molecules with roles in cell signaling, membrane transport, actin cytoskeleton rearrangement, cell development, cell survival, and transcriptional regulation (Toker, 2002). They fulfill these functions by recruiting effector proteins to specific membrane sites where cellular functions are then carried out. Organelle identity is also crucial for directing transport vesicles from one cellular compartment to another. Figure 10 gives an overview of the organelle-specific distribution of the major phosphoinositides in the cell. For the purpose of this thesis, we will consider $\text{PI}(4,5)\text{P}_2$, $\text{PI}(4)\text{P}$ and $\text{PI}(3,4,5)\text{P}_3$ to be most important, because of their role in the SV cycle and, as will be elaborated on shortly, because they are substrates of Synj1.

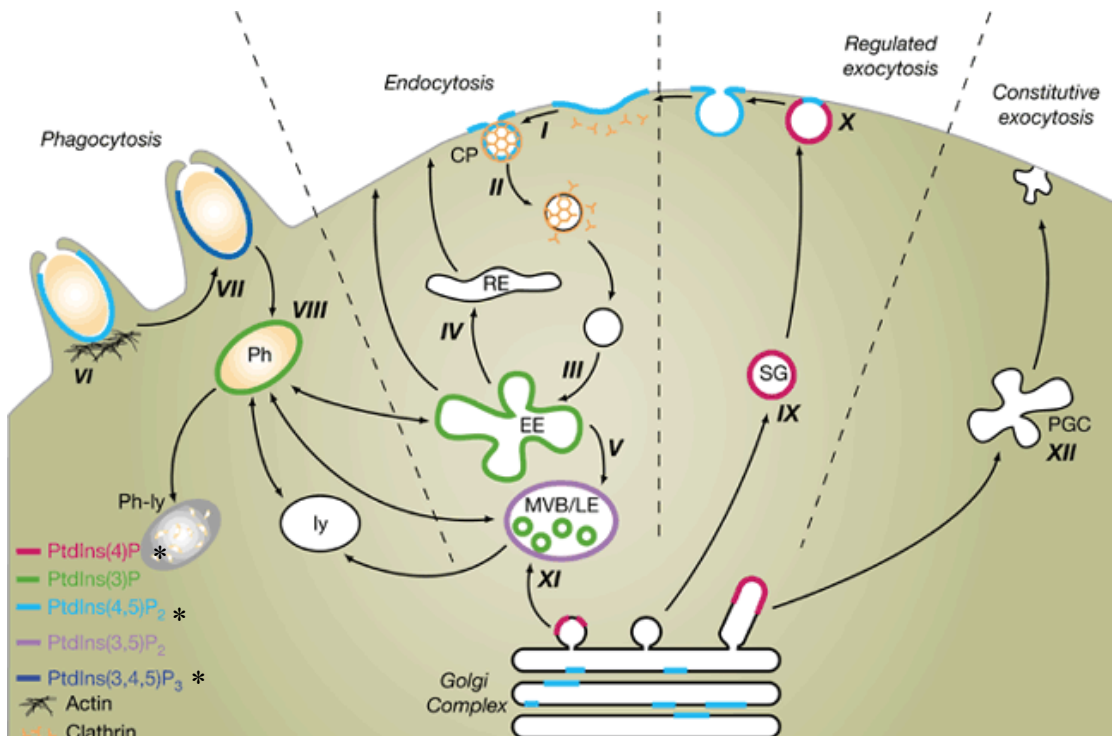


Figure 10. Phosphoinositide patterns in the major transport processes of the cell. $\text{PI}(4)\text{P}$ is highly enriched at the Golgi and secretory granules, $\text{PI}(4,5)\text{P}_2$ at the plasma membrane, where it acts as a cue for endocytosis. $\text{PI}(3)\text{P}$ populates early endosomes, and $\text{PI}(3)\text{P}$ and $\text{PI}(3)\text{P}_3$ are found in phagosomes (De Matteis and Godi, 2004). * substrates of Synj1.

2.7.2 Clathrin-Mediated Endocytosis

CME is a highly modular, highly adaptive process that relies on a network of tightly regulated proteins and lipids. While great strides towards understanding it have been made, it is far from fully understood. Yet the general principle appears simple enough (Figure 11).

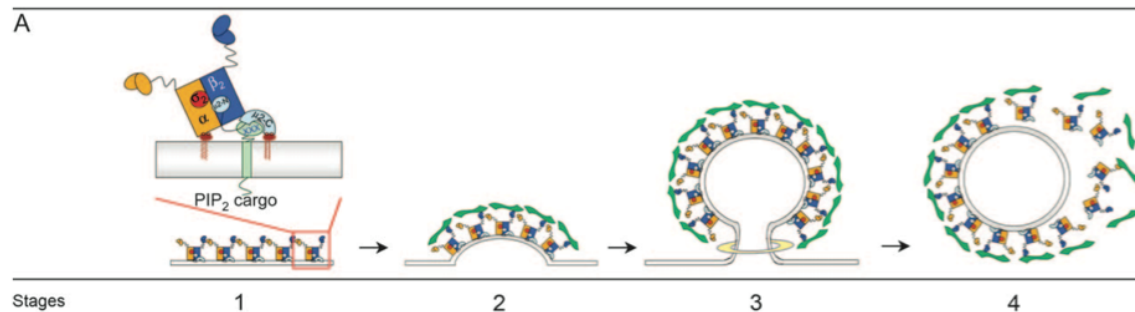


Figure 11 The four stages of CME (Jung and Haucke, 2007). In stage 1, cargo and PIP₂ in the plasma membrane are recognized adaptor molecules (APs). In stage 2, the APs act as a molecular scaffold, and assemble clathrin and other molecules to form a clathrin-coated pit. In stage 3, tubulation occurs and the pit invaginates from the membrane, to be finally pinched off by dynamin. In stage 4, the vesicle moves away from the site of endocytosis and the clathrin coat is shed.

A trigger event enables recruitment of an adaptor protein to the membrane, where it binds to cargo and membrane. The adapter then recruits the endocytic machinery and clathrin, to form endocytosis-capable patches. Within these patches, membrane curvature is induced by parts of the endocytic machinery. The clathrin lattice changes its conformation, assisted by ENTH and BAR domain proteins, and the clathrin-coated pit is further stabilized. Dynamin and the actin-cytoskeleton are recruited, and begin squeezing the neck of the clathrin-coated pit. At the same time, myosins push the head of the pit away from the membrane, while immobilizing the Dynamin ring, creating an invagination. Dynamin constricts further, and due to actin nucleation, and perhaps myosin action, the vesicle-to-be moves further away from the membrane, now sitting on a thin stalk of membrane. Synaptojanin 1-145 is recruited to the bud and changes the phospholipid environment. This reduces the affinity of the adaptors to the

membrane and allows for the recruitment of Auxilin. Auxilin actively removes the Clathrin coat. There are indications that the interaction between Auxilin and Dynamin is required for scission. Scission of the neck coincides with recruitment of cortactin and presumably with either with Auxilin recruitment or with the shedding of the Clathrin coat (Merrifield et al., 2005). Figure 12 shows the results of a stereotypical experiment using TIRF microscopy performed by Merrifield et al. to discern the timecourse of events during CME.

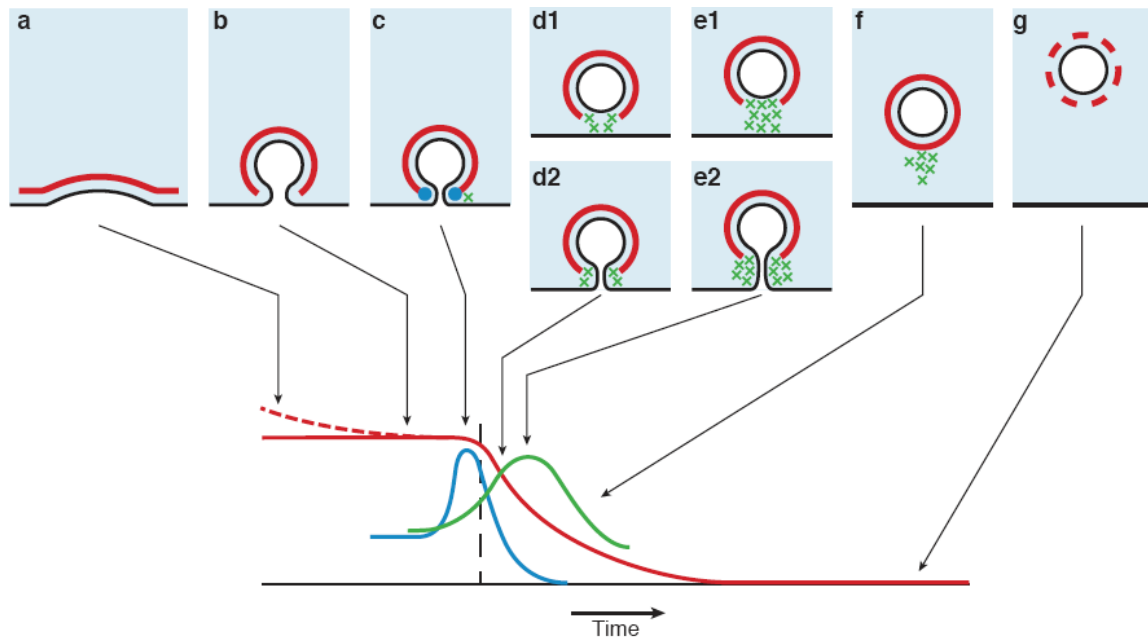


Figure 12. Fluorescence changes and endocytotic structures. Arrows indicate the relationship between possible intermediates in endocytosis and the fluorescence changes shown schematically below. Schematic representations of the structures seen in electron micrographs are shown (top). The continuous black line represents the plasma membrane, light blue represents the cytosol and the thick red line represents the clathrin coat. The dark blue dot in c represents dynamin, green crosses in d-f represent short actin filaments. d1, d2 and e1, e2 represent alternative scenarios that are not distinguished in this experiment. The bottom panel is a schematic representation showing the fluorescence of clathrin (red line), clathrin EF:epifluorescence ratio (dashed red line), dynamin (blue line) and actin (green line). The vertical dashed line indicates the time of departure. (Merrifield et al., 2002). Note: scenario d1,e1 was later ruled out by the authors (Merrifield et al., 2005).

2.7.3 Bulk Endocytosis

Bulk endocytosis is a mode of endocytosis by which nerve terminals can take up fairly large amounts of membrane at a time. First described by Takei et al. (Takei et al., 1996), it was thought to be an “emergency” compensation mechanism, utilized in times of extreme nerve activity (Royle and Lagnado, 2003). More recent evidence indicates that bulk endocytosis may be among the standard repertoire of endocytosis in nerve terminals (Clayton et al., 2007; Leenders et al., 2002; Lenzi et al., 2002) (Figure 13). Within only 1-2s of stimulation, large areas of presynaptic membrane are invaginated (Teng et al., 2007). A large vacuole-like structure forms and may remain attached to the plasma membrane for quite some time after stimulation (Gad et al., 1998). From this structure, single SVs can bud off repeatedly (Takei et al., 1996).

Because of its rapid onset, it has been suggested that bulk endocytosis, like “regular” synaptic endocytosis, might be under the control of calcineurin (Clayton et al., 2007). This would argue against the idea that it is the accumulation of SV membrane in the plasma membrane that triggers the event. The molecules that govern bulk endocytosis are still relatively unknown. Bulk endocytosis has been likened to macropinocytosis, which is controlled by rho GTPases and depends on the actin cytoskeleton (Fiorentini et al., 2001). Disruption of actin functions inhibits bulk endocytosis, as does the inhibition of PI3K (Richards et al., 2004). According to (Evans and Cousin, 2007b), dephosphins, which are involved in regular SV endocytosis, also govern bulk endocytosis. In addition, Dynamin 1-interacting protein Syndapin I has been proposed as a player (Anggono et al., 2006). The phosphorylation status of Dynamin 1 is controlled by Calcineurin (Liu et al., 1994). A strong stimulus with high Ca^{2+} influx will result in dephosphorylation of Dynamin and binding to Syndapin, which will trigger bulk endocytosis. A normal stimulus with some influx of Ca^{2+} will result in partial or no dephosphorylation of Dynamin 1 and binding to Amphiphysin, the default binding partner, which will result in regular, CME (Anggono et al., 2006). Syndapin will mediate the interaction with the cytoskeleton by binding to the Actin-nucleating protein N-WASP (Kessels and

Qualmann, 2002), and may, in addition, possess lipid tubulating activity due to its F-BAR domain.

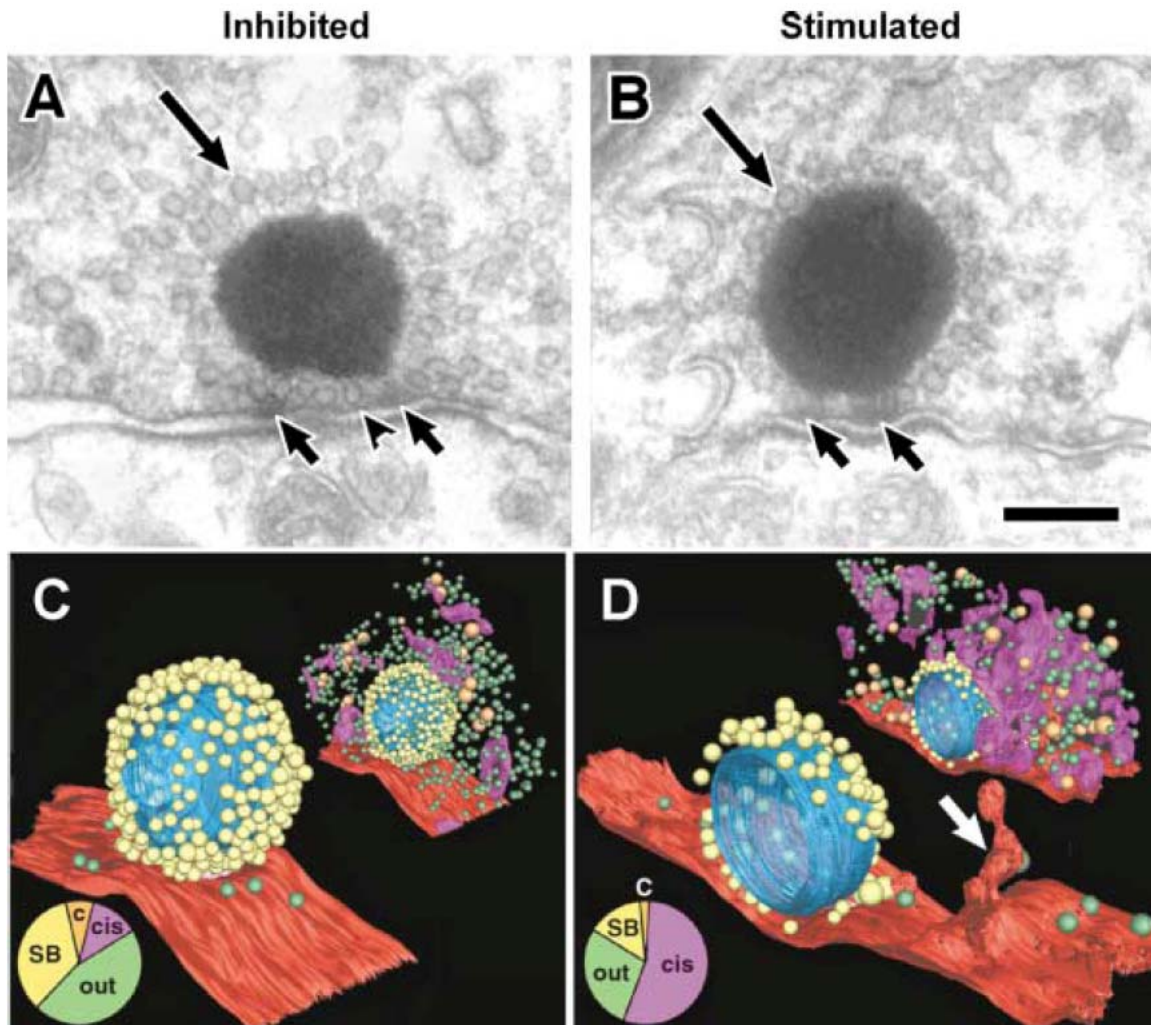


Figure 13. Membrane redistribution at a ribbon synapse after strong stimulation. A, B, TEM of synapses incubated with 0- Ca^{2+} (inhibited, A) and high- K^+ saline (stimulated, B). SVs surround the ribbons (long arrows). Short arrows show the presynaptic density. Scale bar, 200 nm. C, D, electron tomographic reconstructions of synapses exposed to 0- Ca^{2+} (C) and high- K^+ saline (D). Renderings show the plasma membrane (red) in relation to the synaptic ribbon (blue), ribbon-associated SVs (yellow) and outlying SVs (green). In D, the plasma membrane forms a tubular invagination (arrow), a hallmark of bulk endocytosis, and cisternae accumulate in the cytoplasm. Pie charts show the relative redistribution of membrane between compartments (SB, ribbon-associated SVs; out, outlying SVs; c, coated vesicles; cis, cisternae) (Lenzi et al., 2002).

2.7.4 Caveolae Endocytosis

Caveolae are smooth-surfaced flask-shaped pits with a typical diameter of 55-65nm (Yamada, 1955). Caveolin-1 is a major constituent of caveolae (Rothberg et al., 1992). Endocytosis of caveolae is Dynamin 1 and Actin-dependent, which localize to the neck of caveolae (Oh et al., 1998). Caveolae may act as stabilizers of lipid rafts at the plasma membrane, and prevent their uptake (Thomsen et al., 2002), as reduction of caveolin increases the uptake of other markers of caveolae, like AMF-R, and overexpression reduces uptake (Le et al., 2002). Few cargos of a lipid raft endocytosis pathway have been described to date. Of note, cholera toxin is taken up into cells via the GM1 receptor in a lipid-raft-dependent way (with or without caveolin), and SV40 entry may occur via a caveosome (caveolin 1 positive endosome), which is trafficked to the smooth ER (Kartenbeck et al., 1989). Caveolin- dependent endocytosis is Tyrosine-kinase- dependent (Pelkmans et al., 2002), and likely too slow to play a role in synaptic vesicle recycling, though CME and caveolae endocytosis pathways converge at the level of the sorting endosome (Tran et al., 1987). Based on the data available, it is rather unlikely that caveolae endocytosis plays a significant role in SV recycling.

2.7.5 Kiss-and-run endocytosis

In kiss-and-run endocytosis, SVs fuse, but do not collapse into the plasma membrane when they release neurotransmitter (Ceccarelli et al., 1973). This is speculated to be achieved by a tight regulation of the fusion pore, which would open transiently and then close again, to allow the SV to pinch off. Kiss-and-run endocytosis is negligible at hippocampal neurons (Granseth et al., 2006). It would appear that kiss-and-run endocytosis is a perfect explanation for the fast phase of SV recycling at ribbon synapses. Experiments with TIRF microscopy and Interference Reflection microscopy using FM dye turnover at goldfish retinal bipolar cell ribbon synapses present strong evidence that kiss-and-run endocytosis is negligible at these synapses, and that in this preparation, SVs fully collapse into the plasma membrane (Zenisek et al., 2002; Llobet et al., 2003).

2.8 The Phosphoinositide Phosphatase Synaptojanin 1

Mammals have two *synaptojanin* (*synj*) genes, *synj1* and *synj2* (Khvotchev and Sudhof, 1998a). As of the release of Zv7 of the Zebrafish Genome Sequence in July 2007, only *synj1* appears to be present in zebrafish (Obholzer and Nicolson, *unpublished observation*). According to Khvotchev et al., the N-terminus and the middle part of human Synj2 are about 55% identical to human Synj1, the C-terminus is not conserved (19%). Human Synj1 is about 78% identical to zebrafish *synj1*, human Synj2 only 52%. Both Synj1 and Synj2 have a SAC domain (described in 2.8.1) and a 5-phosphatase (5PPT) domain, (described in 2.8.2). Because of Synj's dual specificity (both 4- and 5-phosphatase) it was likened to *Janus*, the two-faced Roman god of doorways. The mammalian *synj1* is well studied. The basic assumption is that as part of the synaptic vesicle cycle, and being controlled by interacting proteins, it turns PI(4,5)P₂ into PI without releasing the intermediate PI(4)P (McPherson et al., 1996; Cremona and De Camilli, 2001). *synj2* appears to have functions that partially overlap with those of *synj1* (Nemoto et al., 2001), but has been more specifically implicated in the regulation of the cytoskeleton via Rac1 and Cdc42 in lamellipodia formation, cell migration and invasion (Malecz et al., 2000; Chuang et al., 2004).

There are two *synj1* isoforms, and both are known to be subject to alternative splicing (Khvotchev and Sudhof, 1998a; Ramjaun and McPherson, 1996). Indeed, the short isoform appears later in development and is generated by the inclusion of an exon that contains a STOP codon and truncates the long isoform. Both isoforms are co-expressed in neurons (Ramjaun and McPherson, 1996). *synj1-170* (for its apparent MW in kDa) is long and ubiquitously expressed. It functions primarily in receptor-mediated endocytosis. *synj1-145* is enriched in the mature vertebrate CNS and gets recruited to the endosome or vesicle after internalization and pinching off (Perera et al., 2006). *synj1-145* has the SAC domain, the 5PPT domain, and a proline-rich domain (PRD). Known interactors of Synj1-145 are Amphiphysin, Endophilin, DAP160/ Intersectin, and Syndapin. The long isoform, *synj1-170*, also includes NPF (EH) motifs and an AP2 binding

site. Known interactors of Synj1-170 are AP2, Amphiphysin, Endophilin, DAP160/Intersectin, Syndapin and Eps15 (Montesinos et al., 2005).

2.8.1 The SAC-Phosphatase Domain

The SAC domain was first observed in yeast Sac1p, which acts as a suppressor of the **actin** mutation, *act1-1^{ts}* (Cleves et al., 1989). A number of SAC-domain containing proteins have since been described (Hughes et al., 2000). The SAC domain is 400 amino acids long, and it contains a highly conserved CX₅R(T/S) motif, which is also present in many metal-independent protein and inositol polyphosphate phosphatases. They have a somewhat broad specificity and can dephosphorylate PI(3)P, PI(4)P and PI(3,5)P₂. SAC domains cannot attack phosphoinositide species with adjacent phosphate groups, such as PI(3,4)P₂ or PI(4,5)P₂.

2.8.2 The Inositol Polyphosphate 5-Phosphatase Domain

The catalytic domain of Inositol (poly)phosphate 5-phosphatases (5PPTs) is approximately 300 amino acids long. Two critical conserved motifs have become apparent: **GD(L/F)N(F/Y)R** and **P(A/S)(C/T)DR(I/V)(L/I)** (Blero et al., 2007). 5PPTs appear to be related to the family of AP endonucleases, and probably share their catalytic mechanism. This is relevant because it allows for precise manipulations, such as the disruption of catalytic activity or changes of substrate specificity. 5PPTs are Mg²⁺-dependent and attack the phosphate in position 5 on inositol rings of inositol phosphates. They can be further subdivided according to their enzymatic activities; however, we will only consider type II 5PPTs, like that of *synj1*. These can dephosphorylate PI(3,5)P₂, PI(1,4,5)P₃, PI(3,4,5)P₃ or PI(4,5)P₂ by removing the 5-phosphate. Most type II 5PPTs have additional protein-protein interaction- or regulatory domains that control their phosphatase activities and localization (Hughes et al., 2000).

2.8.3 Ptlins-Phosphates and Other Lipids in Endo- and Exocytosis

PIs represent only a minor fraction of membrane lipids. Yet, PI metabolism has an important role in synaptic function (Hawthorne and Pickard, 1979; Di Paolo and De Camilli, 2006). PI(4,5)P₂ is the most abundant PI in the plasma membrane, and regulates membrane trafficking (Martin et al., 2001). Interestingly, the dense core vesicles (DCVs) of neuroendocrine cells differ in their exocytosis mechanism from SVs. PI(4,5)P₂ is required for DCV exocytosis, but not for exocytosis of vesicles filled with GABA or Glutamate (Khvotchev and Sudhof, 1998b). In neuroendocrine cells, PI4-kinase and the PI5-kinase PITP α generate PI(4,5)P₂ from PI to prime DCVs at the plasma membrane (Cremona and De Camilli, 2001). Finally, the protein CAPS, which also binds to PI(4,5)P₂, has been suggested as a Ca²⁺ sensor, triggering secretion.

For SV exocytosis, effector proteins that are recruited by PI(4,5)P₂ include Synaptotagmin (Syt) and Rabphilin, DOC (differentially expressed in ovarian carcinoma) and MUNC13. Anchoring proteins for SVs at chemical synapses are Rim and Piccolo (Wang et al., 1997), (Fenster et al., 2000). Syt regulates vesicle fusion and membrane targeting in a Ca²⁺-dependent manner. Its C2B domain acts as a switch for Syt's preference for either PI(4,5)P₂ or PI(3,4,5)P₃ (Schiavo et al., 1996). MUNC13-1 primes SVs for fusion, and lack of the protein leads to a dramatic reduction in the releasable pool of glutamate (Augustin et al., 1999). MUNC18-1 binds Syt and is required for SNARE-mediated SV fusion (Matos et al., 2000).

However, recent data suggests that other lipids are involved in the regulation of SV exo- and endocytosis. Phosphatidic acid (PtdOH), diacylglycerol (DAG) and PIs have been found to be essential for vesicular transport (Simonsen et al., 2001; Odorizzi et al., 2000). Phospholipase-C turns PI(4,5)P₂ into IP₃ and DAG, which is recognized by MUNC13 and serves as a membrane signal for vesicle exocytosis. SVs contain an unusually high amount of cholesterol (Takamori et al., 2006). Synaptophysin (Syp), and Syt form cholesterol-dependent complexes with synaptic membranes (Jia et al., 2006). This is also

relevant for SV endocytosis, in which the SV protein complement can be preserved (Murthy and Stevens, 1998; Aravanis et al., 2003).

A major pathway for SV endocytosis is driven by a specialized CME (Gad et al., 2000). PI(4,5)P₂ function in the endocytic pathway involves adaptor proteins AP-2 and AP180 for clathrin coat assembly in a PI(4,5)P₂- dependent manner (Jost et al., 1998; Gaidarov and Keen, 1999). AP-2 binds to PI(4,5)P₂ via its α -adapatin subunit. AP180 binds to PI(4,5)P₂ via its N-terminal ENTH (Epsin **N**-**T**erminal **H**omology)-like domain. ENTH domains are present in Epsin, AP180 and CALM (C**l**athrin **A**ssembly **L**ymphoid **M**yeloid leukemia) proteins. During CME, ENTH domains assist in the invagination of the plasma membrane through PI(4,5)P₂ interactions, and the clathrin coat connects to this scaffold. Because AP180, CALM and related proteins have an N-terminal domain with a distinct fold, this domain was also named the ANTH domain (A**P**180 **N**-terminal **H**omology domain). ENTH/ANTH domains are found in scaffolding proteins.

As in neuroendocrine cells, PI4-kinase and the PI5-kinase P1TP generate PI(4,5)P₂ at the plasma membrane, prior to SV endocytosis. Indeed, the turnover of PI(4,5)P₂ correlates with synaptic activity (Di Paolo et al., 2004) (Figure 14).

The formation of clathrin-coated pits can be completely disrupted by the depletion of PI(4,5)P₂ from the plasma membrane (Zoncu et al., 2007). Amphiphysin and Endophilin can bind to PIs, and Amphiphysin interacts with Clathrin. In addition, Amphiphysin and Endophilin also bind to Dynamin, which in turn can bind to PI(4,5)P₂. The affinity of Dynamin to PI(4,5)P₂ is abrogated when Dynamin is phosphorylated by Cdk5, and enabled by Calcineurin-mediated dephosphorylation. The binding of Dynamin to PI(4,5)P₂ is crucial for endocytosis (Vallis et al., 1999). According to (Perera et al., 2006), Synj1-170 is recruited to the plasma membrane during early clathrin-coated pit (CCP) formation. This appears to be independent from Endophilin, and mediated through interaction with receptors, EPS15 or AP2. Inactivation of the 5PPT domain of Synj1-170 arrests CCP formation, which lead to the idea that Synj1 function may be required for coat maturation (Perera et al., 2006). Synj1-145 is recruited in a burst by Endophilin to late CCPs, just prior to vesicle fission. Its role is the

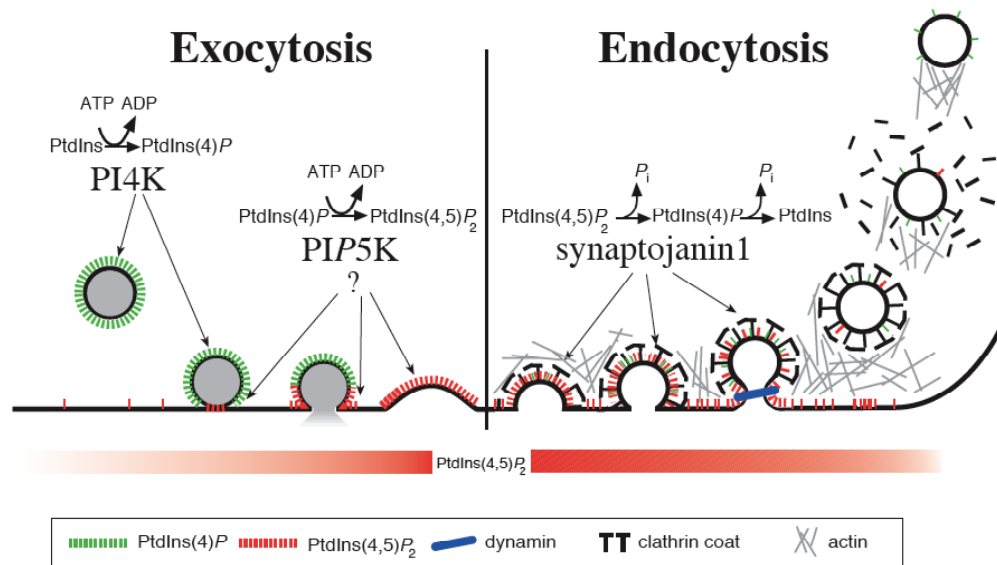


Figure 14. A putative link between membrane traffic at the synapse and PI(4,5)P₂ synthesis/ dephosphorylation. The model proposes a PI cycle nested within the SV cycle. PI4-K, PI 4-kinase; PIP5-K, PIP-5 kinase (Cremona and De Camilli, 2001).

dephosphorylation of PI(4,5)P₂ in the endocytosed vesicle membrane as a step in the shedding of the clathrin coat. PI(4,5)P₂ must be degraded by Synj1 for scission of clathrin-coated vesicles (Perera et al., 2006). The conversion of PI(4,5)P₂ to PI(4)P in the vesicle membrane could allow for the recruitment of auxilin/gak via its PI(4)P-binding domain (Massol et al., 2006), and is required for uncoating (Lee et al., 2005). Synj1 can also hydrolyze PI(3,4,5)P₃, but the purpose of this is unclear. 3-phosphorylated inositol lipids play important roles in regulating trafficking and protein sorting at the endosomal compartment. For example, PI(3)P populates the endosomal systems, specifically the early endosomes (EE). There also appears to be a role for the lipid kinase PI-3K C2α in clathrin-dependent budding reactions (Domin et al., 2000), given the C2B-domain switch in Syt, and the high affinity of AP-2 towards PI(3,4,5)P₃. In conclusion, PI- and other lipids are present at every step in SV turnover and recycling, and the fine control over these lipids may determine the pathway into which SVs are sorted. This could have a profound effect on the efficiency and particularities of SV recycling at specific kinds of synapses.

2.8.4 *synптоjanin1* as a Regulator of Endocytosis and the Cytoskeleton

Synj1 occupies a key position in the regulation of endocytosis and cytoskeletal dynamics (Figure 15). PIs can promote actin nucleation by recruiting WASP Rho-GTPase family members (Rohatgi et al., 1999) and actin nucleation plays a critical role in endocytosis (Kaksonen et al., 2006). Synj1 function indirectly depends on Ca^{2+} , and serves to control the PI levels at the plasma membrane and in the endocytotic cycle. Synj1 interfaces with both a PI- and, through ARF proteins, a GTPase cycle that may act as an amplifier to *synj1*'s actions, or to which Synj1 might be a negative regulator.

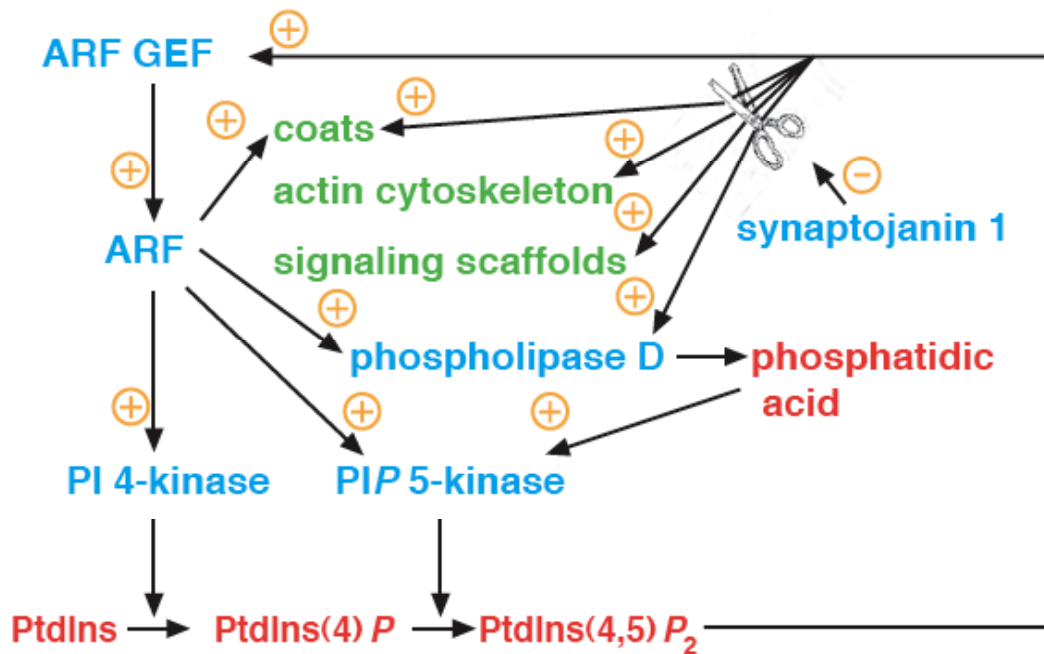


Figure 15. Diagram illustrating a positive feedback loop through which activation of the GTPase ARF leads to enhanced PIP₂ generation, which in turn further activates ARF (Cremona and De Camilli, 2001). Synj1 acts as a major “OFF” switch in this loop.

2.8.5 Consequences of a *synaptojanin1* Loss

Deletion of all three yeast *synaptojanin*-like (Sjl) proteins causes lethality. This lethality is a consequence of a dramatic increase of PI(4,5)P₂ levels (Stefan et al., 2002). The other observed phenotypes in Sjl knockouts are defective actin cytoskeleton, endocytosis and protein sorting from the Golgi to the vacuole. The yeast *synaptojanins* had also been found to be important in cellular events that require clathrin and have been shown to interact genetically with clathrin (Bensen et al., 2000). *synj1* mutants have been reported to show slowed endocytosis in *C.elegans*, drosophila and mice (Verstreken et al., 2003; Dickman et al., 2005), depletion of SVs, accumulation of clathrin-coated vesicles (see Figure 16), and aggregation of cortical actin (Cremona et al., 1999; Harris et al., 2000).

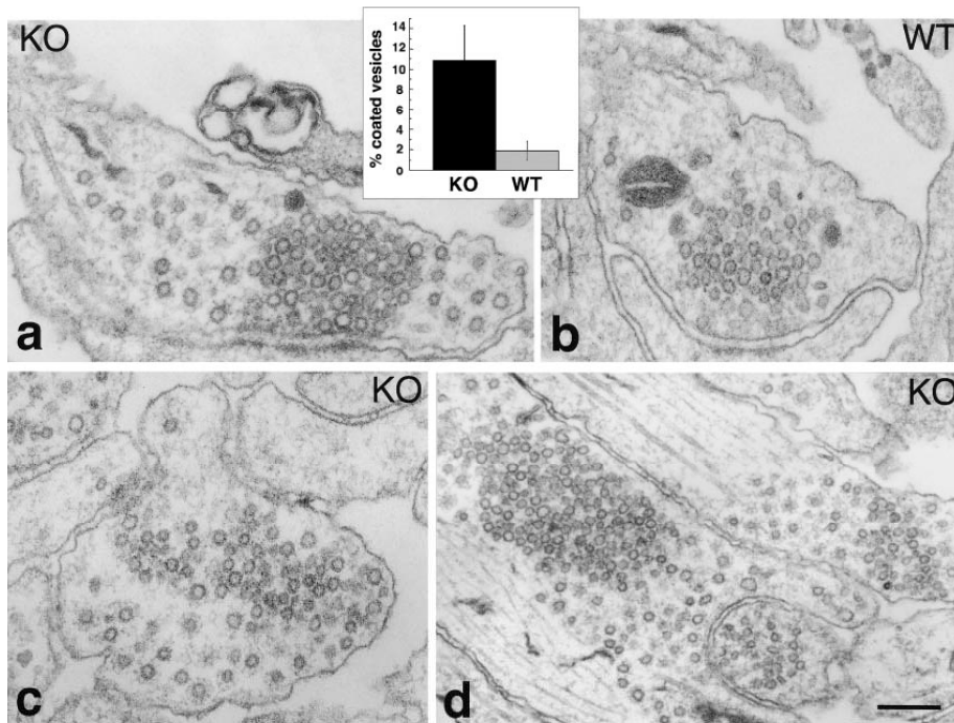


Figure 16. Accumulation of clathrin-coated vesicles in nerve terminals of *SYNJ1* knockout (KO) animals. (a-d) Electron microscopy of synapses in 20-day-old cultures from cortical neurons of KO (a, c, and d) and wild-type (WT) (b) mice. In synapses from knockout animals, the typical cluster of tightly packed SVs is surrounded by less tightly packed SVs that appear suspended in a cytoskeletal matrix. Bar, a, b: 160 nm; c, 170 nm; d, 230 nm. Inset, morphometric analysis of coated SVs versus total SVs in cortical neurons. Data represent means \pm SD, $n = 5$, $p < 0.01$ (Cremona et al., 1999).

Surprisingly, *synj1* appears to be largely expendable for household CME (Cremona and De Camilli, 2001) (Figure 17). This may be due to functional overlap with *synj2* (in mammals), or other lipid phosphatases. At synapses, *synj1* seems to be required for proper functionality. In vertebrates, like in yeast, deletion of *synj1* is lethal, but only post-natally. *synja1*^{-/-} mice show weakness, ataxia, seizures and die within 2 weeks (Cremona et al., 1999). These mice also had increased levels of PI(4,5)P₂ in the brain. *synj1*-deficient “*nrc*” (*no optokinetic response c*) zebrafish have visual defects and floating synaptic ribbons in photoreceptors, but not in bipolar cells (Allwardt et al., 2001; Van Epps et al., 2004). For drosophila, an increased number of boutons at the NMJ has been reported (Dickman et al., 2006). Drosophila mutants also show strong depression of neurotransmitter release at high frequency (10Hz) stimulation, but not at 1Hz (Verstreken et al., 2003). Loss of Endophilin causes similar, but not identical defects (Schuske et al., 2003), because Synj1 function relies on its interaction with Endophilin for recruitment (de Heuvel et al., 1997). It has recently been reported, that inactivation of the 5PPT domain of Synj1-170 leads to the accumulation of clathrin-coated pits at the plasma membrane, or the arrest of endocytosis at this stage (Perera et al., 2006). Many consequences of a loss of *synj1* have been described, but it seems *synj1* may have yet more parts to play.

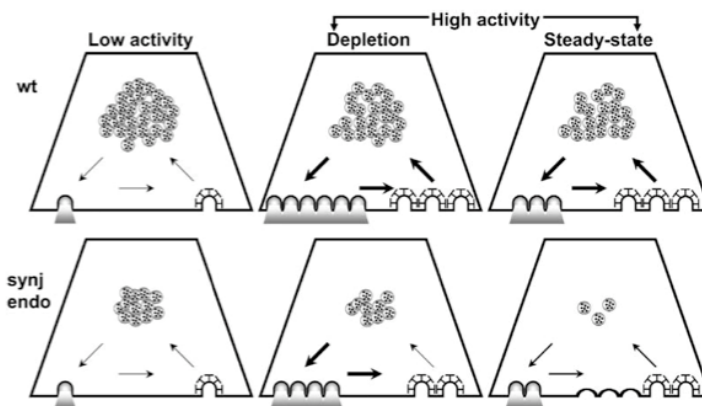


Figure 17. A slow classical endocytosis pathway can explain the endocytic defects in *synj* and *endo* mutants (Dickman et al., 2005). Under conditions of low activity (left panels), a functional SV pool and an EJP with normal amplitude can be maintained in both WT and mutant terminals.

Figure 17.ctd. High-frequency stimulation increases the rate of exocytosis (center and right panels), but, in WT terminals, endocytic rates increase to maintain a functional SV pool of nearly prestimulus size. In *synj/endo* mutants, however, endocytosis rates cannot adequately increase. The SV pool is depleted, and EJP amplitude declines. A new steady state depends upon the balance of exo- and endocytosis rates. The thickness of the arrows represents the rates at which SVs are cycled.

t
l
t
-
s
-

3 Results

3.1 Part 1: Identification and Characterization of *synptojanin1* in Zebrafish

The *comet* strain of zebrafish was isolated during the 2000 Tubingen screen for ENU mutants, a large-scale screen for behavioral and other mutations (Nicolson, unpublished results). Zebrafish that are homozygous for *comet*, hereafter called “*comet* (mutant) larvae”, die around day 8 post fertilization. Death likely occurs due to uncoordinated locomotion, which results in a failure to feed, and failure to inflate their swimbladders. *comet* mutant larval HCs have normal hair-bundle morphology and show wild-type levels of FM 1-43 uptake (unpublished results), indicative of normal mechanotransduction (Gale et al., 2001; Seiler and Nicolson, 1999). *comet* mutant larvae of all three alleles exhibit a normal touch-response, and react to acoustic stimuli such as tapping on the petri dish. However, they display a balance defect that is observable and becomes more obvious over time when mutant larvae are swirled in water, suggesting fatigability. Due to the striking similarity of the *comet* phenotype with that of the *nrc* mutant (S.Brockhoff, personal communication), we performed complementation analysis between the strains and find failure to complement. We sequenced three alleles of the *comet* gene, and report here that it encodes *synptojanin 1* (*synj1*).

The “*nrc*” *synj1* mutant zebrafish line has been previously described by (Allwardt et al., 2001) and (Van Epps et al., 2004). *nrc* mapped to linkage group 10, between the markers EST fb79h03 and Z7504. The genomic lesion of *nrc* is a C-T transition, converting Arg499 (CGA) to STOP (TGA). The premature termination codon (PTC) leads to a truncation of Synj1 after the SAC domain. This has the same effect as a knockdown of the whole protein by a translational morpholino (Van Epps et al., 2004). In the same study, the *nrc* mutant shows a marked decrease in the processing capability of both PI(4)P and PI(4,5)P₂, which provides evidence for a complete loss of function, or *functional null* phenotype. Due to the comparable balance defect (not shown) and failure of *nrc* to complement *comet*, our basic assumption is that the *comet* alleles are also *functionally null*.

3.1.1 Positional Cloning of *synaptojanin1*

We sequenced cDNA and genomic DNA from three alleles of *comet/synaptojanin1*: IG459, JV039 and HT039 (Figure 18). It is important to note again that homozygous mutant larvae of all three alleles display identical behavioral phenotypes. Sequencing IG459, we detect a GT>GA splice site transversion mutation that results in the inactivation of the donor splice site of exon2 – intron3, and thereby leads to the omission of exon2 from the processed *synj1* mRNA. Since exon2 contains the start-of-translation codon (ATG), we assume that no Synj1 protein product is made in the mutant. In the case of allele JV039, we detect a C>T transition mutation in coding sequence bp 886, resulting in a premature termination codon (PTC) after amino acid 296. This should lead to the truncation of Synj1 protein product after amino acid 296 for all known transcripts of this gene. We detect a G>A transition mutation in HT039 (bp 2828), this time resulting in a PTC and truncation of Synj1 protein product after amino acid 940 for all known transcripts of this gene.

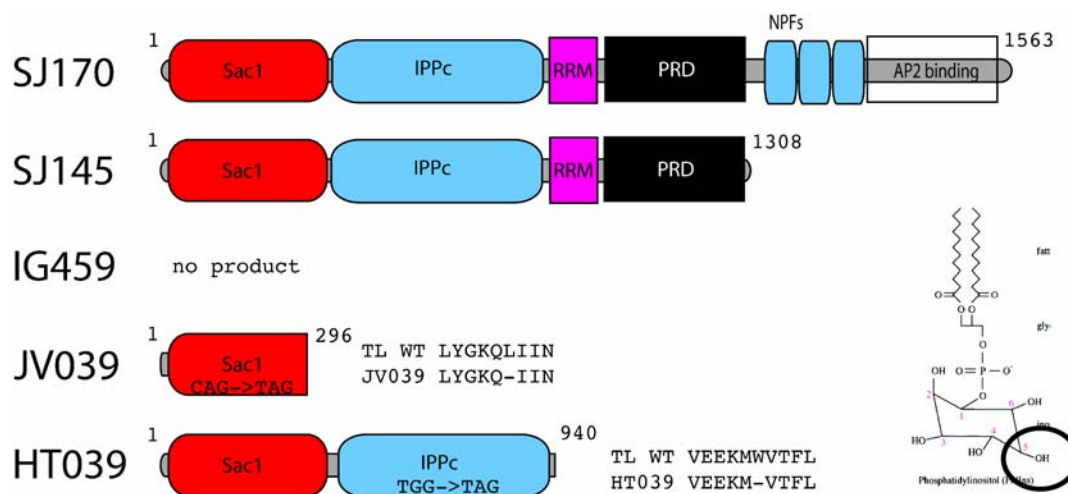


Figure 18. Splice variants and *comet* alleles of *synj1*. SJ170 is the long, ubiquitous variant of *synj1*. SJ145 is enriched in the nervous system. IG459 *synj1* mRNA lacks exon2 with the START codon. JV039 causes an early truncation within the SAC domain. HT039 causes an early truncation after the 5PPT (IPPc) domain. Inlay: PtdIns with circle marking position 5, point of attack for the 5PPT/IPPc domain, which dephosphorylates PI(4,5)P₂, creating PI4P.

3.1.2 *In situ* Expression Analysis of *synптоjanin1*

While it has been shown that *synj1* is expressed in the zebrafish brain and retina (Van Epps et al., 2004), we performed *in situ* analysis on 48- 72 hpf larvae to show the expression of *synj1* in HCs to obtain clues to the origin of the balance defect in *comet* larvae. Indeed, *synj1* is expressed in HCs of the inner ear (Figure 19). This is interesting, because even though brain function is likely impaired in *comet* mutant larvae, the vestibular sensory information sent to the brain must first be encoded by HCs. In addition, our sections reveal higher resolution of expression in the retina compared to previously published results (see above), especially in photoreceptors and between the inner plexiform layer and the ganglion cell layer. We also observe *synj1* expression in the brain.

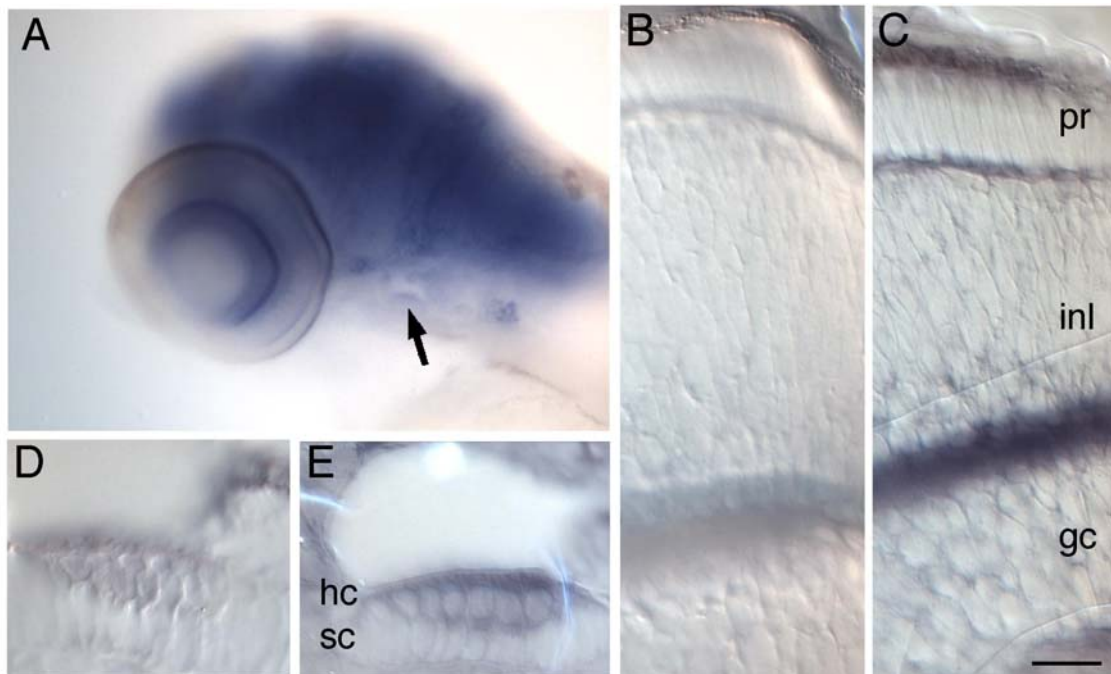


Figure 19. Whole mount *in situ* hybridisation of 72 hpf zebrafish larvae for *synj1*. *A*, Overview shows labeling of the brain, retina, several ganglia including the posterior lateral line ganglion, and the ear (arrow). *B*, Section of the retina, negative (sense) control. *C*, Section of the retina with antisense probe. pr= photo receptor, inl= inner plexiform layer, gc= ganglion cells. Note: labeling of basal ends of bipolar cells (inl). *D*, macula HCs (negative control). *E*, macula HCs with antisense probe. hc= hair cell, sc= supporting cell.

3.1.3 Cloning of the *myosin6b* Promoter for Hair Cell Specific Expression

In order to allow for HC-specific expression of transgenes, we cloned a total of 6.5kb of the zebrafish *myosin6b* promoter (Kappler et al., 2004). To this end, we first performed a 5'RACE on *myosin6b* to obtain the full 5'UTR sequence. We compared this sequence to the ZV3 assembly of the zebrafish genome project (www.sanger.ac.uk/zebrafish) to identify intronic sequences. We find that exon2 contained the ATG of *myosin6b*, and that intron1-2 spans about 20kb. Using this data, we analyzed the DNA 30kb upstream of the start of translation of *myosin6b* using public domain software for promoter prediction and transcription factor binding site identification available on the internet (*transfac*, *promoterscan*, etc.). We identified several regions within intron1-2 and upstream of exon1 that were repeatedly predicted to be important using high cutoff values for stringent conditions. We cloned 1534bp of intron1-2 and 5109bp of upstream genomic DNA (Figure 20). When fused and inserted into a pEGFP-N1 backbone (Clontech), the promoter fragment gives rise to high levels of expression in HCs.

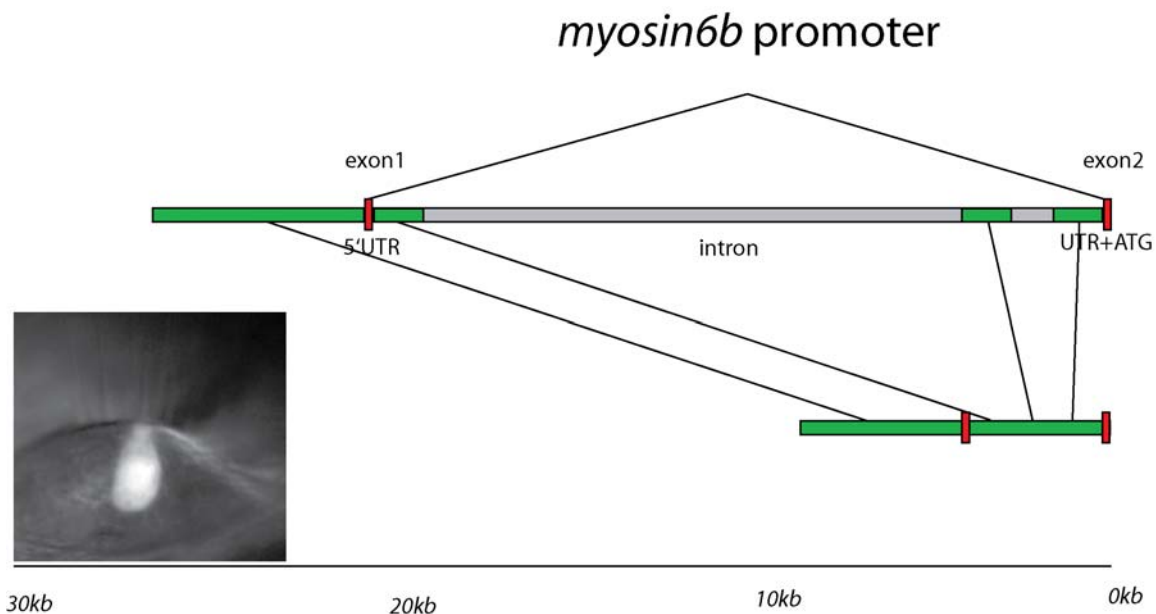


Figure 20. Cloning of the *myosin6b* promoter, and HC-specific expression pattern (inset). 1534bp of intron1-2 were cloned in three fragments from genomic DNA and fused with 5109bp of exon1-upstream genomic DNA to obtain a functional HC promoter.

3.1.4 Cellular Localization of *synaptojanin1-egfp*

We cloned full-length cDNAs for *synj1-145* and *synj1-170* and fused them with a C-terminal EGFP tag in our *myo6b* promoter HC expression vector. We then transiently expressed these constructs in zebrafish larvae, and monitored the cellular localization of the fusion proteins in live animals (Figure 21).

Both Synj1-145-EGFP and Synj1-170-EGFP are diffusely distributed throughout the HC cytosol, but occasionally appear to form clusters. Synj1-170-EGFP appears to be less diffuse, more clustered, and enriched at the basal end of the HC. Perera et al. have shown that Synaptojanin 170 is present at the site CCP internalization before Synj1-145 is recruited to budding clathrin-coated vesicles by Endophilin in order to help shed the clathrin coat after scission (Perera et al., 2006). It can also be recruited to sites of endocytosis by Endophilin. We find that, according to our fluorescence microscopy data from live and fixed HCs, C-terminal tagging of either Synj1 variant with EGFP does not appear to mislocalize the protein (Figure 21A, B). Furthermore, we do not see colocalization of Synj1 and Ribeye-a, a ribbon synapse marker that we tag with mRFP (Figure 21C). Also, Synj1 fusion proteins can be expressed in zebrafish HCs without apparent adverse consequences: transfected larvae behave normally (data not shown).

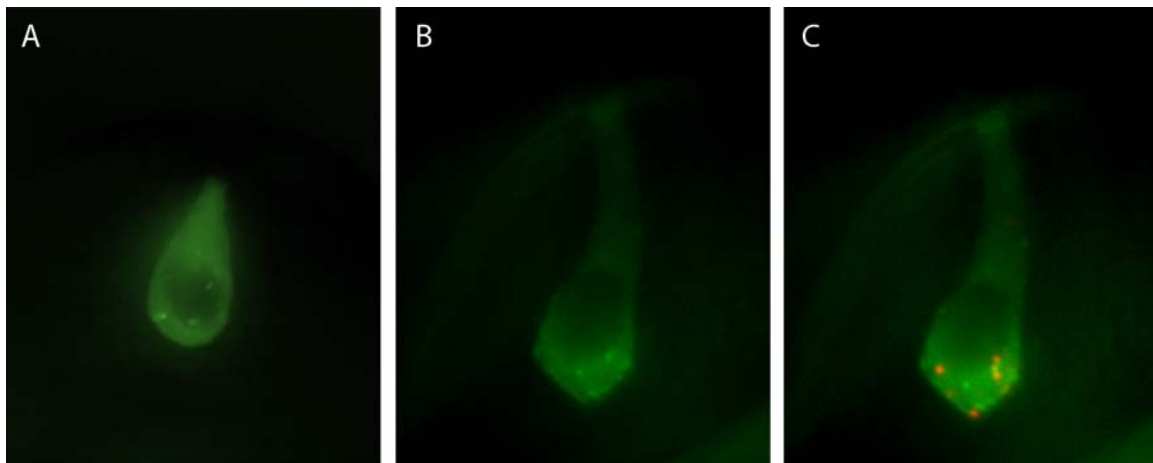


Figure 21. Cellular localization of Synaptojanin1-EGFP isoforms in HCs. Both Synaptojanin 145 and 170 localize to the cytosol, and cluster near the plasma membrane. A, *myo6: synj1-145-egfp* in HC B, *myo6:synj1-170-egfp* in HC. C, *myo6:synj1-170-egfp* and *myo6:ribeye-a-mRFP* coexpression.

3.1.5 Cellular Localization of Markers of the SV cycle in *comet* Mutants

We hypothesize that a loss of *synj1* activity may, due to slowed endocytosis, lead to a redistribution of proteins from the SV pool to the plasma membrane. We analyzed the distribution of the putative SV markers Otoferlin A (Roux et al., 2006) and Vglut3 in wild-type and in mutant *comet* HC after stimulation using immunohistochemistry, and the distribution of Clathrin light chain A (CTLA) and Vglut1 by transient expression of *myo6b:ctla-egfp* and *myo6b:vglut1-egfp*, respectively. We find that the gross cellular distribution of SV markers is unaffected in stimulated day 5 (d5) *comet* mutant vs. WT larvae (Figure 22). Alternatively, the effect might be too subtle to observe using our protocol. While potential overexpression of Vglut1 or the addition of an EGFP moiety may mask differential distribution, Vglut3 is detected by antibody labeling and should not suffer from this caveat.

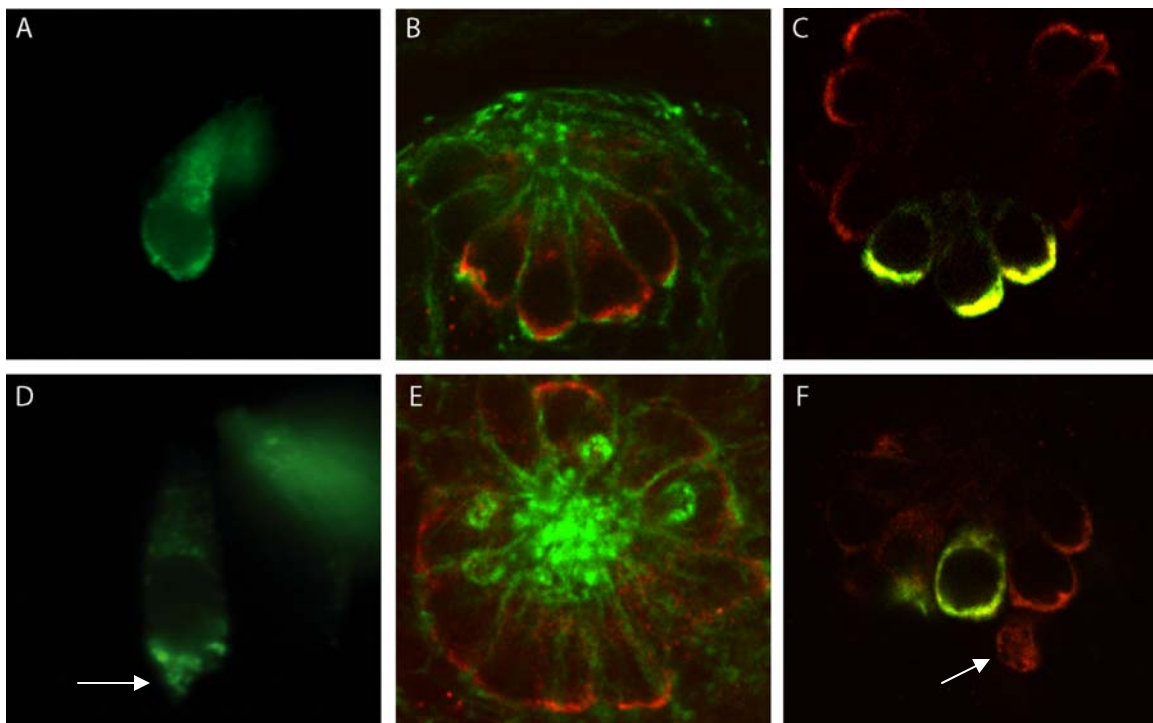


Figure 22. Cellular localization of SV markers in *comet* mutants. The gross cellular distribution of SV and SV cycle markers is unaffected in stimulated d5 *comet* vs. WT larvae. A, WT; *myo6b:ctla-egfp*. B, WT; red: Otoferlin, green: actin. C, WT HC; green: *myo6b:vglut1-egfp*, red: Vglut3 D, *comet* mut; *myo6b:ctla-egfp*. E, *comet* mut; red: Otoferlin, green: actin. F, *comet* mut; green: *myo6b:vglut1-egfp*, red: Vglut3. arrows: blebs

3.1.6 Loss of *synaptojanin1* Results in No Change in HC Ribbon Numbers, Which Are Indicators of Synapse Formation

During development, vestibular HCs undergo synaptic refinement. When a ribbon synapse is established in mouse HCs, two or more ribbons may be present and juxtaposed to each afferent bouton. When the synapse matures, the number of ribbon bodies per active zone is reduced to one (Johnson et al., 2005). The zebrafish vestibular system is fully functional at d5, and the *comet/synj1* mutant behavioral phenotype is apparent at that time.

To examine the possibility of an improper synapse refinement like that observed in endocytosis mutants at the drosophila NMJ (Dickman et al., 2006), or the appearance of floating ribbons like in the *nrc* mutant photoreceptors (Allwardt et al., 2001; VanEpps et al., 2004), we raised an antibody against the N-terminus of Ribeye-a and -b to detect synaptic ribbons in WT and *comet/synj1* mutant HCs. To outline HCs with a genetic marker, we crossed the *brn3c:gap43-egfp* line into the JV039 *comet* allele. Using immunofluorescence, we counted an average of about 3 ribbons per lateral line HC in both d5 wild-type and *comet/synj1* mutant larvae (Figure 23).

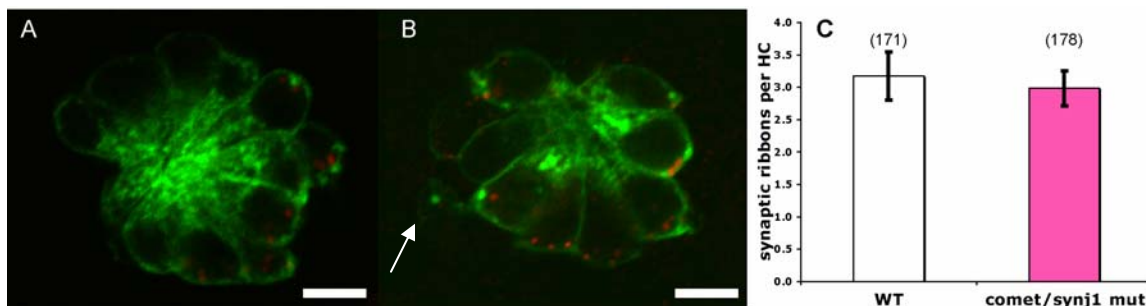


Figure 23. Synaptic ribbon quantification in d5 *comet/synj1* WT vs. mutants by wholemount antibody labeling. *brn3c:GAP43gfp/comet* larvae were labeled for Ribeye-b on d5. *A*, WT neuromast expressing *brn3c:GAP43gfp* (green) and labeled for Ribeye-b (red). *B*, *comet/synj1* mutant neuromast expressing *brn3c:GAP43gfp* (green) and labeled for Ribeye-b (red). *C*, bar diagram showing the average number of synaptic ribbons per HC (mut: 3.2 ± 0.37 , $n = 178$ cells, 6 larvae observed. WT: 3.0 ± 0.27 , $n = 171$ cells, 6 larvae observed.). scale bar: 3 μ m. arrow: bleb. Error bars denote standard deviation. Number of total larvae observed in parentheses.

3.1.7 Morpholino-Mediated Knockdown of *synj1-145* Generates a Fatiguability-of-Balance Phenotype

We speculate that the balance defect in *comet/synj1* mutant larvae is caused by insufficient vesicle recycling. There are two *synj1* isoforms, and both are known to be subject to alternative splicing (Khvotchev and Sudhof, 1998a; Ramjaun and McPherson, 1996). Both isoforms are co-expressed in neurons (Ramjaun and McPherson, 1996). *synj1-170* (for its apparent MW in kDa) is long and ubiquitously expressed and functions primarily in receptor-mediated endocytosis. *synj1-145* is enriched in the mature vertebrate CNS and is recruited at a late stage of clathrin-coated pit formation (Perera et al., 2006). The 145kD isoform is generated by the insertion of one exon (exon30) into the *synj1* transcript, which truncates the long isoform, *synj1-170* (Figure 24 A). We used a morpholino (145MO) against the splice donor site of exon 30 (blue arrow, Figure 24 A) to suppress the generation of *synj1-145* in developing WT larvae and to determine if *synj1-145* specifically is needed for efficient HC SV recycling. As a positive control, we injected the translation-blocking morpholino (atg MO) (Van Epps et al., 2004), a sense control morpholino, and a combination of atg MO and 145MO, and tested for balance at 96 hpf. After the assay, we confirmed 145MO action by RT-PCR from mRNA isolated from the tested larvae (Figure 24B).

We find that at high concentrations, the atg MO phenocopies the *comet* mutant with some efficacy, and causes a balance defect in $48 \pm 9.5\%$ of injected larvae after extended (up to 30 minutes) stimulation (Figure 24 C). The 145MO alone does not phenocopy *comet*, but causes $24 \pm 2.7\%$ of injected larvae to fatigue and lose balance in a behavioral test. The atg MO in conjunction with the 145MO has about the same effect as atg MO alone ($52 \pm 4.4\%$). We conclude that *synj1-145* is likely not specifically needed for HC function, and that *synj1-170* can compensate unless the stimulation is extended. Alternatively, the current model of splicing (Ramjaun and McPherson, 1996) is incorrect and *synj1-145* splices to a different exon/UTR than exon 31, resulting in functional Synj1-145 protein. However, we performed a 3'RACE with cDNA from 145MO larvae and do not detect such a 3'UTR (data not shown).

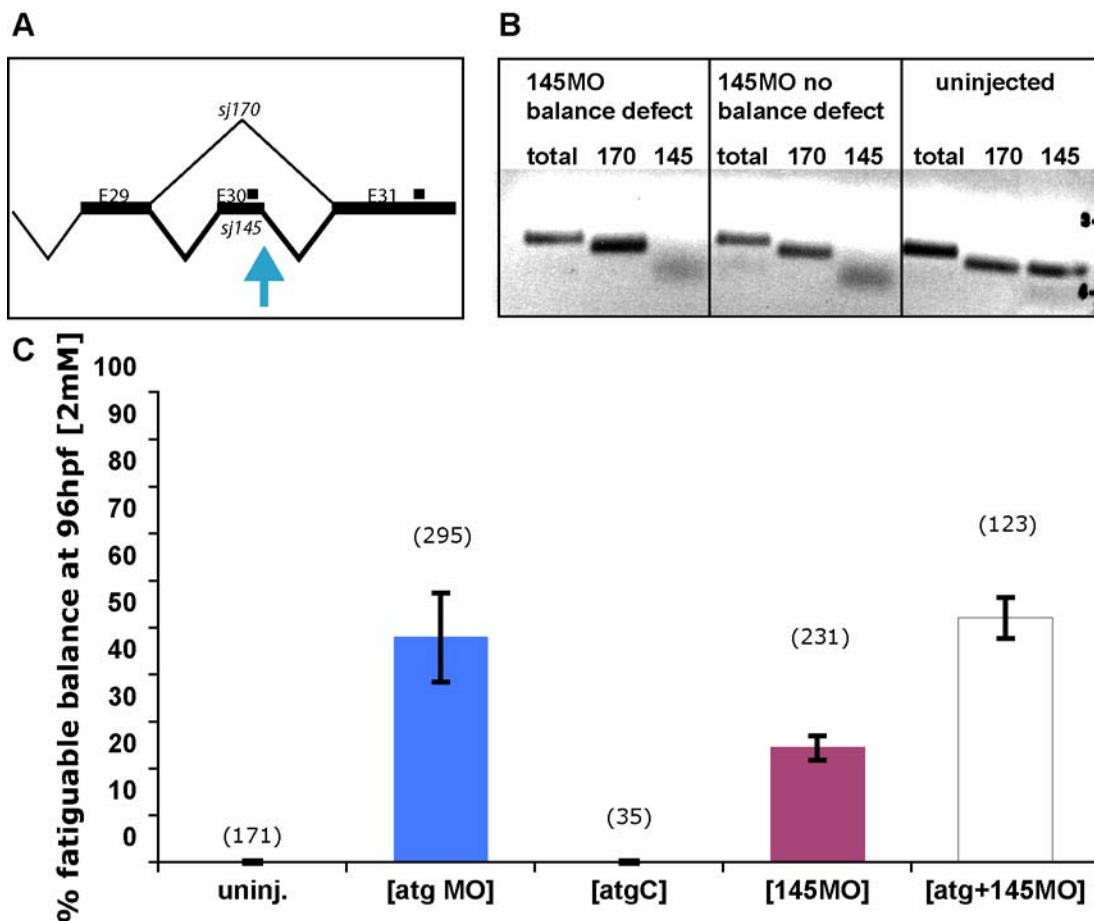


Figure 24. Morpholino-mediated knockdown of total *synj1* versus the short isoform *synj1-145*. **A**, Diagram of last three *synj1* exons and their splice sites. Alternative splicing gives rise to either *synj1-145* or *synj1-170*, depending on the inclusion of exon30. Black boxes mark a stop codons. Blue arrow marks morpholino target site, the donor splice site of *synj1* exon 30. **B**, 1.5% agarose gel showing the RT-PCR control amplification of total *synj1*, *synj1-170* and *synj1-145* after mRNA isolation from observed larvae after the behavioral assay. To achieve splice variant specificity, *synj1-170* forward primer and *synj1-145* PCR primers are exon-spanning. Due to lack of template, *synj1-145* PCR primers generated some primer dimer. **C**, Bar graph showing a failure of balance (in % larvae observed) in the extended balance test at 96 hpf after the injection of 2 mM or 2nL morpholino. uninjected: 0 ± 0%, atg MO: 48 ± 9.5%, atgC: 0 ± 0%, 145MO: 24 ± 2.7%, and atg MO+ 145MO: 52 ± 4.4%. Error bars denote standard deviation. Number of larvae observed in parentheses.

3.1.8 Morpholino-Mediated Knockdown of *synj1-145* Induces Compensatory Overexpression of *synj1* and Forces Overexpression of *synj1-170*

To further characterize the effects of 145MO splice suppression, we analyzed transcript levels of total *synj1* and *synj1-170* versus *synj1-145* in uninjected versus 145MO-injected larvae at 96 hpf using real-time quantitative PCR (RT-qPCR). We expect to see suppression of *synj1-145* due to morpholino action, and an increase of *synj1-170* copy number as a result. While we detect a modest increase of *synj1-170* (about 2.1 ± 0.5 fold, Figure 25) and a complete suppression of *synj1-145* mRNA, we see a drastic increase of total *synj1* mRNA (6.8 ± 2.1 fold), perhaps a result of compensatory up-regulation as a response to the lack of functional *synj1-145*.

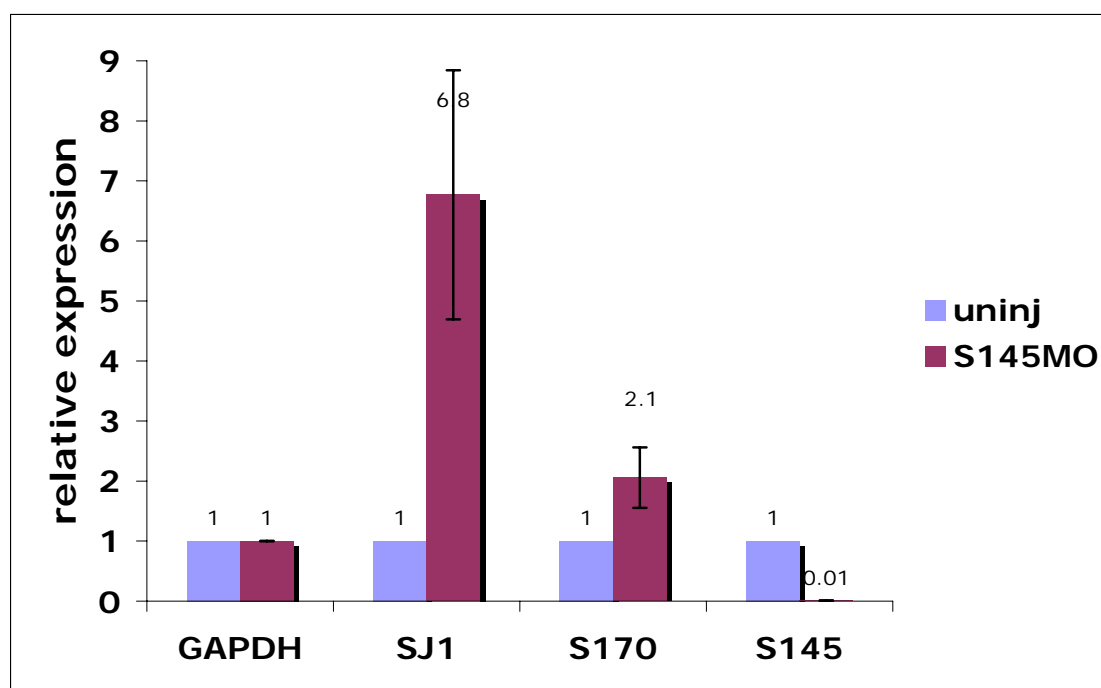


Figure 25. Quantitation of *synj1* mRNA transcript by RT-qPCR in 145MO-injected larvae by splice variant. *gapdh* was used as internal standard. All expression levels are in comparison to the uninjected control. *synj1* transcript levels were 6.8 ± 2.1 fold of the control, *synj1-170* 2.1 ± 0.5 fold, and *synj1-145* was barely detected in 145MO-injected larvae (0.01 ± 0.0). Each transcript was tested in triplicates per dilution over a dilution series spanning 3 orders of magnitude, for a total of 9 reactions per biological replicate. 2 biological replicates were assayed. Data values are the average of all 18 reactions, the standard deviation between biological replicates was used to calculate error bars.

3.2 “Blebbing” as a Novel Phenotype in *comet* Mutant Hair Cells

A previous study reported capacitance measurements that showed that membrane turnover in HCs can reach approximately 1.4 times the amount of the initial cell surface within several seconds of maximal stimulation (Schnee et al., 2005). In a wild-type HC, the rate of endocytosis approaches, but does not quite match, that of exocytosis. Therefore, in *comet/synj1*, we expect slowed endocytosis, which might lead to an accumulation of membrane and HC swelling.

Physiologically, *synj1* mutants have been linked to blindness (Allwardt et al., 2001; Van Epps et al., 2004) and motor fatigue (Verstreken et al., 2003; Dickman et al., 2005). Ultrastructurally, loss of *synj1* was connected to slowed endocytosis, an accumulation of endocytic intermediates, a smaller synaptic vesicle (reserve) pool, an increase in the number of clathrin-coated vesicles, detached ribbons in photoreceptors, but not in bipolar cells (Allwardt et al., 2001; Van Epps et al., 2004) or HCs (this study), and aggregation of the actin cytoskeleton. A previously undescribed phenotype that we observe in HCs is the looping out, or expulsion of basolateral membrane, much like a bud, or sometimes a tube or spill. At times, these structures appear to be completely detached from the cell body, other times, they are clearly connected to the soma. We call this phenotype “blebbing.”

3.2.1 Detection of Membrane Blebs in *comet* by Labeling With FM1-43, *plcδ-PH-egfp*, *myo6b:egfp* and *brn3c:gap43ΔC-gfp*

When we transiently express *myo6:plc-PH-egfp* to compare PI(4,5)P₂ levels in HCs between WT and *comet/synj1* mutant HC, we do not observe any obvious differences. What we find instead is that labeling of HC plasma membranes reveals basolateral blebs in *comet* mutant HCs (Figure 26). We confirmed this previously unobserved phenotype by expressing either soluble GFP or another membrane label, GAP43 membrane domain fused to GFP. Expressing soluble GFP also reveals blebs in HCs and supplies evidence that blebbing was not simply caused by interfering with the plasma membrane. By using the soluble dye, FM1-43, we ruled out that blebbing was an artifact of general exogenous protein expression or transient transfection.

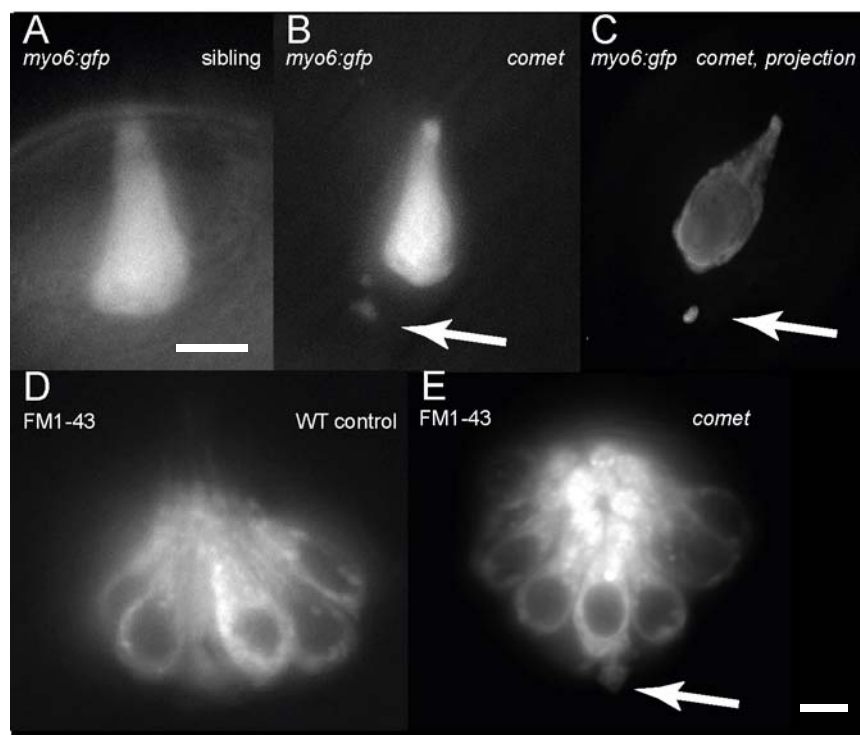


Figure 26. *comet/synj1* mutant HCs display a “blebbing” phenotype. *A*, wild-type HC transiently expressing soluble GFP. *B*, *comet* HC transiently expressing soluble GFP. *C*, *comet* HC transiently expressing soluble GFP (max intensity projection). *D*, wild-type neuromast HCs loaded with FM1-43. *E*, *comet* neuromast HCs loaded with FM1-43. Blebs are indicated by arrows. Scale bar, a-c and d, e, 3 μm.

3.2.2 Blebbing in *comet* Mutants is Activity-Dependent

synja/endo mutant cells show impaired endocytosis in drosophila (Dickman et al., 2005). We hypothesize that an imbalance between exo- and endocytosis promotes blebbing in HCs. We attempt to uncouple exo- and endocytosis by stimulating HCs for 30 minutes (Figure 27). When we stimulate the vestibular and lateral line HCs of d5 to 6 larvae on a rotator at 8 rpm for 30 minutes at room temperature, blebbing is barely observed in *comet/synj1* siblings (6.8 ± 3.5 vs. 7.7 ± 4.0). Blebbing is clearly observed in *comet/synj1* mutants and even more pronounced after stimulation (26.3 ± 7.5 vs. 42.6 ± 24.4). *gemini/cav1.3* mutants, which have no synaptic transmission (Sidi et al., 2004), are comparable to wild-type siblings (5.4 ± 4.0 vs. 5.1 ± 5.5). After crossing the *comet/synj1* mutation into *gemini/cav1.3* background (compound), blebbing is suppressed (6.1 ± 6.1 vs. 6.0 ± 4.9).

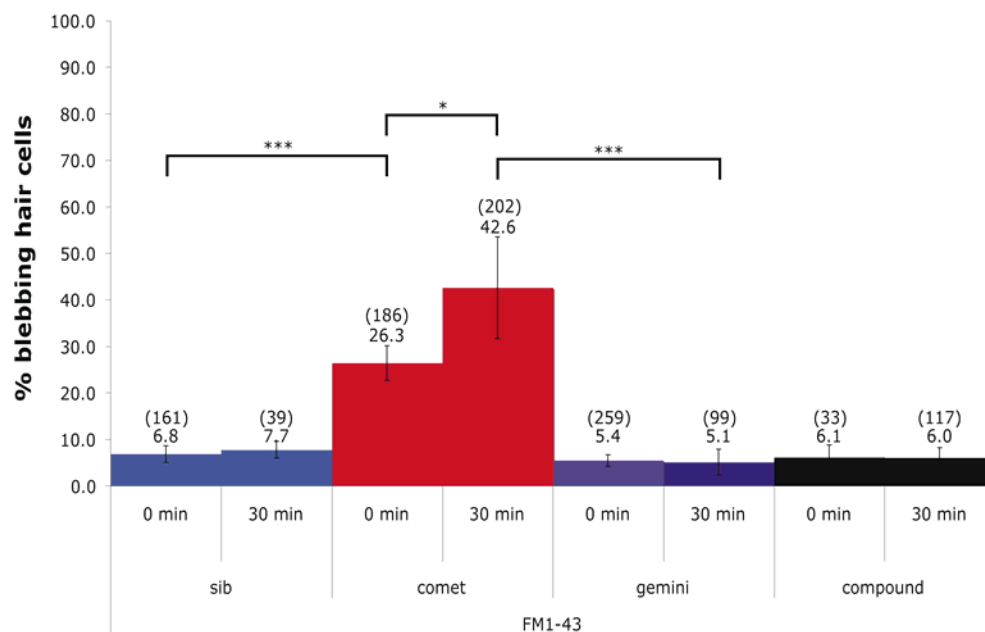


Figure 27. Activity-dependence of hair cell blebbing. Vestibular and lateral line HCs of zebrafish were stimulated for either 0 min or 30 min, and checked for blebbing by loading HC with FM1-43 dye. Percentage blebbing in *comet/synj1* siblings (6.8 ± 3.5 vs. 7.7 ± 4 , *comet/synj1* mutants (26.3 ± 7.5 vs. 42.6 ± 24.4). *gemini/cav1.3* mutants (5.4 ± 4.0 vs. 5.1 ± 5.5 , *comet/gemini* (compound) mutants (6.1 ± 6.1 vs. 6.0 ± 4.9). * = $p < .05$; *** = $p < .001$ (unpaired student's t-test), number of HCs in parentheses.

3.2.3 Blebs are Promoted by Latrunculin A

We speculate that failure of endocytic actin polymerization (Kaksonen et al., 2006) due to the absence of Synj1 might be involved in blebbing. Latrunculin A is a common reagent for blocking CME (Merrifield et al., 2005). According to our hypothesis, perturbing monomeric actin might therefore induce blebbing in HCs of wild-type larvae. When we incubate d5- 6 wild-type larvae with Latrunculin A for 15 min. at room temperature and visualize HC shape with FM1-43, we observe concentration- dependent basal blebbing (Figure 28). High concentrations of Latrunculin A (>2 $\mu\text{g}/\text{mL}$) and prolonged exposure (>20 min), however, eventually lead to general loss of cell shape and cell death. Adding the drug carrier (DMSO) alone has no effect (data not shown). However, theoretically, Latrunculin A might mimic *comet/synj1* mutants by affecting the cortical cytoskeleton. Mammalian Synj1 is known to interact with cytoskeletal regulators like Rac and Cdc42 (Qualmann et al., 2002), and might induce active cell-shaping processes.

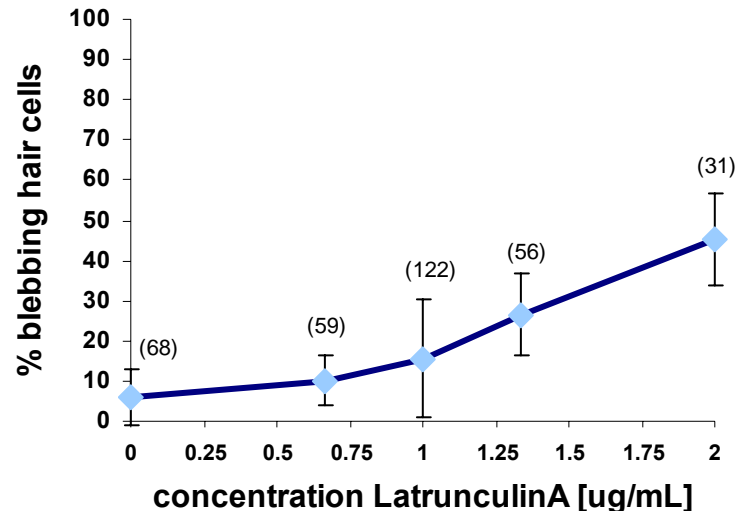


Figure 28. Latrunculin A induces blebbing in wild-type HCs in a concentration-dependent manner. D5 to d6 wild-type larvae were incubated with 0 $\mu\text{g}/\text{ml}$ to 2 $\mu\text{g}/\text{ml}$ of Latrunculin A for 15 min at room temperature. Blebs were visualized by loading HCs with FM1-43. Values: 0 $\mu\text{g}/\text{ml}$: $5.8 \pm 5\%$, 0.66 $\mu\text{g}/\text{ml}$: $10.2 \pm 7\%$, 1 $\mu\text{g}/\text{ml}$: $15.6 \pm 6\%$, 1.33 $\mu\text{g}/\text{ml}$: $26.5 \pm 15\%$, 2 $\mu\text{g}/\text{ml}$: $45.2 \pm 10\%$. Concentrations higher than 2 $\mu\text{g}/\text{mL}$ caused general toxicity and eventually HC death. Error bars, SD. Number of total HCs observed in parentheses. 3- 6 larvae tested per concentration.

3.2.4 Blebs Contain Normal Amounts of Actin and Tubulin

We hypothesize that since the cytoskeleton is involved in the generation of budding structures, perhaps this is also the case for the generation of HC membrane blebs. We stimulated the vestibular and lateral line systems of d5 to 6 *brn3c:gap43-gfp/JV039 comet* mutant and sibling larvae on a rotator at 8 rpm for 30 minutes at room temperature, then immediately fixed the larvae on ice for wholemount immunohistochemistry. To visualize the cytoskeleton, we labeled for either actin or tubulin (Figure 29), and for Ribeye-b to indicate ribbon synapses. GAP43-GFP provides a HC outline. We find that blebs label most strongly by GAP43-GFP. We detect only very weak labeling for actin and tubulin in blebs. Therefore, it appears that neither actin nor tubulin is enriched in the basal blebs of HCs, and that blebbing is probably not driven by the actin cytoskeleton. This result provides evidence for blebbing as a passive process driven by the addition of SV membrane to the basal plasma membrane. However, we acknowledge the detection limit of light microscopy.

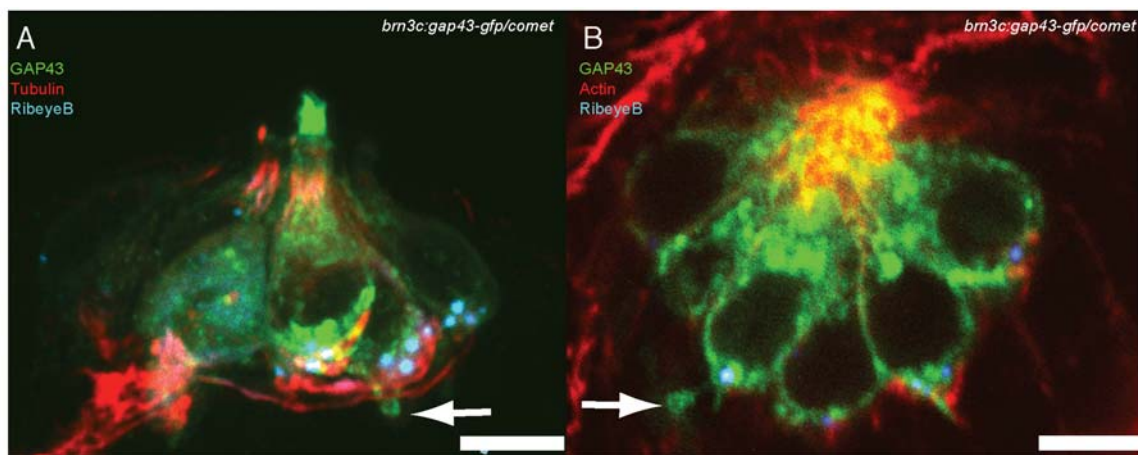
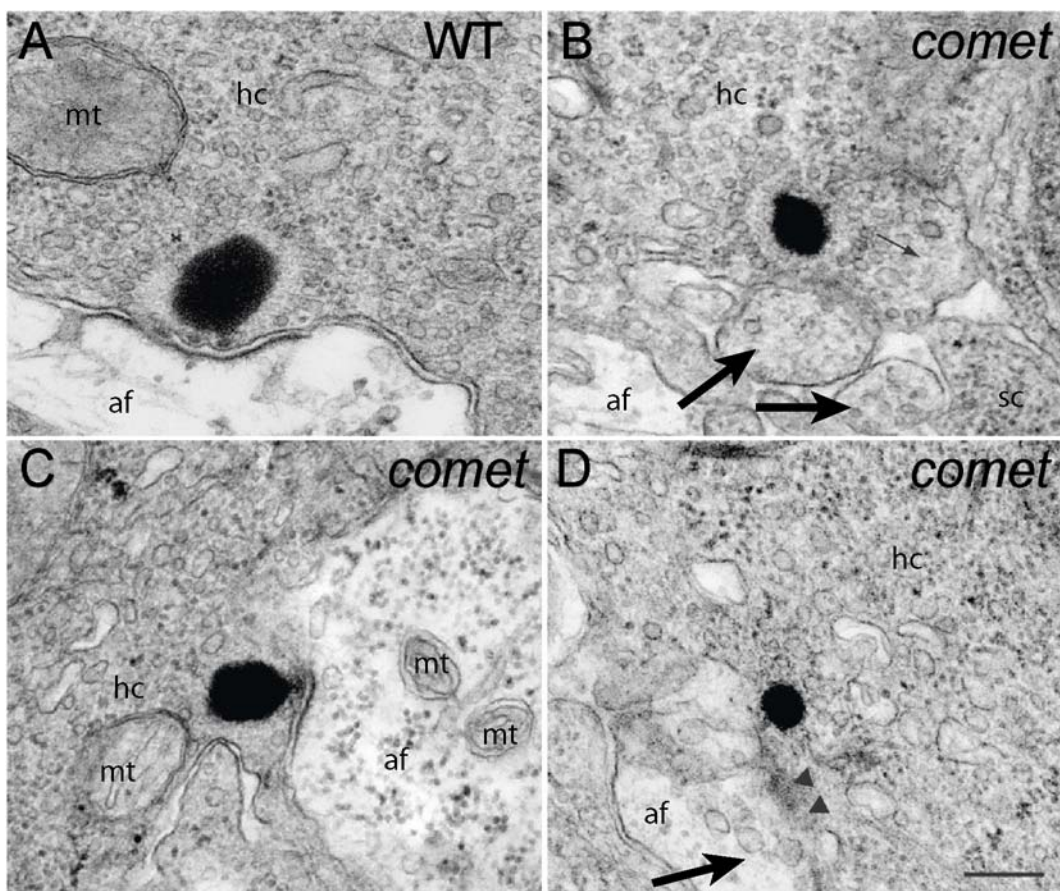


Figure 29. Actin or tubulin are *not* enriched in blebs. *A*, *comet/synj1* mutant neuromast expressing *brn3c:gap43-egfp* and double-labeled for tubulin (Cy3 = red), and Ribeye-b (Cy5 = cyan). *B*, *comet/synj1* mutant neuromast expressing *brn3c:gap43-egfp* and double-labeled for Actin (rhodamine = red), and Ribeye-b (Cy5 = cyan). Arrows: blebs; Scale bar: 3 μ m.

3.2.5 Detection of Blebs Using Electron Microscopy

We proceeded to use electron microscopy (EM) to confirm the existence and composition of basolateral blebs, and to observe other *synj1* mutant phenomena at the ultrastructural level (Figure 30). 5 larvae each of stimulated d5 *comet* siblings and mutants were analyzed. We find that blebs appear to contain mostly cytoplasm and vesicles, and are distinguishable from the cell body only by the fact that they are enclosed by membrane that does not connect to the cell body. Yet blebs are clearly of a different composition than supporting cells (darker), or the afferent post-synapse or boutons of efferents (largely empty of cytoplasmic density) synapsing onto the HC. However, we find a reduced average ribbon diameter (*comet*: 293 ± 83.4 nm vs. WT: 408 ± 108 nm) that coincides with a reduced number of ribbon-associated SVs (*comet*: 21.9 ± 12.3 vs. WT: 36.2 ± 6.4), while the surface packing density is comparable (data not shown).



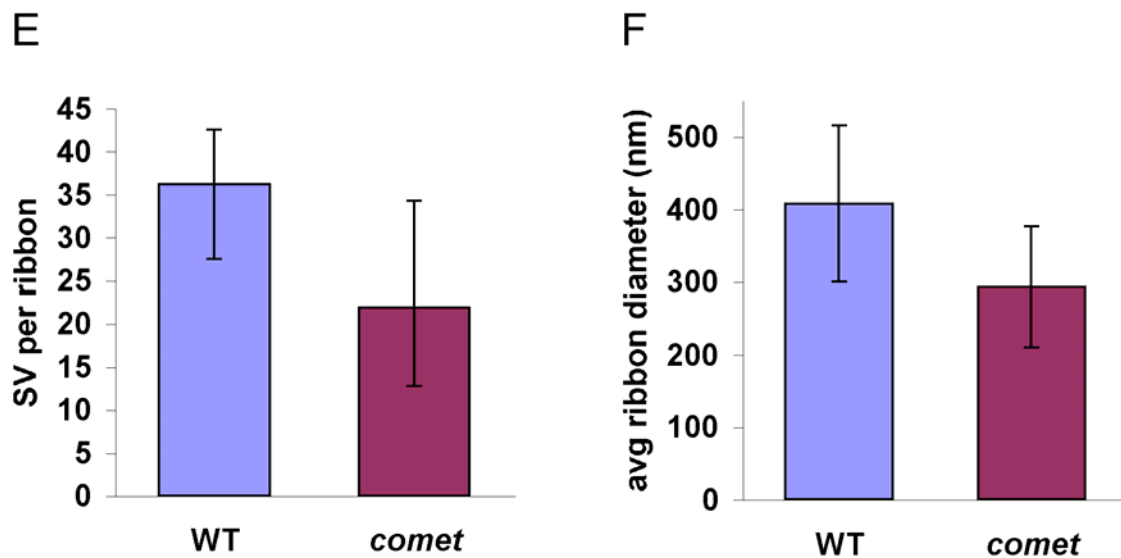


Figure 30. HC synapses of *comet* mutant larvae bleb and have a reduced ribbon diameter that coincides with fewer coordinated synaptic vesicles. *A*, representative wild-type HC afferent synapse. Only vesicles with a diameter of 30-50 nm and proximity to the ribbon were counted. *B-D*, sections through mutant afferent synapses. Arrows indicate blebs. hc = hair cell, af = afferent postsynapse, sc = supporting cell, mt = mitochondrion *A-D*, scale bar: 400 nm. *E*, synaptic vesicle counts from wild-type and mutant HCs and *F*, Ribbon diameter; wild-type ribbons (24) average 408 ± 108 nm and coordinate 36.2 ± 6.4 SVs, compared to 293 ± 83.4 nm and 21.9 ± 12.3 vesicles for mutant ribbons (23); $p < .001$, Student's t-test. 3 mutant and 5 wild-type sibling larvae are analyzed. Error bars in *E-F* represent standard deviation. Sample size in parentheses.

comet mutants also show some of the manifestations typical for *synj1*- or *endophilin* mutants, as described in *Drosophila* or mice at conventional synapses (Dickman et al., 2005; Cremona et al., 1999). Among these are signs of slowed or arrested endocytosis, such as clathrin-coated pits and endocytic intermediates, and invaginations. Furthermore, detached or “floating” ribbons in HCs as described in zebrafish *nrc* mutant photoreceptors, but not bipolar cells (Allwardt et al., 2001; Van Epps et al., 2004) or in the pineal gland (Allwardt and Dowling, 2001) are not apparent. Concomitantly, we do not observe strings of vesicles, or actin aggregates, which may be for technical reasons, or due to the specifics of our cell type.

3.2.6 Conclusions of Part 1: *synptojanin1*

In conclusion, *synj1* is expressed in HCs and appears to be necessary for HC synaptic transmission and vestibular function. We observe that in *comet* /*synj1* mutant HCs, synaptic ribbons are smaller, and though they show equal packing densities as in the WT, they coordinate fewer vesicles. Whether the smaller effective readily releasable pool leads to altered release kinetics at the HC afferent synapse, remains to be investigated.

Counter to our expectation of accumulation at the plasma membrane due to slowed endocytosis, putative SV- or SV cycle markers like Otoferlin A, Vglut1 and Vglut3, or Clathrin light chain A localize normally in *comet* mutant HCs, even after HC stimulation. Also, in contrast to data from drosophila endocytosis mutant NMJs and zebrafish *nrc/synj1* mutant photoreceptor cells (Allwardt et al., 2001; Van Epps et al., 2004), synaptic ribbons in *comet* mutant HCs appear to localize normally and are not increased in numbers.

We also describe structural evidence for blebbing, a novel phenotype, in our *comet/synj1* mutant HCs. We find that HC blebbing is synaptic activity-dependent and can be suppressed by eliminating voltage-dependent presynaptic Ca^{2+} currents in a *comet/gemini* compound mutant HC. Though blebbing can be reproduced by Latrunculin A, it appears to be caused by excessive SV membrane addition to the basal plasma membrane, or by the lack of compensatory membrane reuptake, rather than it being an active, cytoskeleton-dependent process.

comet mutant larvae have a balance defect that becomes more apparent when larvae older than 96 hpf are challenged by swirling the water in their dish. Using this simple assay, we can phenocopy the *comet* mutant balance defect with a translation-blocking morpholino (atgMO), but not with one suppressing the splice variant *synj1-145* (145MO), the predominant *synj1* isoform in the nervous system. While 145MO induces a balance defect at very high concentrations (2mM), it appears that *synj1-170* can compensate fairly well for *synj1-145* under the conditions tested. However, this result is preliminary in the absence of protein data (e.g. Western Blot), which will be important to confirm its significance.

3.3 Part 2: *vglut3* is Required for Hearing and Balance in Zebrafish

The *asteroid* mutant was identified in the same ENU mutagenesis screen that identified *comet* (chapter 3.1). Unlike *comet* mutant larvae, *asteroid* mutant larvae display a “deaf circler” phenotype, which includes a lack startle response (presumably deaf), inability to orient to gravity, and a spiraling swim trajectory. Like *comet* mutants, *asteroid* mutants die around d8, presumably from a failure to feed and to inflate their swimbladders. Morphologically, *asteroid* mutant larvae appear normal, and mutant HCs take up FM 1-43, suggesting that mechanotransduction is normal (data not shown). These observations suggest that the *asteroid* defect lies downstream of mechanotransduction, perhaps in synaptic transmission.

HCs are glutamatergic. Previously, Furness et al. have found Vglut1 expression at the electron microscopic level at HC ribbon synapses in mice (Furness and Lawton, 2003). In following, I will show that in the zebrafish, both Vglut1 and Vglut3 are present in the HC, and probably involved in neurotransmitter release. Furthermore, Vglut3 appears to be HC-specific, and is required for hearing and balance. *asteroid* mutants have a splice-site mutation in *vglut3* mRNA that leads to a non-functional Vglut3 protein. This mutation leads to a decrease in the number of synaptic vesicles at the HC ribbon synapse. Beyond loading of SVs with neurotransmitter, this may indicate a function for Vglut3 in SV biogenesis and trafficking.

3.3.1 Positional Cloning of *vglut3* in *asteroid* Mutants

Positional cloning with polymorphic markers was performed by Boehland, Wolfson and others (unpublished) and resolves a ~5 Mb critical interval that contains a number of gene predictions (Figure 31 A). One candidate was *vglut3*, an isoform of the vesicular glutamate transporter. RT-PCR of the *vglut3* N-terminal coding sequence from *asteroid* wild-type and mutant mRNA results in a 662 bp band in the wild-type, and 530 bp and 406 bp bands in the mutant (Figure 31 B). Sequencing shows a partial (530bp) or complete (406bp) deletion of exon2 from the mutant cDNA.

All bands are also detected in *asteroid* sibling cDNA, indicating that the *asteroid* mutation might cause a splicing defect in *vglut3* mRNA. Sequencing the donor splice site in intron 2 of the *asteroid/vglut3* gene results in the expected genomic lesion, a GT>GC transition that causes the complete or partial deletion of exon2 during mRNA splicing by accessing a cryptic splice site within exon2, or skipping exon2 entirely (Figure 31 C). We could efficaciously phenocopy the *asteroid* mutant using an antisense morpholino (GT MO) targeting the intron2 splice-donor site (Figure 31 B, E). Interestingly, the GT MO always leads to accession of the cryptic splice site within exon2 (Figure 31 B).

Both splicing defects observed in the mutant result in a frameshift and premature stop codon for the predicted translations of the resulting cDNAs. This likely causes the termination of Vglut3 translation prior to its first transmembrane segment (Figure 31 D), resulting in non-functional protein. Furthermore, we could also phenocopy the *asteroid* mutant with a translation-blocking (directed against the start codon) morpholino, ATG MO. A 5-base mismatch control MO had no effect (Figure 31 E). We conclude that *vglut3* is the *asteroid* gene, and that the *asteroid* mutation is a *functional null*.

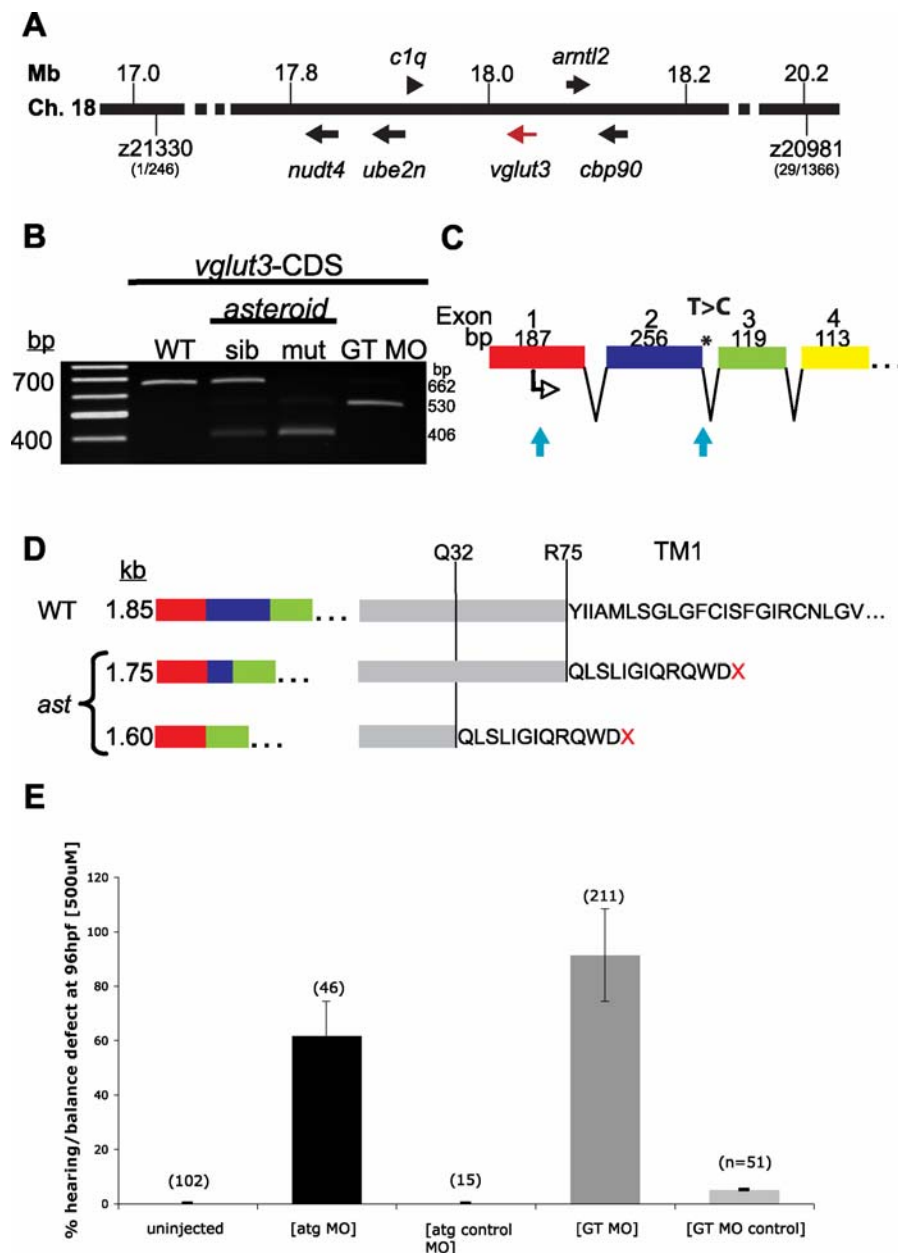


Figure 31. Positional cloning and identification of the *asteroid* gene. *A*, Critical interval of the *asteroid* gene, including polymorphic markers and the number of meiotic recombinants at each end. *B*, cDNA spanning exon2 of *vglut3* amplified from wild-type, *asteroid* sibling and mutant, and *vglut3* splice donor site (GT) morpholino-injected larvae. *C*, Exon/intron structure of *vglut3*, and position of the genomic lesion (asterisk), a GT>GC donor splice site mutation (blue arrows indicate the morpholino target sites). *D*, Reading frames of the wild-type and mutant transcripts. *E*, Morpholinos against *vglut3* phenocopy the hearing and balance defect of the *asteroid* mutant (uninjected: 0 ± 0%, atg MO: 62 ± 13%, atg control MO: 0 ± 0%, GT MO: 91 ± 13%, GT control MO: 5 ± 7%).

3.3.2 *In situ* Expression Analysis of *vglut3* and other *vglut* genes

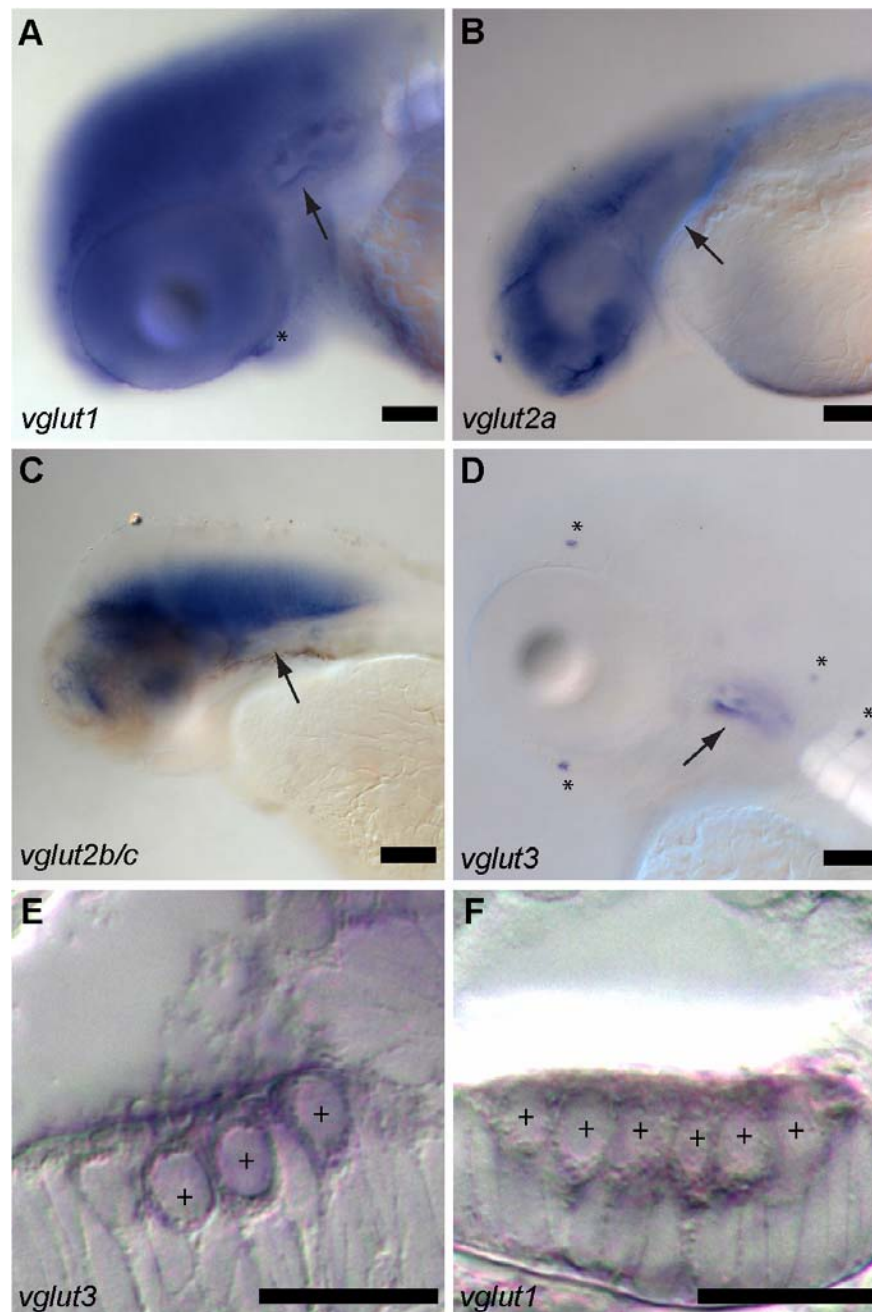


Figure 32. *vglut* expression in the developing zebrafish. mRNA (blue/purple) was detected at 72 hpf by whole-mount *in situ* hybridization with *vglut1* (A), *vglut2a* (B), *vglut2b* and *c* (C), and *vglut3* (D) antisense riboprobes. A-D Lateral views of the larval head region. E,F, 14 μ sections of the ears from A and D, respectively. Asterisk: neuromast; arrow: ear; +: HC. A-D scale bar: 100 μ m. E,F scale bar: 10 μ m.

In rat, *Vglut3* expression is reported for brain and the vestibulum (Herzog et al., 2004). In order to better understand if the mutation in *asteroid* causes sensorineural or central deafness, and if *vglut3* is the only vesicular glutamate transporter expressed in the ear, we performed *in situ* hybridization for the three zebrafish *vglut* isoforms. *vglut1* shows a widespread distribution in the brain, and is also expressed in the larval inner ear (Figure 32 A, F). *vglut2* has three isoforms, which we also detect in some parts of the brain, but not in the inner ear (Figure 32 B, C). *vglut3*, however, is only detected in inner ear HCs and in the neuromast HCs of the lateral line organ (Figure 32 D, E). Sections of the inner ear imaged at 63x magnification (Figure 32 E, F), and whole mounts of 96 hpf larvae (data not shown) show that both *vglut1* and *vglut3* are present in the auditory/ vestibular and lateral line sensory epithelia.

Since both *vglut1* and *vglut3* appear to be expressed in HCs, we speculate that *asteroid* mutant larvae may overexpress *vglut1* in an attempt to compensate for loss of *vglut3*. We sectioned and analyzed staining levels in HCs of 10 larvae after detecting *vglut1* by *in situ* hybridization. Interestingly, we do not observe increased *in situ* levels of *vglut1* mRNA in *asteroid* mutants versus siblings (Figure 33).

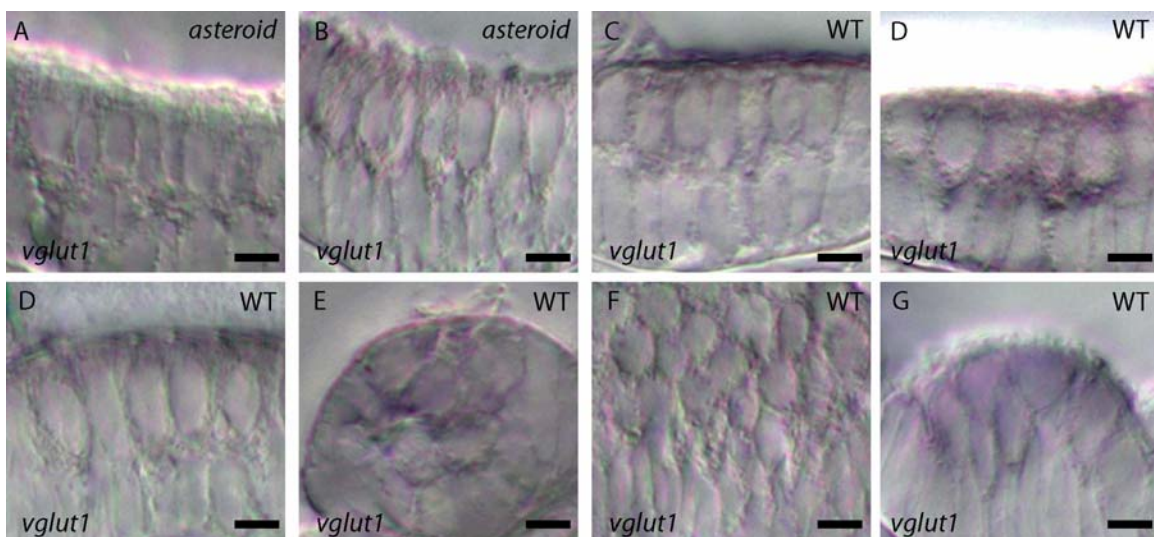


Figure 33. *vglut1* expression levels are comparable between *asteroid* mutant and sibling inner ear HC at 96 hpf. A,B, mutant HCs. C-G, sibling HCs. Scale bar: 3 μ m. Images taken from 14 μ m sections of whole-mount *in situ*.

3.3.3 Semiquantitative PCR Shows No Up-regulation of *vglut1* in *asteroid* Mutant Larvae

To confirm that *vglut1* is not up-regulated in *asteroid* mutants, we performed real-time PCR to measure transcript levels in 120 hpf *asteroid* sibling and mutant larvae. Primers specific for *vglut1*, *vglut3* (total) and *vglut3* (exon2), reveal no significant up-regulation of *vglut1* (“VG1N1”) or *vglut3* (“VG3N8”) in *asteroid* mutant versus wild-type larvae (Figure 34). As expected, *vglut3* exon2 (“VG3E2”) is not detected in the mutant. While this result is in agreement with our *in situ* data, we predict that with glutamatergic neurons potentially in 100-fold or more excess of HCs in 120 hpf zebrafish larvae, a moderate increase of transcript might be below the detection threshold. However, we expect to recognize a large increase of transcript level at the *in situ* level. Therefore, it appears as if there is no compensatory up-regulation of *vglut1* in mutant HCs.

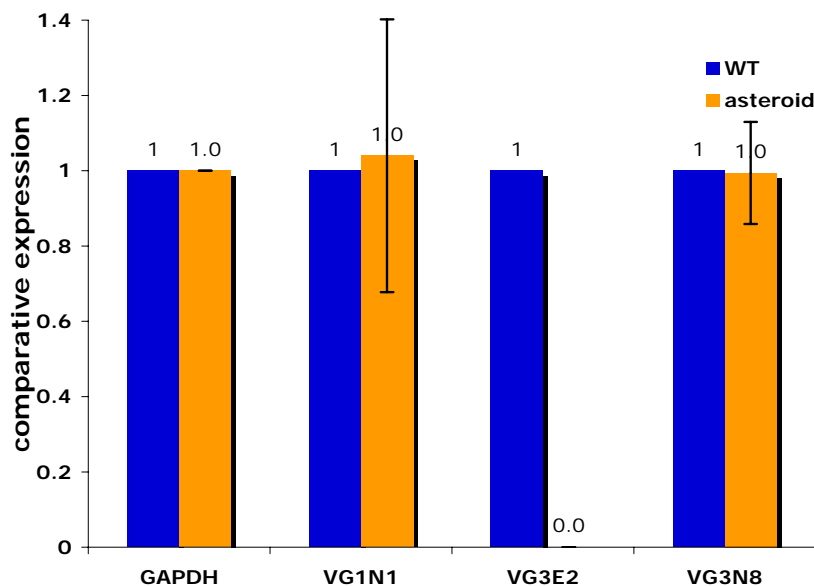


Figure 34. Neither *vglut1* nor *vglut3* expression levels are significantly changed in *asteroid* mutant larvae. *gapdh* serves as internal standard. *vglut1* (“VG1N1”): 1.0 ± 0.4 , *vglut3* (“VG3N8”): 1.0 ± 0.1 , *vglut3* exon2 (“VG3E2”): 0.0 ± 0.0 . WT levels are defined as “1-fold expression”. Error bars denote standard deviation. Data from 3 biological replicates.

3.3.4 Morpholino Knockdown of Vglut1 Causes Vestibular and Other Defects

We detect both *vglut1* and *vglut3* mRNA in HCs of larvae between 72 hpf and 120 hpf. Despite *vglut1*'s role as the main vesicular glutamate transporter in the vertebrate brain (Takamori, 2006), we hypothesize that, due to the high vesicle turnover in HCs, a relatively small reduction of functional Vglut1 might result in a vestibular deficiency. To address this, we injected a morpholino (VG1_GT MO) targeting the exon 2 donor splice site of *vglut1*, resulting in an early truncation similar to that of the *asteroid* mutation. Knockdown of Vglut1 in this way causes deafness and balance defects in $34 \pm 6\%$ of free-swimming larvae (Figure 35). As an aside, *vglut1* morphants also have additional defects, like small eyes, and less activity or responsiveness to touch. These defects may be based on morpholino interference with Vglut1 function in the brain and retina.

While *vglut1* is seen expressed in HCs of the inner ear and throughout the nervous system, *vglut3* is apparently HC specific. Neither Vglut1 nor Vglut3 appear to compensate for the loss of the other in *asteroid* mutant or *vglut1* morphant larvae, under the conditions tested.

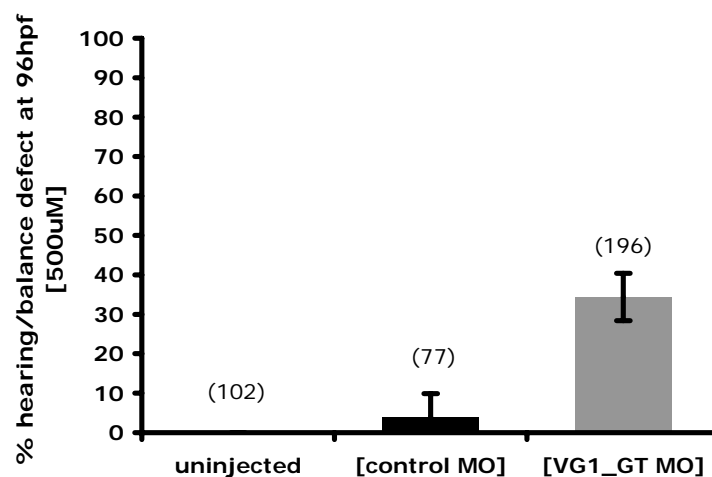


Figure 35. Morpholino-knockdown of Vglut1 causes deafness and a balance defect in 96 hpf larvae. The morpholino targets the exon2 donor splice site (GT) of *vglut1*. Percentage larvae with auditory/vestibular defects: $0 \pm 0\%$ uninjected; $4 \pm 6\%$ control MO; $34 \pm 6\%$ GT MO; ($p < .001$, Student's t-test). Error bars denote standard deviation. Number of total larvae observed in parentheses.

3.3.5 Cellular Localization of Vglut3 Using Immunofluorescence: Vglut3 is Localized to the Basal End of Hair Cells

To examine the subcellular distribution of Vglut3, we raised an antibody against the C-terminus of Vglut3 (amino acids 530-590) and performed immunohistochemistry on 14 μm sections of 120 hpf larvae (Figure 36). Cell bodies of HCs were outlined by antibody labeling against acetylated tubulin (Figure 36B, C, E, F). We observe Vglut3 immunoreactivity in densely packed punctae in the basal halves of inner ear and neuromast HCs (Figure 36 A, C). Vglut3 immunoreactivity is absent in *asteroid* mutant HCs (Figure 36 D, F), providing strong evidence for the identity of *vglut3* as the *asteroid* gene and specificity of the anti-Vglut3 antibody.

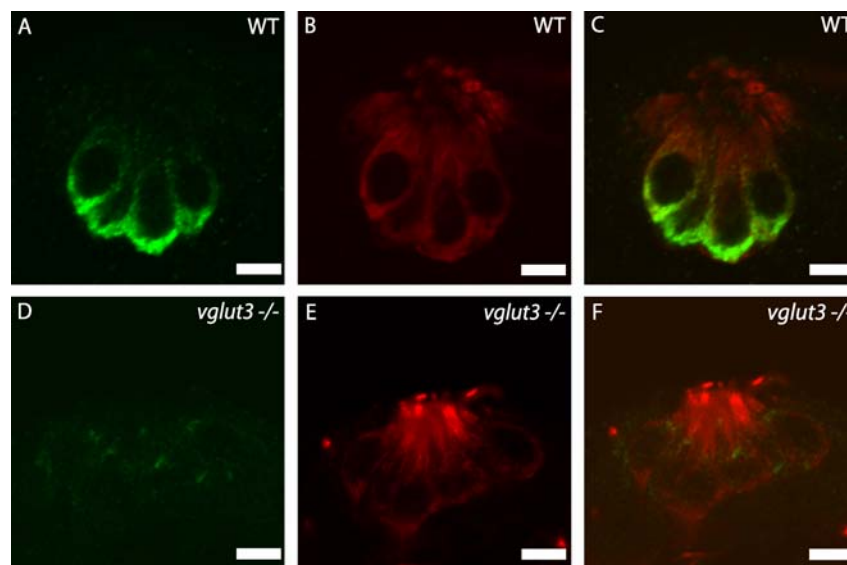


Figure 36. Vglut3 protein is absent in *asteroid/vglut3* mutants. *A-F*, Immunolabeling of Vglut3 protein in thick sections of wild-type and mutant *asteroid/vglut3* neuromast HCs at 120 hpf. *A,D*, Vglut3 (green). *B,E*, acetylated tubulin (red). *C,F*, Overlay of tubulin and Vglut3 labeling. Three or more neuromasts were observed per specimen ($n = 8$ for both sibling and mutant larvae). Scale bar: 3 μm .

3.3.6 Antigen Competition Eliminates Vglut3 Immunolabel

To gather additional evidence for the specificity of our antibody against Vglut3, we repeated the immunohistochemistry on 120 hpf larvae as an antigen competition assay (Figure 37). Anti-Vglut3 antibody was preincubated either with a one-fold molar excess of antigen or PBS. Any immune complexes were removed by pelleting. Sections were then labeled with the respective mixtures using our standard protocol. Phalloidin-rhodamine was used as a counterstain for actin. We find that Vglut3 immunoreactivity is absent in the wild-type only in HCs of those sections labeled with antigen-containing solution, confirming the specificity of the antibody against Vglut3.

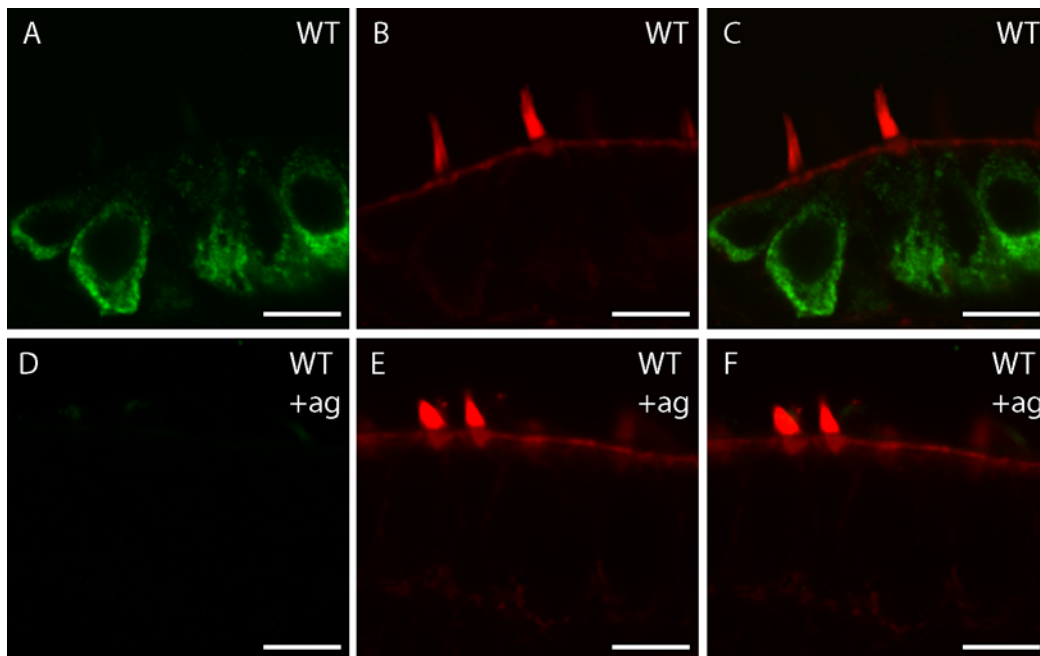


Figure 37. Vglut3 immunolabel is lost in WT under antigen competition. A-F, Immunolabeling in thick sections of wild-type inner ear HCs at 120 hpf. A, D, Vglut3 (green). B, E, actin (red). C, F, Overlay of Vglut3 and actin labeling. Three or more ears were observed in each of two larvae. Scale bar: 3 μ m.

3.3.7: Vglut1 Localizes to the Basal Half of the Cell

Currently antibodies reactive with zebrafish Vglut1 protein are not available, thus we fluorescently tagged Vglut1 and transiently expressed *vglut1-gfp* in HCs using the *myosin 6b* promoter (see 3.1.3) for tissue specificity. To outline HCs, we co-expressed GAP43-tomato, a soluble membrane marker. Like Vglut3, Vglut1-GFP is largely confined to the basal end of HCs (Figure 38). GFP tags are a known caveat for this type of localization experiment. This will be discussed in section 4.1. It is unlikely that *vglut1* is over-expressed by the *myo6b* promoter, given that HCs contain hundreds of thousands of vesicles. While the neuromast HCs in Figure 38 are pear-shaped, the possibility exists that the basal end is brighter simply because it contains more cytoplasm. However, GAP43-tomato expressed by the same cells is largely cytosolic and does not look equally enriched at the base of the cell.

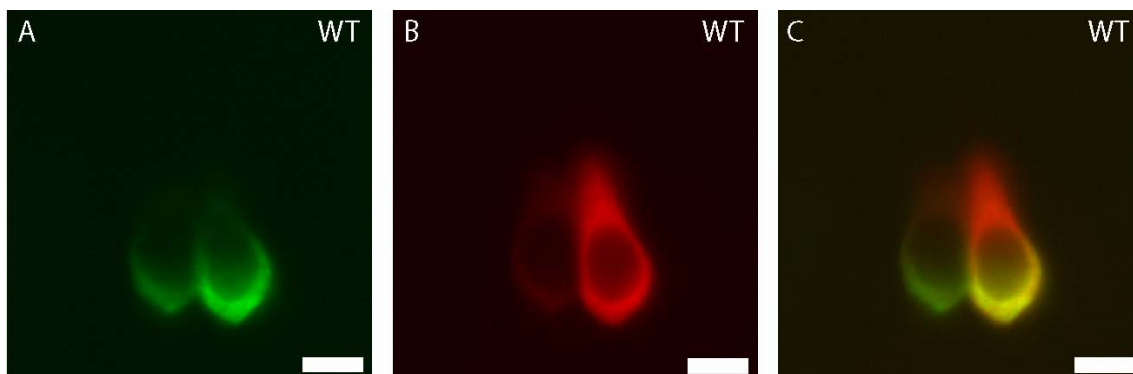


Figure 38. Vglut1-GFP localizes to the basal half of hair cells. *A*, Vglut1-GFP fluorescence in neuromast HCs driven by the *myo6b* promoter ($n=5$). *B*, Same cells expressing *myo6b:gap43-td tomato*, filling the cell bodies. *C*, Overlay of *A* and *B*. Scale bar: 3 μm .

3.3.8: Synaptic Vesicle Numbers Are Reduced in *asteroid/vglut3* Mutants

A recent study of *vglut1* knockout mice reported a ~ 60% reduction in reserve pool SVs at central synapses (Fremeau et al., 2004a), and similar results were observed in zebrafish (Smear et al., 2007). Perhaps a reduction in SVs would also be observed in at the HC afferent synapse of *asteroid/vglut3* larvae. To investigate this possibility, we analyzed HCs from larval *asteroid/vglut3* siblings and mutants by transmission electron microscopy (Figure 39). A typical HC ribbon body is spherical to ovoid, electron-dense, and surrounded by a filamentous halo that coordinates synaptic vesicles. We occasionally observed ribbon anchors, which connected ribbon bodies to the plasma membrane at the active zone (Figure 39A).

For counting ribbon-associated *bona fide* SVs, we required the following characteristics: a vesicle must (a) be in the first row of vesicles surrounding the ribbon; (b) be approximately circular; and (c) measure 30-50 nm in diameter (Schnee et al., 2005). We therefore excluded the reserve pool of SVs, as well as endosomal intermediates near the ribbon body and limited our analysis to readily-releasable SVs at the ribbon.

Figure 39 shows representative sections through wild-type and *asteroid/vglut3* mutant ribbons (B and C, respectively). Ribbon halos extend approximately 50-100 nm from the ribbon body. There appears to be no difference in ribbon area or halo width between wild-type and mutant synapses (Figure 39D; data not shown). Also, *asteroid/vglut3* HC ribbons show a ~ 60% decrease in coordinated SVs compared to those from wild-type siblings (Figure 39E; 12.8 ± 1.0 SVs for wild-type ribbons, 5.34 ± 0.6 ; for *asteroid/vglut3* mutant ribbons; $p \ll 0.001$, Student's t-test).

This result is comparable to data from other synapses lacking *vglut1* (above), which may be interpreted as evidence that *vglut3* may fulfill a similar function in HCs as *vglut1* at central synapses. This is especially interesting considering that *vglut1* is co-expressed with *vglut3* in HCs.

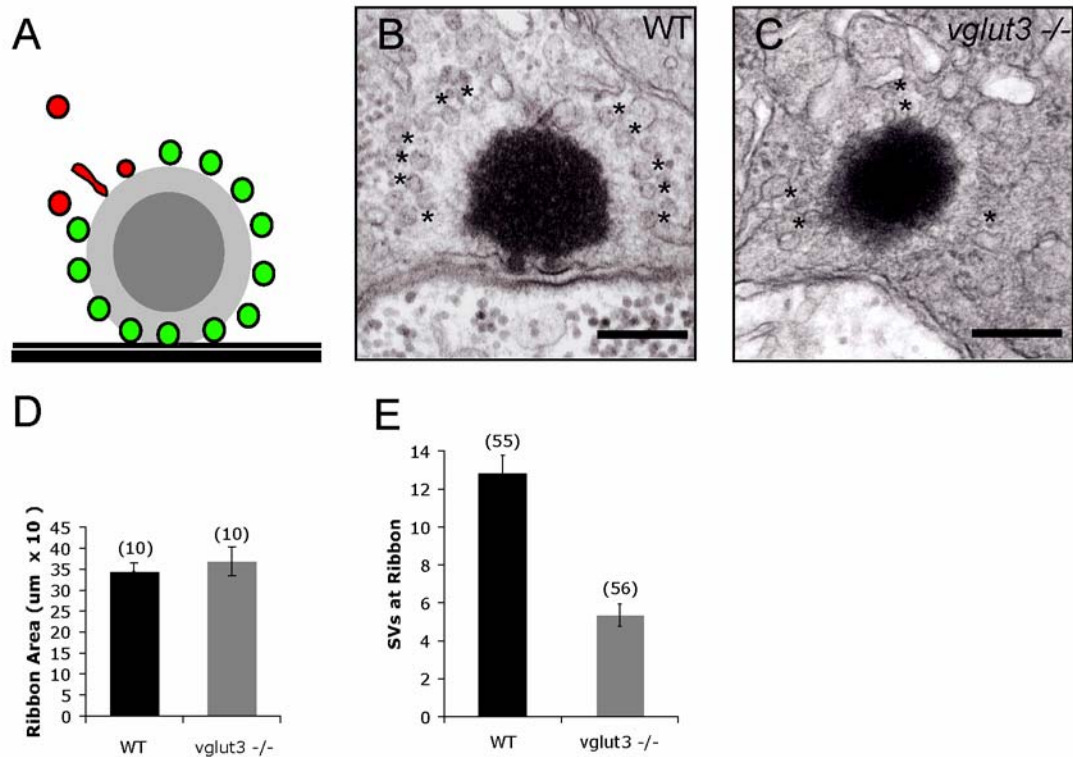


Figure 39. *asteroid/vglut3* mutants have a reduced number of ribbon-associated synaptic vesicles. *A*, Schematic of the HC afferent synapse. Only vesicles with a diameter of 30-50 nm and proximity to the ribbon were counted (green); outliers (red) were ignored. *B*, A representative wild-type ribbon; asterisks indicate synaptic vesicles included in analysis. *C*, A representative section through a mutant ribbon. *B-C*, scale bar: 200 nm. *D*, Cross-sectional area of ribbon bodies in wild-type and mutant *asteroid/vglut3* HCs. No significant difference is seen (n=10 in each case). *E*, Vesicle counts from wild-type and mutant HCs; wild-type ribbons coordinated 12.8 ± 1.0 SVs, compared to 5.34 ± 0.6 for mutant ribbons ($p < .001$, Student's t-test). Error bars in *D* and *E* represent standard error of the mean. Sample size in parentheses.

3.3.9 Conclusions of Part 2: *vglut3*

HCs transmit information via glutamatergic ribbon synapses, which presumably have the highest synaptic vesicle turnover of all chemical synapses. We have identified *asteroid* as the vesicular glutamate transporter 3 (*vglut3*), which is critical for HC function. *asteroid* mutant larvae are deaf and display a profound balance defect, while HC bundle morphology and FM 1-43 dye uptake appears normal, suggesting a transmission failure downstream of mechanotransduction. Consequent sequencing of the *asteroid* mutant allele IJ001 revealed a donor splice site mutation in exon2 of *asteroid/vglut3*, which results in a severe truncation of the protein product. We can phenocopy *asteroid* phenotype by injecting morpholinos directed against the *vglut3* ATG/start site or the affected splice junction into the wild-type. *In situ* hybridization shows that *vglut3* appears to be exclusively expressed in HCs of the ear and lateral line organ. Also, antibodies against Vglut3 exclusively label the basal end of HCs, can be blocked by antigen competition, and labeling is absent in *asteroid/vglut3* mutants. We find that *asteroid* mutants show a 60% decrease (12.8 ± 1.0 SVs, WT, 5.34 ± 0.6 mutant) in the number of ribbon-associated synaptic vesicles at the ultrastructural level. Ribbon diameters are comparable between *asteroid* mutants and WT. Using *in situ* hybridization, we also detect *vglut1* transcript in HCs, but the presence of *vglut1* does not compensate for loss of *vglut3* under the conditions tested. In support of this notion, our qPCR data indicates that *vglut1* is not significantly upregulated in *asteroid/vglut3* mutants.

Our data indicates a role for *vglut3* in synaptic vesicle biogenesis and/or trafficking in HCs, but Vglut3 is not the sole component required for these processes.

4 Discussion

In the following chapter, I will reexamine the evidence we have generated in this study and attempt to interpret its meaning and relevance for the field. I will also provide a thematic outlook, as well as propose additional experiments.

Even after decades of research, the current understanding of the mechanisms of hearing and balance is fundamentally lopsided. On one hand, the vertebrate and even human cochlea and vestibulum are extremely well characterized in terms of physiology. Electrical recordings are possible and data is available from all electrically active cell types in these organs. And from these data, highly sophisticated models of cochlear function have been generated. Today, cochlear implants are available and are routinely used in clinical practice (Waltzman, 2006). Similarly, the availability of cochlear-vestibular implants is expected for the near future (Wall et al., 2002; Shkel and Zeng, 2006). In contrast to these striking successes, knowledge about the molecular composition and the mechanisms that govern the HC, the sensory receptor for hearing and balance, is limited. While the current implants are of great benefit for the patient, in order to obtain a true (genetic) cure, and in order to understand nature's machinations, we need to elucidate the exact molecular composition and function of the mechanotransduction and -transmission apparatus. What progress has been made in the understanding of the molecular components and mechanisms in the HC in the past decades has largely come from genetics, especially mouse genetics, but also from other vertebrates, like the zebrafish. One reason for this is the high number of genetic diseases that affect hearing, which fall into the natural "jurisdiction" of geneticists. Additional reasons are the scarcity of material, which forestalls most biochemical approaches: a mammalian cochlea contains some 36,000 HCs; and the inaccessibility of the cochlea, which is encased in bone. In this study we have identified, cloned and characterized two genes from the zebrafish that are required for proper HC transmission. Both *synj1* and *vglut3* are involved in SV generation and recycling, and absence of at least one functional copy of each gene leads to transmission defects at the HC afferent synapse.

4.1 Vesicular Glutamate Transporter 3 in the Zebrafish Hair Cell

Vesicular glutamate transporter 3 (Vglut3), which is absent in the *asteroid* mutant strain, is critical for HC function. *asteroid* mutant larvae are deaf and display a profound balance defect, while HC bundle morphology and FM 1-43 dye uptake appear normal. This phenotype suggests a transmission failure downstream of mechanotransduction. In the *asteroid* mutant, the *vglut3* gene contains a T>C transitional mutation in the splice-donor site of intron2 that leads to partial or complete deletion of exon2 during mRNA splicing. The deletion of exon2 or selection of a cryptic site within this exon results in a frameshift and premature stop codon prior to the first transmembrane domain, which we expect to generate a severely truncated Vglut3 protein. Indeed, Vglut3 immunoreactivity is not seen in *asteroid* mutants using an antibody against the Vglut3 C-terminus, and can be blocked by antigen competition in the wild-type. We interpret these data, combined with the finding that morpholinos against *vglut3* replicate the *asteroid* mutant phenotype, as proof that *vglut3* is identical with *asteroid*.

Although the precise identity of the neurotransmitter transporters had not been determined, it was previously reported that HCs are glutamatergic (Glowatzki and Fuchs, 2002). We can deduce from this result that a vesicular glutamate transporter is likely required for hearing and balance, and *vglut1* had been previously detected in the guinea pig cochlea by immunohistochemistry (Furness and Lawton, 2003). In addition, another group recently reported the immunodetection of VGLUT3 in rat cochlear sensory epithelium (Wang et al., 2007). Yet it is unexpected that both Vglut1 and Vglut3 are co-expressed in HCs, and that Vglut3 has a role directly related to hearing and balance. The three Vglut isoforms (*vglut1*, -2, and -3) are expressed in complementary distributions in the mature mammalian CNS, but it has been reported that neurons in the developing brain may transiently co-express Vglut1 and -2 (Fremeau et al., 2004a). It remains to be seen if the co-expression of Vglut1 and Vglut3 in larval zebrafish HCs is a transient phenomenon, yet larval HCs are fully operational by d5, the timepoint which we observed. It is clear from the above results that, unlike in immature mammalian neurons, the presence of these two Vglut

isoforms does not provide any functional redundancy in larval HCs. Loss of either Vglut3 or Vglut1 alone is sufficient to abrogate balance in these larvae and to severely impair hearing, although electrical recordings of the auditory brain stem would be required to prove without doubt that these larvae are truly deaf. Alternatively, it is possible to record action potentials from the posterior lateral line ganglion (the first order neurons of the lateral line) to characterize the nature and extent of the remaining HC transmission in *asteroid* mutant larvae.

In Vglut1 and -2 co-expressing mammalian neurons, these transporters appear to be segregated to distinct vesicle populations that traffic to separate presynaptic boutons (Fremeau et al., 2004b). It appears that Vglut1 and -2 specific SV populations also show distinct release kinetics, perhaps with Vglut1-containing vesicles mostly making up the reserve pool (Fremeau et al., 2004a). While we do not yet know whether the same is true of Vglut1 and Vglut3 in larval zebrafish HCs, we detect both transporters diffusely at the basal end of HCs. We interpret this as circumstantial evidence that Vglut1 and Vglut3 do not segregate to different ribbon synapses. Yet two caveats for all exogenous expression experiments classically apply: overexpression and mislocalization. While the *myo6b* promoter is very strong, we do not think overexpression likely. HCs have reserve pools in excess of 600,000 SVs, each of which must have at least one molecule of glutamate transporter (Daniels et al., 2006). HCs must therefore be used to high turnover of all SV proteins. As for mislocalization, a C-terminal EGFP-tag may or may not interfere with correct protein localization. Vgluts are currently not known to control SV localization to the synapse, which may be rab-dependent (Sudhof, 2000). Interestingly, Vglut1 C-terminus has been shown to interact with Endophilin, AP2 and AP3 (Voglmaier et al., 2006; Jung and Haucke, 2007) for endocytosis at the plasma membrane. Because we do not see accumulation of fluorescence at the plasma membrane in HCs expressing *myo6b:vglut1-egfp*, we assume that these interactions are not disrupted by the addition of an EGFP tag. A conclusive answer to the question if Vglut1 and Vglut3 localize to the same or different vesicle pools and to the same synapses

in HCs would require immuno-gold labeling, ideally as a co-label for Vglut1 and Vglut3 using antibodies generated in different host species. Electrical recordings from HCs or the lateral line ganglion in *asteroid* mutant larvae, wild-type larvae after *vglut1*-knockdown, and *asteroid* mutant larvae after *vglut1*-knockdown should be able to give meaningful functional data to elucidate the kinetics of Vglut1- and Vglut3-containing SV release in HCs, and shed light on the question of if there are different SV pools that are distinguishable by their Vgluts (Fremeau et al., 2004b; Fremeau et al., 2004a).

asteroid mutants show a 60% decrease (12.8 ± 1.0 SVs; WT, 5.34 ± 0.6 mutant) in the number of ribbon-associated synaptic vesicles at the ultrastructural level (synaptic ribbon diameters are comparable between *asteroid* mutants and WT). This is comparable to a similar reduction in SVs within 300 nm of the active zone at central synapses in *vglut1* knockout mice (Fremeau et al., 2004b), and indicates a role for Vglut3 in synaptic vesicle biogenesis and/or trafficking, even though Vglut3 is not the sole component required for these processes in HCs. It remains to be investigated if this function depends on glutamate loading of SVs, or if it is mediated by protein-protein interaction with other factors.

We speculate that if Vglut1-containing SVs are sorted to the synapse independent of Vglut3 and account for the remaining SVs that we observe at the *asteroid* mutant HC synaptic ribbon, we should be able to record electrical activity at the postsynapse in response to residual glutamate release from *asteroid* mutant HCs. In this scenario, we would expect altered kinetics of vesicle release compared to wild-type, either because of the reduced SV pool or because of distinct Vglut1-containing SV pool kinetics. In contrast, if Vglut3 is required for the generation and/or trafficking of mature, glutamate-loaded SVs in HCs, we should not record evoked postsynaptic currents from *asteroid* mutant larvae. These data could be complemented by semi-quantitative immunolabeling of glutamate in HCs, where we would expect the strongest label in the wild-type, intermediate label in *asteroid* mutants and little to no label in HCs of *asteroid* mutants with *vglut1* knock-down. Recent data supplied by Daniels et al. indicates that a single Vglut molecule is sufficient to load a SV with glutamate (Daniels et

al., 2006). Interestingly, in their landmark study, Takamori et al. report that on average, we can expect a stoichiometry of 1-3 Vglut molecules per SV (Takamori et al., 2006). If SV protein distribution during biogenesis/ recycling is a stochastic process, set on average to generate SVs with an excess of (two) Vglut copies, this would provide a failsafe mechanism *in vivo*, which could save *asteroid* carrier siblings from a gene-dosage effect. However, the data from Takamori et al. could also be interpreted such that there is always only one Vglut copy per SV, for which there would then likely be a molecular quality control checkpoint of some sort, and the range of 1-3 copies/SV simply signifies a limit of accuracy in the mass spectrometry experiment. In this case, Vglut1 might be more stable in *asteroid* carrier siblings, or the transcription level of *vglut1* is not a bottleneck in Vglut1 production. Combining our *in situ* and qPCR data, perhaps neither *vglut1* nor *vglut3* can be up regulated in *asteroid* HCs because expression is already at the maximum in the wild-type. Of course, *vglut1* and *vglut3* gene regulation might simply be independent from one another, and *vglut1* expression levels therefore immune to changes in *vglut3* expression, and *vice versa*. The traditional argument against gene dosage would be that *asteroid* is a recessive mutation, and there appears to be little to no behavioral difference within the sibling group, at least under the conditions observed. Also, statistical analysis (S. Wolfson, personal communication) shows no significant difference between individuals in the sibling group in terms of readily-releasable pool- or ribbon size. It would be interesting in this regard to look at the reserve pool size between individuals of the sibling group, in order to rule out a behaviorally neutral bottleneck at the translational level for *asteroid* carriers leading to a reduced reserve pool size that is not apparent in the release kinetics observed under physiological stimuli.

For further analysis of the effect of Vglut3 on SV recycling in HCs, we propose the expression the N- or C-terminus of Vglut3 for a dominant-negative effect on Vglut3 sorting, if the respective part of the protein is involved. Ideally, we would construct a hybrid *myosin6b* promoter, which includes a small molecule (e.g. Tetracycline or Ecdysone) control element, thus generating an inducible HC-specific promoter (Chang, 2007). A transgenic line expressing parts of *vglut1*

or *vglut3* in HCs under this promoter would be equivalent to a conditional knockout mutant, which might be useful in a number of physiological experiments. The peptide could also be tagged with a GFP-moiety for localization, and even pulse-chase experiments in the live animal are possible by using photoconvertible protein tags (Schafer et al., 2006). Vglut3 and Vglut1 secretion kinetics at the HC synapse could be characterized by creating transgenic lines expressing *myo6b:vglut1/3-phlourin*, and analyzing SV exocytosis by two-photon microscopy, similar to experiments done with *vglut1* by Voglmaier et al. in cultured Δ VGLUT1 neurons (Voglmaier et al., 2006). In order to address putative differential sorting of Vglut1 and Vglut3 into distinct SV pools, we envision the generation of molecular chimeras between *vglut1* and *vglut3*, and using rescue of *asteroid* mutants as a functional readout.

Through our experiments, we learned much that may be applicable to all vertebrate HC synapses, yet we find some indications for significant differences between teleosts and mammals in terms of Vglut3 utilization. In rats, VGLUT3 is present in vestibular sensory epithelia cells and in afferent fibers in the maculae and ampullary cristae (Wang et al., 2007). In addition, VGLUT3 expression has been described for the hippocampus and cortex (the striatum, caudate-putamen, the olfactory tubercle, the nucleus accumbens, the interpeduncular nucleus and the dorsal and medial raphe nuclei, (Herzog et al., 2004). VGLUT3 expressing neurons are scattered and include serotonin and possibly dopamine neurons, cholinergic interneurons, and GABAergic interneurons (Seal and Edwards, 2006b), which, according to the authors, suggests an “unsuspected function” of vesicular glutamate transport in some interneurons and in neuromodulatory neurons. In stark contrast to the data obtained from rat, our *in situ* hybridization and immunohistochemistry data show that *vglut3/Vglut3* appears to be exclusively expressed in HCs of the ear and lateral line organ in developing zebrafish larvae. Perhaps Vglut3 acts as a vesicular glutamate transporter with transporter properties specifically fit for high-throughput synaptic activity? We are now ready for a more detailed functional analysis of Vglut3.

4.2 *synaptojanin 1* in the Zebrafish Hair Cell

We characterized the *comet* mutant from the 2000 Tübingen mutagenesis screen. *comet* encodes the lipid phosphatase *synaptojanin 1* (*synj1*), which plays an important role in CME by modulating the PI lipid composition of the membrane undergoing endocytosis (Cremona and De Camilli, 2001). *comet* mutant larvae display a balance defect that increases in severity over time of HC stimulation, perhaps due to insufficient SV recycling. We sequenced three alleles of *comet/synj1*, all of which encode severe truncations that presumably manifest as *functional null* mutations, and all of which display identical phenotypes under the conditions tested. The allele IG459 encodes a donor splice site mutation of exon2, which contains the start-of-translation codon, ATG. This is predicted to lead to the complete elimination of Synj1 protein in IG459 mutant larvae, and the identity of behavior between IG459 and other *comet* alleles represents an important piece of circumstantial evidence for our claim of *comet* being functionally *null*.

There are currently copious amounts of literature concerning *synj1* available. Yet, neither the exact function or timing of Synj1 action, nor the greater role of Synj1 in the regulation of SV turnover and other processes at the synapse are fully understood. In addition, the molecular players of fast and slow endocytosis at the ribbon synapse have not yet been identified. In this study, we attempted to use the *comet* strain of zebrafish to help address the mechanisms underlying SV recycling in HCs, with a particular focus on CME.

A number of splice variants are proposed for *synj1* in rat, including a Δ SAC variant (Woscholski et al., 1998). This variant was claimed to lack the original N-terminus of Synj1, including the SAC domain, and encode a shorter protein that starts with the 5-phosphatase domain instead. While we find several new minor splice forms from direct sequencing, we detect no such variant in zebrafish (not shown). In addition, since the original claim, there has not been further report in the publication record. Perhaps then it is also interesting that *Synj2*, a paralogue of *Synj1* in mammals (Malecz et al., 2000), does not appear to be present in zebrafish (this study, data not shown). Note that the possibility of

partial functional compensation for *synj1* in its absence through other lipid phosphatases still exists.

synj1 expression has been proposed to be ubiquitous to low levels for *synj1-170*, and *synj1-145* is highly co-expressed in the nervous system in addition (Ramjaun et al., 1996). In this study, we confirm the expression of *synj1* in the CNS in zebrafish larvae and in addition show its expression in HCs of the ear by *in situ* hybridization. Apparently, we detected a particular form of *synj1-145* mRNA, since we do not observe labeling in outside the brain, ear or the lateral line ganglia. However, our result shows *synj1* expression in HCs, and warrants investigation of the role of HCs in the *comet* phenotype.

Interestingly, the *comet* mutant phenotype was not replicated using morpholino-mediated knockdown of the short splice variant of *synj1*, *synj1-145* alone, whereas injection of a translation-blocking morpholino against *synj1* does appear to produce a true phenocopy. Phenocopy by knockdown of total *synj1* at the translational level is expected, as this would indirectly replicate our IG459 allele *comet* mutant. However, failure to phenocopy the *comet* mutant by a *synj1-145*-specific morpholino is surprising, since *synj1-145* is highly enriched in the wild-type nervous system (Ramjaun et al., 1996), and is thought to act in a different step of endocytosis than Synj1-170 (Perera et al., 2006). The rationale behind this experiment is to suppress the inclusion of exon30 by forcing its skipping during mRNA processing by masking its donor splice site, therefore leading to the generation of the *synj1-170* splice variant only, presumably without the reduction of the gross level of *synj1*. This would give insight into two questions: a) does Synj170 compensate for Synj1-145 at the synapse? and b) since Synj1-170 and Synj1-145 have identical enzyme activities and both interact with Endophilin for localization (Schuske et al., 2003), what is significant to the short splice variant?

At first glance, it appears as if morpholino knockdown of Synj1-145 is without effect on hearing or balance in zebrafish larvae. Furthermore, the efficacy of 145MO is substantiated by our quantitative PCR data, showing what amounts to complete suppression of *synj1-145*, as measured by the presence of exon30

in *synj1* transcripts, and a 2-fold increase of the amount of *synj1-170* mRNA. The comparatively small increase in *synj1-170* levels might be explained by the fact that *synj1-145* is only expressed in the nervous system, whereas *synj1-170* is expressed ubiquitously. Even though recent TIRF microscopy data has shown that Synj1-145 and Synj1-170 are normally recruited into the endocytic process at different time points (Perera et al., 2006), this result indicates that *synj1-170* may compensate for *synj1-145* in our behavioral test.

However, this interpretation does not account for the drastic (around 7-fold) increase in overall *synj1*, as measured by the amplification of exon29, which is present in all known splice variants of *synj1*. On the technical side, great care was taken assure the validity of results (see section 5.2.1.12). Technical aspects aside, unless cryptic splicing within the small (24bp) exon30 occurs, it appears that 145MO injection induces up regulation of *synj1*, and suppression of exon30. But perhaps the morpholino leads to the accession of a cryptic splice site within exon30, or deletion of exon30 does not cause the generation of *synj1-170* as a consequence. To examine if this is the case, I propose a 3'RACE experiment to determine the nature of the *synj1* message composition in 145MO morphants. Also, if a Synj1 antibody was available, a western blot could shed light on which protein products are generated from the resulting messages. An alternative experiment for the relevance of *synj1-145* versus *synj1-170* would be to generate a transgenic rescue with *synj1-170* in an animal of the *comet* background. This could be achieved utilizing either the *myosin6b* promoter for HC-specific analysis or the *synj1* endogenous promoter, both of which I have cloned for this study (*synj1* promoter not shown).

In addition, transgenic animals would provide much needed functional evidence for Synj1 action resolved by isoform and/or domain. Perera et al. have reported that mutation of the 5-phosphatase domain of *synj1-170* leads to the arrest of endocytosis at the stage of clathrin-coated pits of transfected COS7 cells in cell culture, thus defining what amounts to an early checkpoint in CME (Perera et al. 2006). It would be highly informative to test this scenario in a transgenic animal, and assess behavior versus SV recycling at the HC synapse.

A battery of behavioral and electrophysiological tests for the whole animal are available, such as the balance test, optokinetic reflex (OKR) test, vestibulo-ocular reflex (VOR) test, recordings from the lateral line ganglion, etc.

In addition to our steps towards a domain-specific functional analysis of the *synj1* splice variants, we observe several defects at the HC afferent synapse. At the electron microscopy level, *comet/synj1* mutants show a decrease in synaptic ribbon diameter (*mutant*: 293 ± 83.4 nm vs. WT: 408 ± 108 nm) that accompanies a reduced number of ribbon-associated synaptic vesicles (*mutant*: 21.9 ± 12.3 vs. WT: 36.2 ± 6.4), while the packing density of the ribbon surface with SVs is comparable (this study). Wild-type ribbons tether a monolayer of synaptic vesicles at approximately 55% of the maximum packing density (Lenzi et al., 1999).

This result begs the question: what about the influence of *synj1* on ribbon formation and/or maintenance? Is ribbon assembly influenced by PI(4,5)P₂ levels, by cytoskeletal components that experience alterations due to the lack of *synj1* or by other, more indirect factors? Dickman et al. have reported a dependence of synapse spacing on endocytic proteins for the drosophila NMJ. Lack of Endophilin, Synaptojanin, Dynamin, AP180 and Synaptotagmin all lead to supernumerary “satellite” boutons in third instar larval NMJ (Dickman et al., 2006). According to Dickman et al., the generation of these boutons is not dependent on synaptic transmission per se, which the authors have previously characterized in these mutants, but on the presence of functional versions of the endocytosis factors they observed. According to Dickman et al., an endocytosis-dependent “spacing function” mechanism (Meinertzhagen et al., 1998) seems to developmentally control synapse density at the terminals of drosophila NMJs. However, this same function does appear to control zebrafish HC synapse formation, as we do not observe abnormal synaptic ribbon body numbers or changes in number or shape in the postsynaptic afferent bouton. In addition, Dickman et al. interpret the morphological changes they observe as compensatory, in order to maintain gross synaptic release as much as possible.

In the zebrafish *gemini* mutant, synaptic transmission is abrogated due to lack of the synaptic Ca^{2+} channel. Yet, HC synapse morphology appears normal (Sidi et al., 2004). We conclude that at least in terms of synapse formation and maintenance, *synj* mutant NMJs cannot be compared with *comet* zebrafish HCs. Homing and establishment of the *comet* HC afferent postsynapse, including refinement, do not appear to be impaired by the absence of *synj1* in zebrafish.

Little is known about ribbon synapse development or maintenance. In d5 *nrc/synj1* mutant photoreceptors, a percentage of ribbons are detached from the presynaptic membrane (Allwardt et al., 2001; Van Epps et al., 2004). The anchoring of ribbon bodies in mice presumably relies on Bassoon (Dick et al., 2003; Khimich et al., 2005). Perhaps Synj1 modulates the interaction between Bassoon and ribbon bodies, or proper ribbon assembly requires the presence of certain endocytic factors, or ribbon size might depend on endocytic capacity, which is impaired in *comet* mutants. Arguing against a dependence of ribbon size on endocytosis alone may be the fact that in the chick cochlea, the synaptic body diameter increases with increasing characteristic frequency (Martinez-Dunst et al., 1997), while we assume that endocytic capacity is the same between HCs. On the other hand, frog saccular HCs display about 20 large synaptic bodies irrespective of the cells' location in the end organ (Roberts et al., 1990; Lenzi et al., 1999; Lenzi et al., 2002). Perhaps ribbon diameter is determined by synapse activity? This could mean that *comet* HC synapses might be less responsive to stimuli and release fewer SVs than a wild-type HC to a stimulus of equal intensity.

In *comet* mutant HCs, we observe a reduced number of ribbon-associated synaptic vesicles. This can be interpreted as evidence for altered release kinetics, because the readily-releasable pool may have different kinetics of release than SVs recruited from the recycling pool (Moser and Beutner, 2000). We propose testing of this hypothesis directly by capacitance measurements of HCs, or indirectly by recordings of evoked action potentials from the lateral line ganglion. Delayed transmission or decreased action potential frequency in response to stimuli (decreased sensitivity) would be a novel finding.

In this study, we also describe the completely novel phenotype for loss of *synj1*; basal membrane blebbing. Basal blebbing is increased in response to stimulation in *comet/synj1* mutant HCs ($26.3 \pm 6\%$ unstim. vs. $42.6 \pm 21.5\%$ post stim.). Moreover, blebbing is suppressed in *comet/gemini* compound mutants that lack synaptic exocytosis due to the absence of the presynaptic Ca^{2+} -channel Cav1.3 (Sidi et al., 2004). Further supporting the hypothesis that uncoupling of exocytosis and endocytosis causes this phenotype is the observation that interfering with endocytosis by exposing larvae to Latrunculin A phenocopies blebbing in wild-type HCs. Finally, we find no indications that the cytoskeleton is actively involved in blebbing- we detect no aggregation of actin in blebs. We conclude from our data that HC blebbing depends on presynaptic activity, and that the source of the bleb's membrane is likely the SV pool, even though we do not see an obvious redistribution of clathrin or of SV protein to the plasma membrane.

Our immunofluorescence data for putative SV proteins may or may not be significant in this regard. While we do not observe obvious aggregation of clathrin, for example, it must be said that this concept comes from electron microscopy data, and a statistically significant increase of clathrin-coated pits and endocytic intermediates need not reflect a large number. For example, Cremona et al. observe an increase in the percentage of clathrin-coated vesicles from 2% of total SVs in the wild-type to 10% at the *synj* mutant synapse (Cremona et al., 1999). We may have missed existing differences in the pattern of clathrin patches at the cell surface simply because of a lack of lateral resolution: the scale of our cells (3 μm diameter, pear-shaped), whereas, for example, Perera et al. used COS7-cells, which were approximately planar and often 100 μm or more in diameter (Perera et al., 2006). Otoferlin A and Vglut3, on the other hand, may be so abundant in the HC that the point spread function alone, which marks a diffraction limit and thus a minimal vertical resolution of light microscopy, may have prevented the observation of a moderate but significant redistribution of protein from the cytoplasm to the plasma membrane. Alternatively, our stimulation protocol may not have depleted the HC recycling pool sufficiently, or

blebbing might be caused by activity-dependent Ca^{2+} influx at the *comet* mutant synapse without requiring a major redistribution of membrane from the SV pool. Such a result could offer evidence against the importance of CME for HC SV recycling, and at the same time might indicate a role for Synj1 in other pathways. While our study falls short of proving that the SV pool is the origin of the blebbing membrane, Lenzi et al. have argued from their capacitance measurements and EM serial reconstructions of frog saccular HCs, that after strong stimulation about 75% of the SV membrane is accounted for by endosomal structures and invaginations (Lenzi et al., 2002). In this light, our blebbing phenotype in *comet/synj1* mutant HCs can yet be explained as due to uncoupling of exocytosis and activity-dependent membrane retrieval (compensatory endocytosis).

However, what is the role of CME in HC SV recycling? Like in other neurons, there are endocytic processes with at least two different time courses, according to the strength of the stimulus (Beutner et al., 2001). The slow time course, observed during capacitance measurements in mouse inner ear HCs in Ca^{2+} -uncaging experiments for low $[\text{Ca}^{2+}]_i$, has a time constant of about 15 s, while the fast time course has a time constant of approximately 300 ms and was observed for high $[\text{Ca}^{2+}]_i$.

The current view of SV recycling in ribbon-synapse containing neurons is that differing amounts of CME versus non-CME and bulk endocytosis occur in different ribbon synapse cells. Photoreceptors probably show a major contribution of CME (LoGiudice and Matthews, 2007) to their compensatory endocytosis. HCs appear to employ bulk endocytosis, CME and non-CME, perhaps in order to increase the available membrane surface for SV biogenesis. Experiments with microperoxidase uptake from goldfish indicate that retinal bipolar cells also use bulk endocytosis when stimulated, since the majority of label is found in endosomal structures and coated vesicles are very rarely observed. In comparison, photoreceptors distribute much more of the label into SVs (LoGiudice and Matthews, 2007). Unfortunately, since HC *in vivo* are deeply embedded in supporting tissue and cannot easily be cultured because of their metabolic sensitivity, accessibility issues have so far prevented similar

experiments in HCs, though with explanted bullfrog HCs, they are a theoretical possibility. A contrasting view is that bulk endocytosis alone is slower than CME plus non-CME. Van Epps et al. observed large endocytic structures unusual to photoreceptors due to the lack of *synj1*, while bipolar cells were almost unaffected (Van Epps et al., 2004). This data could be interpreted as the result of a switch from rapid to slow compensatory endocytosis in the affected cells. In this scenario, bipolar cells would be able to “sit out” a bottleneck in endocytosis due to their very large reserve pool (>600,000). This would make a HC synapse a hybrid between that of a photoreceptor and a bipolar cell, since HCs have a similarly large SV pool as bipolar cells, yet cannot rely on their SV reserves alone because their exocytosis rates (up to 1000/s per ribbon, up to 20 ribbons/HC in frog saccular HCs (Roberts et al., 1990) would quickly deplete the SV pool.

Interestingly, when CME is inhibited in goldfish bipolar cells by dominant negative peptides or proteins, the fast phase of endocytosis, as measured by membrane capacitance, is largely unaffected (Jockusch et al., 2005). However, it quickly saturates and is insufficient to compensate for exocytosis. Jockusch et al., conclude that CME must be responsible for the slow phase of endocytosis. Yet according to LoGiudice and Matthews, EM data do not show sufficient clathrin-coated intermediates to support this hypothesis (LoGiudice and Matthews, 2007). In addition, LoGiudice and Matthews point out that many of the previous capacitance measurements may have been skewed by induced changes in intracellular osmolarity or hydrostatic pressure, which apparently can modulate the slow component of endocytosis.

Perhaps some of the confusion about the slow and fast components of compensatory endocytosis stems from the fact that bulk endocytosis is broadly viewed as an emergency mechanism for membrane uptake in neurons (Royle and Lagnado, 2003). Selective strength of stimulation in frog motor nerve terminals shows fast or slow uptake of FM-dye into different vesicle pools (Richards et al., 2000). In contrast, FM-dye and peroxidase uptake experiments under selective stimulation protocols, Ca^{2+} monitoring and block of cdk5 in primary neuronal cultures suggests that, in central nerve terminals, bulk

endocytosis may be a regular Ca^{2+} -dependent uptake mechanism with fast kinetics and rapid activation upon stimulation (Evans and Cousin, 2007a; Evans and Cousin, 2007b; Clayton et al., 2007). If bulk endocytic effectors are indeed members of the dephosphins, meaning that they are activated by calcineurin during synaptic activity, bulk endocytosis would easily fit into the current model of synaptic compensatory endocytosis. However, since the assumed dwell time of a recycled SV in the endosomal pathway is 10-15 minutes (Clayton et al., 2007), this may not explain the assumed rapid rejoining of the releasable pool demanded by a HC. It would be interesting to determine if the reactivation of a SV recycled by bulk endocytosis is faster in a HC. However, this would first require the dissection of extant SV recycling pathways in HCs. To do so, we could block CME selectively (see below), then stimulate HCs expressing SV markers like VAMP, Vglut1 or Vglut3 as fusion proteins with pHlourin (pH sensor) and/or Kaede (light-induced switch in emission wavelength) for tracing vesicles. In this two-pronged approach, we would measure the fluorescence intensity of VAMP-pHlourin in a HC at rest. We would then stimulate the HC, perhaps with a water jet, and monitor the rise and decay of fluorescence, as recycled SVs reacidify. The results of this experiment would include the presupposition that SV luminal acidity correlates with a reentry into the recycling pool. Similarly, we could perform a light-activated pulse-chase of SVs, and trace their cycling. Using these tools, wild-type HCs could then be compared to *comet* mutant HCs, or wild-type HCs in which we chemically interfere with different endocytosis pathways. For example, in order to show the importance of compensatory CME in HCs, we first propose morpholino-mediated knockdown of Dynamin 1, which provides most of the synaptic Dynamin function (Ferguson et al., 2007). In a mouse model, elimination of *dynamin 1* does not cause prenatal developmental defects (same study). Therefore, we should be able to analyze HC function in d5 larvae. We expect to observe a balance defect similar to that of the *comet* mutant. Hearing would likely be subtly affected, and may only be distinguishable from wild-type by electrical recordings. Since SV recycling is severely impaired in synapses lacking Dynamin 1, we would test for HC blebbing in Dynamin 1

morphants. Analysis of the SV marker distribution might observe SV pool depletion (by EM) and perhaps an increase in bulk endocytosis in these larvae.

Alternatively, or perhaps in addition to a Dynamin 1 knockdown, we could apply non-hydrolysable forms of GTP or GDP ($\text{GTP}\gamma\text{S}$, $\text{GDP}\gamma\text{S}$) to inhibit CME by titrating out all Dynamin action. Similarly, we could apply $\text{ATP}\gamma\text{S}$ to block clathrin-mediated compensatory endocytosis to determine the contribution of bulk- and clathrin-independent endocytosis to compensatory endocytosis in HCs. We could drive expression of a dominant negative clathrin heavy chain fragment (Liu et al., 1998) with our HC specific *myo6b* promoter, or with a heat-shock inducible promoter in a transgenic line, or with our to-be-constructed repressible *myo6b* promoter (transiently or as a transgenic line). With these larvae we would then perform the same battery of tests as above, before and after stimulation. Finally, we could fuse VAMP to Kaede, and perform pulse-chase experiments to determine time courses of SV membrane uptake when specific endocytic pathways are blocked.

Furthermore, we could determine if Vglut1 and Vglut3 are sorted into distinct SV pools by different endocytosis pathways by co expressing *myo6b:vglut1-gfp* and *myo6b:vglut1-mRFP* in HCs, for example. We could then selectively block different endocytic pathways as described above and observe any potential segregation. These data could be backed up by immunofluorescence labeling with our anti-Vglut3 (and anti-Vglut1, once available) antibody or immuno-EM. In all cases, recording of evoked action potentials from the posterior lateral line ganglion should predict the efficiency of transmission at the HC afferent synapse.

In conclusion, a summary of our perception of endocytosis at the zebrafish HC synapse in a model is provided in Figure 38. Drawing from the recent landmark paper from (Ferguson et al., 2007), we speculate that three modes of endocytosis are present at the HC synapse. During a weak stimulus, slow, mostly Dynamin 2, but also Dynamin 1/3 (depending on the availability of Ca^{2+}) dependent CME take place. During a strong stimulus, Dynamin 2 is silenced by high $[\text{Ca}^{2+}]$, and both fast, Dynamin 1/3-dependent CME as well as bulk endocytosis occur. Bulk endocytosis appears as fast, because it takes up considerable amounts of membrane quickly. However, it quickly saturates. Dynamin 1-mediated endocytosis is faster than Dynamin 2, and operates with different accessory proteins (AP180, etc.). The vesicles endocytosed by Dynamin 1/3 mostly follow the AP2 pathway and return to the recycling pool directly, some get sorted into the AP3 pathway and are trafficked to endosomal intermediates. Membrane and protein from bulk endocytosis forms endosomal intermediates and is slowly processed AP3-dependently into SVs.

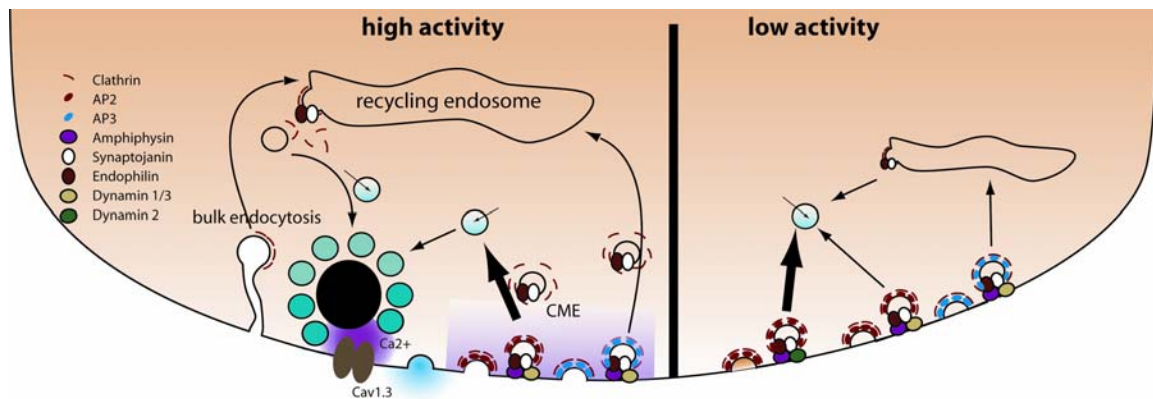


Figure 38. Schematic of putative synaptic vesicle turnover at the HC ribbon synapse. *Left:* High activity (high $[\text{Ca}^{2+}]$) scenario. SV endocytosis is mostly clathrin- and Dynamin 1-dependent, with a significant contribution by bulk endocytosis. Vesicles are sorted into both the AP2 and AP3 pathway. *Right:* low activity (low $[\text{Ca}^{2+}]$) scenario. SV endocytosis is mostly clathrin- and Dynamin 2-dependent, with a no contribution by bulk endocytosis. Vesicles are sorted into both the AP2 and AP3 pathway.

4.3 Concluding Remarks

HC ribbon synapses are high-performance chemical synapses that are closely tied to the senses of vision, hearing, and balance. Much research has yet to be done to understand the remarkable transfer properties of these synapses, but also their development and maintenance. Ribbon synapses have a number of structurally and molecularly unique features, such as the ribbon body itself, but also an apparently unique protein complement that acts in SV generation, trafficking, secretion, and recycling. What is more, there is growing evidence of the existence of unique differences between ribbon synapses of different cell types, such as photoreceptors, bipolar cells, and even different types of HCs. Indeed, perhaps the molecular variety between synapses is a general principle in biology. In this study, we have employed the strategy of forward genetics to identify and begin to characterize *synj1* and *vglut3* in HCs, and we are confident that many more molecular players in HCs will be identified in this way. In addition, we generated a set of tools that will allow us to further dissect the functional characteristics of HC ribbon synapses.

synj1 and *vglut3* occupy key positions in the synaptic vesicle cycle, one as traffic controller, the other one as functional vesicle marker. We can now optically trace these molecules and tie their observed molecular roles to a functional examination of the electrical transfer properties of the HC afferent synapse, and then compare these data to vertebrate animal behavior. In other words, in a genetically tractable vertebrate, we can now examine the senses of hearing and balance along the entire dynamic range from single molecule to the whole animal.

5 Materials and Methods

5.1: Materials

All standard chemicals and reagents were purchased from either Sigma-Aldrich (Saint Louis, MO, USA), Invitrogen (Carlsbad, CA), Fischer Scientific (Hampton, NH, USA), ISC Bioexpress (Kaysville, UT, USA) or VWR (West Chester, PA, USA). QIAquick PCR Purification Kit, QIAquick Gel Extraction Kit and QIAprep Spin Mini Prep Kit from QIAGEN (Valencia, CA, USA); GenElute Plasmid Maxiprep Kits from Sigma-Aldrich (Saint Louis, MO, USA); electron microscope film from Kodak (Rochester, USA); Donkey and Goat serum from Hyclone, Fisher Scientific.

5.1.1: Enzymes and kits

Restriction enzymes, Antarctic (alkaline) phosphatase, Klenow fragment, Mung bean nuclease and the corresponding buffers were purchased from New England Biolabs (Beverly, MA, USA); T4 Ligase from Fermentas (Glen Burnie, MD, USA), ExoSAP from USB (Cleveland, Ohio, USA). BD Advantage polymerase mix, the RT-for-PCR kit and the Marathon cDNA kit were from BD/Clontech/Takara (Madison, WI). The GeneRacer and SuperScript III kits were from Invitrogen. Phusion was from FinnZymes (Espoo, Finland), Herculase II from Stratagene (Cedar Creek, Texas, USA). GeneRuler 100bp and 1kb DNA ladders from Fermentas. Other kits used were Mini “Qiaprep”, Midi and Maxiprep kits “HiSpeed” (Qiagen); TOPO TA and TOPO Zero Blunt Cloning Kit (Invitrogen); QuickChange Mutagenesis and QuickChange II XL (Qiagen); QIAquick Gel Extraction and PCR cleanup kits (Qiagen); GeneClean II kit (Q-BIOgene Carlsbad, CA, USA). MicroPoly(A)purist (mRNA isolation kit), and the Megaclear RNA cleanup kit were from AMBION (Austin, TX, USA), as were the mMessage Machine T7 and SP6 *in vivo* mRNA transcription and poly(A) tailing kits. SP6/T7 *in vivo* transcription kit for biotinylated *in situ* probes was from Roche, as were the DIG Wash and Block Buffer set (1 585 762), 20x SSC (1666681), and BM Purple substrate. The ProLong Antifade Kit (P-7481) was from Invitrogen: Molecular Probes.

5.1.2: Primers and oligonucleotides

Primers for cDNA cloning, subcloning and sequencing were ordered from either Invitrogen (Carlsbad, CA, USA) or Integrated DNA Technologies (Coralville, IA, USA). PCR primers were dissolved in ddH₂O to 20 μM, or 100 ng/μl for SDM primers or oligos. PCR was carried out with a variety of polymerases, most commonly the BD Advantage Taq DNA Polymerase Mix (BD Biosciences, San Jose, CA).

The most important primers were:

PRIMER NAME	PRIMER SEQUENCE (5'-N-3')
Common sequencing primers	
M13F (TOPO)	TGT AAA ACG TGC CGG TC'
M13R (TOPO)	CAG GAA ACA GCT ATG AC
M6BP_F	GAT TTG CAT TCT TGT CTG CG
cPCR (EGFP_seqR)	CTG GAC GTA GCC TTC GGG CAT G
mCherry cPCR	GCG CTC CCA CTT GAA GCC CTC
Genotyping primers	
<i>comet</i> IG459 (genomic)	
IG459SEQ 2_3 F	CCA CAA CCC CTG TGT CAT TTG CTT TAT ATG
IG459SEQ 2_3 R	GTT ATG AAA ACA AAC AGA ATT AGC AAG TAC CCG C
<i>comet</i> HT039 (genomic)	
IG459SEQ_23_25F	AAGGCAACCATGCCTAGTGAGAGTACACCC
IG459SEQ_23_25R	CAGACAGACAGAGATTACATAGTGTTACCCCA
<i>comet</i> JV039 (genomic)	
IG459SEQ 8_9 F	ACAGTAATCTTTATCTATTTCTGAGAAATCGAAAAGCTTT
IG459SEQ 8_9 R	TCACAGTAAAATTGTACCGAAGTCCCTTGAAAAAC
<i>asteroid</i> IJ001 (genomic)	
vglut3 I1X2_F (WT specific)	GCTGAACTGTAAGGAGAATAATATCACCTTACTCCC
vglut3 I1X2_R (WT specific)	CCGTATACCGTGAAACCGTCAAACCGT
vglut3_I1 6F (mut specific)	TCCGTTATCTGACAGATAGAGGACAAAGCAAAGA

vglut3_I2 1R (mut specific)	ATTAACATGAGAGAGGAACGGAAATCTCATTTT
vglut3 partial CDS (Nterm)	
<i>vglut3</i> cl F1.2 (FWD)	AGTCCAGTGCAGGAGAGGATGCG
<i>vglut3</i> R2N (REV)	CGCACAAACATCACACAACCATAGTGAACC
Site-directed mutagenesis Primers	
phosphatase dead mutants of <i>synaptojanin1</i>	
IPPc_D838G_F	GGCAGAGCTGAGCTGAAAACATCTGgTCACAGACCTGTGGTGGC C
IPPc_D838G_R	GGCCACCACAGGTCTGTGAcCAGATGTTTTTCAGCTCAGCTCTGCC
SJIPPc_PDR_AAG_F	GCCGCA CAg CGG CCT GGA CCG cCg GTG TGC TGT GGA AAA G
SJIPPc_PDR_AAG_R	CTTTCCACAGCACACcGgCGGTCCAGGCCGcTGTGCGGC
SJSAC_CS_F	CTGGCTTCTGAGATTGATGTcTGGTGGCGTGGAGATCCGCACC
SJSAC_CS_R	GGTGCGGATCTCCACGCCACCAGACATCAATCTCAGAAGCCAG
Oligonucleotides:	
FMD-A12 V2A/B sequence for peptide self-cleavage ("next-gen IRES"), Agel	
Agel-PV GSGLLNFDLLKLAGDVESNPGP -Agel	
FWD- ACCGGT cggaagtggattattaaacttcgacttattaaagtagctggagacgttgagagtaaccctgg ACCGGT	
REV- ACCGGT ccagggttactctcaacgtctccagctaactttaataagtcgaagttaataatccactccg ACCGGT	
T7_SJ1_5UTR_Kozak	
tttgaattc TAATACGACTACTATAGGG agCTGTTCTTGAACCTACCTGCCCGCTAATCATTTTgT TTCTAGCCATATACGATATCCAACCGGGGCAAGACAGGCACAACCTCTGACAGGTCTGAAATA GGTTGTGTCGAGCCgccaccgaattctttt	
T7_SJ1_5UTR_Kozak RC	
aaaagaattcggtggcGGCTCGACACAACCTATTTTCAGACCTGTCAGAGTTGTGCCTGTCTTGCCC CGGTTGGATATCGTATATGGCTAGAAAcAAAATGATTAGCGGGGCAGGTAGTTCAAGAACAG ctCCCTATAGTGAGTCGTATTAgattcaaaa	
GAP43 membrane targeting oligo (for Klenow fill-in) "MLCCIRRTKPVEKTKPVEKNEE"	
G G>AATT<C tgCACGAAACC ATG CTGTGCTGCATCAGAAGAACTAAACCGGTTGAGAAGACTAAACCGGTT GAGAAGAATGAAGAG>gatc<c ACCGGT catg	
FWD GGAATTCTGCACGAAACCATGCTGTGCTGCATCAGAAGAACTAAACCGGTTGAGAAG	
REV CAT GAC CGG TGG ATC CTC TTC ATT CTT CTC AAC CGG TTT AGT	

5.1.3: Antisense Morpholinos

Morpholinos, targeting either start codons or splice sites were obtained from GeneTools, LLC (Philomath, OR) as lyophilized solids and resuspended in RNase-free ddH₂O to 2 mM. Injection solutions were made by diluting this stock with ddH₂O and KCl to final concentrations of 1 mM, 500, 250, 100 and 50 uM for MOs, and 2mM for KCl. Phenol red was added to a final volume of 5% as an injection tracer.

Morpholino	SEQUENCE
VG1-ATG	CGCGACTTTCAGGTCCGACCGG
VG1-ATG-C	GGCCAGCCTGAGCTTTCAGCGC
VG1-X2del	CAGCACTGATACTGACCACTATGAC
VG3-ATG	CCAGTGGCATCTCTCCTTCCCTTTC
VG3-ATG-C	CCAcTGcCATCTgTCgTTCCgTTTC
VG3-X2del	GCTGGCTAAACAATGCAAACATTAG
VG3-X2del-C	GCTcGgTAAAgAATcCAAAGATTAG
VG3-X2del2	ATTTATTTCTGGTTTCACCTGCATG
VG3-X2del2-C	ATTTtTTTgTGGTTTgACgTGgATG
p53 MO	GCGCCATTGCTTTGCAAGAATTG
Anti-SJ145MO	ATGACTTAATCCAGTACCTGTTAAC
SJ ATG MO	GATAACCTTTACTGAATGCCATG
SJ ATG ctrl	CATGGCATTTCAGTAAAGGTTATCGT

5.1.4: Plasmids and constructs

Basic constructs

pCDNA3.0 (Invitrogen):

Eukaryotic expression vector for constitutive expression; contains a CMV promoter and a T7 promoter, neomycin resistance cassette

pCRII-TOPO and pCR-Blunt II-TOPO (Invitrogen):

TOPO-cloning vector for “TA-cloning” of PCR products, contains a T7 promoter and an SP6 promoter. blunt-end PCR products, contains a T7 promoter and an SP6 promoter.

pEGFP-N1 (Clontech):

Eukaryotic expression vector for constitutive expression; it encodes the green fluorescence protein GFPmut1 variant which contains the double-amino-acid substitution of Phe-64 to Leu and Ser-65 to Thr. Genes cloned into the multiple cloning sites (MCS) will be expressed as fusions to the C-terminus of EGFP if they are in the same reading frame as EGFP. A Neomycin resistance cassette (Neo^R), consisting of the SV40 early promoter, the neomycin/kanamycin resistance gene of Tn5 and polyadenylation signals from Herpes simplex virus thymidine (HSV TK) kinase gene allows stably transfected eukaryotic cells to be selected for using G418.

pEGFP-N1 Δ CMV M6BP “pEGFP M6BP”:

modified version of pEGFP-N1 in which the CMV promoter was excised using the flanking *AseI* and *NheI* sites. These sites were subsequently filled in using *Klenow* fragment, polished using *pfu* polymerase, and ligated, thus generating the intermediate **pEGFP-N1 Δ CMV**. 6.5kb of the *myosin 6b* promoter (M6BP) were then inserted into the multiple cloning site using *SacI* and *EcoRI* sites.

pEGFP-N1 Δ CMV DEGFP M6BP td-tomato “pM6BP tomato”, or “ptom”:

modified version of pM6BP in which EGFP was excised and replaced by tandem dimer (td) DsRed fluorescent protein “tomato” a gift from Roger Y. Tsien (Shu X et al., 2006), using the *AgeI* and *NotI* sites flanking EGFP.

pEGFP-N1 Δ CMV DEGFP M6BP cherry “pM6BP cherry”, or “pCherry”:

modified version of pM6BP in which EGFP was excised and replaced by a modified DsRed fluorescent protein “mcherry”, a gift from Roger Y. Tsien (Shu X et al., 2006), using the *AgeI* and *NotI* sites flanking EGFP.

pEGFP-N1 Δ CMV Meganuclease M6BP “MN M6BP EGFP” , or “MN EGFP”:

modified version of pM6BP used to generate transgenic zebrafish. Meganuclease recognition sites were added upstream of the *myosin 6b* promoter and downstream of the SV40 poly adenylation site for digest prior or during injection.

pEGFP-N1 Δ CMV Meganuclease M6BP cherry “MN M6BP cherry” , or “MN cherry”:

modified version of pCherry used to generate transgenic zebrafish. Meganuclease recognition sites were added upstream of the *myosin 6b* promoter and downstream of the SV40 poly adenylation site for digest prior or during injection.

pEGFP-N1 Δ CMV Meganuclease M6BP td-tomato “MN M6BP tomato” , or “MN tomato”:

modified version of ptom used to generate transgenic zebrafish. Meganuclease recognition sites were added upstream of the *myosin 6b* promoter and downstream of the SV40 poly adenylation site for digest prior or during injection.

pEGFP SJP

modified version of pEGFP-N1 in which the CMV promoter was excised using the flanking *AseI* and *NheI* sites. These sites were subsequently filled in using *Klenow* fragment, polished using *pfu* polymerase, and ligated, thus generating the intermediate **pEGFP-N1 Δ CMV**. 6.5kb of the *synaptojanin1* promoter (SJP) were then inserted into the multiple cloning site using *AscI* and *EcoRI* sites. **Notably, this construct includes the *synaptojanin1* start codon upstream of the *EcoRI* site, leading to a translation of the multiple cloning site in frame 1.**

5.1.5: Fusion Protein Expression Constructs

-*xfp* could be either EGFP, mCherry or tdTomato.

mFruits are second-generation monomeric red fluorescent proteins (mRFPs) that have improved brightness and photostability compared to the first-generation mRFP1. The emission and excitation maxima are distributed over the remarkably large ranges of about 550-650 and 540-590 nm, respectively; however, the variations in the spectra can be traced to a few key amino acids. Spectroscopic and atomic resolution crystallographic analyses of three representatives, mOrange, mStrawberry, and mCherry, reveal that different mechanisms operate to establish the excitation and emission maxima. Evidently, they all undergo the second oxidation step to produce an acylimine linkage in the polypeptide backbone. In comparison to the progenitor DsRed, direct covalent modification to this linkage (mOrange) and indirect modification of the chromophore environment (mStrawberry and mCherry) produce strong blue- and red-shifted variants. The blue shift of mOrange is induced by an unprecedented covalent modification of the protein backbone. The electron-density map indicates the formation of a third heterocycle, 2-hydroxy-dihydrooxazole, upon the reaction of Thr 66 Ogamma with the polypeptide backbone, which in turn reduces the conjugation of the carbonyl at position 65 with the rest of the chromophore. In mStrawberry and mCherry, the movement of charged Lys 70 and protonation of Glu 215 are proposed to modify the chromophore electron-density distribution, inducing the red shift. pH-dependent spectral shifts of mCherry and mStrawberry appear to result from the titration of Glu 215, although, for mStrawberry, partial cyclization of Thr 66 may contribute at high pH.

myo6b:plcdPH-xfp

was obtained by inserting rat PLCd (AAP31521 [gi:30352160]) PH domain (aa 11-140) into pEGFP M6BP using the KpnI and BamHI sites of the MCS. This generated a fusion protein (PLCdPH-EGFP) that targeted PIP2 in the plasma membrane.

myo6b:GAP43-xfp

For membrane targeting, the sequence encoding the first 20 amino acids of zebrafish GAP43 (Kay et al., 2004) was generated from two overlapping oligonucleotides, which also contained a *Xenopus* β -globin ribosomal binding site. The oligonucleotides were annealed, filled in with Klenow Polymerase, digested and cloned into MN M6BP -xfp using EcoRI / BamHI sites.

myo6b:ribeye A-xfp

was obtained by inserting zebrafish *ribeyeA* full-length CDS (AY878349 [gi: 60459326]) into MN M6BP-xfp.

myo6b:ribeye B-xfp

was obtained by inserting zebrafish *ribeyeB* full-length CDS (lab records) into MN M6BP-xfp.

myo6b:ctfA-xfp

was obtained by inserting zebrafish *ctfA* full-length CDS (zgc:73358 and lab records) into MN M6BP-xfp.

myo6b:endo A-xfp

was obtained by inserting zebrafish *endoA1* full-length CDS (gb|BC045942.1] and lab records) into MN M6BP-xfp.

myo6b:synj1_170-xfp

was obtained by inserting zebrafish *synj1-170* full-length CDS (NM_001007030.1, GI:55742459 and note lab records!) into MN M6BP-xfp.

myo6b:synj1_145-xfp

was obtained by inserting zebrafish *synja-145* full-length CDS (NM_001007030.1, GI:55742459 and note lab records!) into MN M6BP-xfp.

myo6b:vglut1-xfp

was obtained by inserting zebrafish *vglut1* full-length CDS (lab records) into MN M6BP-xfp.

myo6b:vglut3-xfp

was obtained by inserting zebrafish *vglut3* full-length CDS (lab records) into MN M6BP-xfp.

expression marker	primers used
<i>myo6b:ribeye A-xfp</i>	FWD 5'-AGAATTCGATGAATGTTGATCTCCAGTAAGCAGTTGCCGATCG3' REV 5'-ATGGATCCCGGTATACATTTTGTCTTGCAGGCCGCC- 3'
<i>myo6b:bactin-xfp</i>	FWD 5'- AAGGGCGAATTCTGATGGATGAGGAAATC GCTGCCCT- 3' REV 5'-ACCGGTGAATTCCGGAAGCACTTCCTGTGAACGAT GGATG-3'
<i>myo6b:ctfA-xfp</i>	FWD 5'-CGAATTCTGATGGACGATTTTCGATATGCTCAGTGC-3' REV 5'-ACCGGTGGATCCCGGCCGACGAGCGGAGCCTG- 3'
<i>myo6b:endo A-xfp</i>	FWD 5'GGAATTCTGATGGATTTCAATGTCAAGAACTAGCGTCGGA3' REV 5'GGGGTACCGTGCTTAGAAGCTCCAGGTATGTGACAGGCACTT3'
<i>myo6b:GAP43-xfp</i>	FWD 5'- GGAATTCTGCACGAAACCATGCTGTGCTGCATCAGAAGAACT AAACCGGTTGAGAAG - 3' REV 5'- CATGACCGGTGGATCCTCTTCATTCTTCTCAACCGGTTTAGT- 3'
<i>myo6b:synj1_170-xfp</i>	FWD 5'-agaattcgatgaATGGCATTAGTAAAGGTTATCGTATTTATCAC- 3' REV 5'-cggtagcgcACCTGAGGATTGCTCCTGCTGTGTTGT- 3'
<i>myo6b:synj1_145-xfp</i>	FWD 5'-agaattcgatgaATGGCATTAGTAAAGGTTATCGTATTTATCAC- 3' REV 5'-gtggcgaccggtggACCTGAGGATTGCTCCTGCTGTGTTGTTGGA-3'
<i>myo6b:synbr1/vamp2-xfp</i>	FWD 5'- ATGTCTGCCCCAGATGCTGCC - 3' REV 5'- GGTAGTAGAAGTACATGAAAGCAATACCCAACAAGATGAT-3'
<i>myo6b:rab5A-xfp</i>	FWD 5'-AAGGGCGAATTCTGATGGCCAATAGGGGAGGAGCAA- 3' REV 5'-ACCGGTGGATCCCGGTTGCTGCAGCAGGGGGCT- 3'
<i>myo6b:vglut1-xfp</i>	FWD 5'- AAGGGCGAATTCTGATGGAGATCCGTCCGGACC- 3' REV 5'-AACCGGTGGATCCCGTGTGAGCTCTTTCTCCCTCTCC -3'
<i>myo6b:vglut3-xfp</i>	FWD 5'-GTGGCGACCGGTATGCCACTGGGGGGGTTTGC- 3' REV 5'GTCGACGGTACCGGTTGATACTGGGTCTGATATTCCCCATTTTCA3'

<i>myo6b:plcdPH-xfp</i>	FWD 5'-GAATTCTGATGGAACAAAACTCATCTCAGAAGAGGATCTG3'
	REV 5'-GGATCCCACTTCTGCCGCTGGTCCATGGA- 3'

5.1.6: Constructs for Antibody Generation

antibody peptide construct	primers used
pCRII_TOPO otoA 400	FWD 5'- CTGGATCGAAAAGCCATGCGTCTAG – 3' REV 5'- TGAAGGTGCCACGAGGGTG – 3'
pCRII_TOPO otoA 1000	FWD 5'- CTCTTGCCGAGGGTGTTCCATC – 3' REV 5'- CCATACATATTCACCCAAAGCCGGACC – 3'
pCRII_TOPO synbr1/VAMP2	FWD 5'- ATGTCTGCCCCAGATGCTGCC – 3' REV 5'- GGTAGTAGAAGTACATGAAAGCAATACCCAA CAAGATGAT-3'
pCRII_TOPO synj1 Nterm	FWD 5'- ATGGCATTTCAGTAAAGGTTATCGTATTTATCAC – 3' REV 5'- GCTTCTCAGTCTTCCCTCCTTTA – 3'
pCRII_TOPO synj1 Cterm	FWD 5'- AGGCCAAGAACATGAATGGAGTCCAA– 3' REV 5'- TTCTCTCAGTGAATCATTCTGGAAGGGAG– 3'
pCRII_TOPO RibA peptide	FWD 5'- TCCAGTAAGCAGTTGCCGATCGG – 3' REV 5'- ATGGTGCTTTCCGAGAGGCCCT – 3'
pCRII_TOPO RibB peptide	FWD 5'- GTGCGAGGCACGGTTCCTCCT – 3' REV 5'- CGTTCACCAGCTGAGGGCGGATA – 3'
pCRII_TOPO vglut3	FWD 5'- TATGCCACTGGGGGGGTTTGC – 3' REV 5'- GGTTGATACTGGGTCTGATATTCCCCATTTTCA – 3'

5.1.8: Fixatives used for EM sample preparation

- (1) 25% EM grade glutaraldehyde from Fisher
- (2) 10% paraformaldehyde freshly prepared (Sigma P1213)

Preparation of 10% stock solution of paraformaldehyde in aqua dest:

10 g paraformaldehyde were added to 75 ml aqua-dest and placed on a combined stirrer/heater in a fume hood. The temperature of the water bath should not exceed 65°C. The solution was kept under constant stirring until all paraformaldehyde had dissolved. It was titrated to pH 7.2. H₂O was added to volume of 100 ml. The solution was filtrated and finally stored in aliquots at -20 °C. Upon thawing the solution would remain white until heated. If it did not get clear, it was not used.

Stock-solution of 0.2 M phosphate buffer:

Buffer A: NaH₂PO₄·1H₂O = 27.6 g in 1000 ml aqua dest

Buffer B: Na₂HPO₄·7H₂O = 53.65 g or

Na₂HPO₄·2H₂O = 35.6 g or

Na₂HPO₄·12H₂O = 71.7 g in 1000 ml aqua dest.

Add 19 ml buffer A to 81 ml buffer B to get 0.2 M phosphate buffer, pH7.4. Check pH and if necessary add more of the appropriate buffer to get pH7.4

5.1.9: Antibodies

5.1.9.1: Primary antibodies

Table 5.2: Primary antibodies and conjugates

Antibodies	Raised in	clonality	dilution	source
RibB_Nterm aa133-483	rabbit	polyclonal	1:100 – 1:200	PTGlab
Synbrv1 aa1-143	rabbit	polyclonal	1:100	PTGlab
synj1_Nterm aa389-748	rabbit	polyclonal	1:100	PTGlab
OtofA_400 aa209-342	rabbit	polyclonal	1:100	PTGlab
OtofA_1000 aa409-545	rabbit	polyclonal	1:100	PTGlab
RibA_Nterm aa1-466	rabbit	polyclonal	1:100 – 1:200	PTGlab
synj1_170Cterm aa1302-1554	rabbit	polyclonal	1:100	PTGlab
anti acetylated tubulin	mouse	IgG2b monoclonal	1:1000	SIGMA
anti synaptophysin	mouse	IgG1 monoclonal	1:1000	SYSY
vglut3_Nterm	rabbit	polyclonal	1:100	PTGlab
vglut3_Cterm	rabbit	polyclonal	1:100	PTGlab
Anti-PIP2	mouse	IgG2b (monoclonal)	1:250	assay designs
phalloidin	NA	NA	1:500	Mol. Probes
Anti-GFP	mouse	IgG1K (mix)	1:500	
Anti-dsRed	rabbit	polyclonal	1:1000	ClonTech

5.1.9.2: Secondary antibodies

All secondary antibodies (coupled to) were purchased from Molecular probes.

Antibody	specificity	dilution	fluorophore
goat-anti-rabbit	rabbit	1:1000	Alexa488
goat-anti-rabbit	rabbit	1:1000	Cy3
goat-anti-rabbit	rabbit	1:1000	A647
goat-anti-mouse	mouse	1:1000	Alexa488
goat-anti-mouse	mouse	1:1000	Cy3
goat-anti-mouse	mouse	1:1000	A647

5.1.10: Common buffer stocks and solutions

(1) 20 X PBS

160g NaCl, 4g KCl, 28.8g Na₂HPO₄, 4.8g KH₂PO₄

(2) 10x TBE buffer

108g Tris base (1300 mM), 55g Boric acid (450mM), 9.3g EDTA (25mM); adjust to 1l with H₂O. Dilute 10-fold with H₂O to obtain 1x buffer, ready-to-use.

(3) 6x DNA loading buffer

-0.25% bromophenol blue, 0.25% Xylen Cynol blue, 30% glycerol in H₂O

(6) LB media

-1% (w/v) peptone, 0.5% (w/v) yeast extract, 170mM NaCl and pH adjusted to pH7.0 using 5N NaOH. Sterilize by autoclaving.

(7) LB/Amp or LB/Carb

100µg/ml ampicillin/carbenicillin in 1L of LB (1mL of 10mg/mLx stock)

(8) LB/Kan

50µg/ml kanamycin in 1L of LB (1mL of 5mg/mL stock)

(9) SOC

Purchase from Invitrogen or add the following to 900ml of distilled H₂O:
20g Bacto Tryptone, 5g Bacto Yeast Extract, 2ml of 5M NaCl, 2.5ml of 1M KCl, 10ml of 1M MgCl₂, 10ml of 1M MgSO₄, 20ml of 1M glucose. Adjust to 1L with distilled H₂O. Sterilize by autoclaving.

5.2: Methods**5.2.1: Methods in Molecular Biology**

Extraction and purification of plasmid DNA from *E.coli* were performed according to the manufacturer's instructions (Qiagen Maxiprep, Midiprep and Miniprep kits). All the standard methods of molecular biology that were not described in this chapter were performed according to Sambrook, Fritsch et al. 1989.

5.2.1.1: Ethanol precipitation of plasmid DNA

1/10 volume of 3M Sodium acetate, pH 5.2 and 2.5 volumes of 100% Ethanol were added to DNA. Solutions were mixed and incubated at -20°C for at least 30min or overnight before centrifugation at 13,000g for 20min. The resulting DNA pellet was washed twice with 70% Ethanol. The pellet was then air dried for 5 min and resuspended in water or TE buffer. DNA was stored at -20°C.

5.2.1.2: Agarose gel electrophoresis

To separate DNA fragments, 0.8%-2% agarose gels were used depending on fragment size. Agarose was dissolved in 1x TBE buffer, 1µg/ml ethidium bromide was added to the agarose solution, which was poured into a gel chamber. DNA samples were mixed with 6x loading buffer in a ratio of 1:6 before loading onto the agarose gel. Electrophoresis was performed in 1x TBE buffer at 150-160V until sufficient band separation was achieved.

5.2.1.3: DNA Restriction Digests

For analytical restriction digest of plasmid DNA, 10 units of appropriate restriction enzymes were used. 50 units of restriction enzymes were used for preparative digestions with starting DNA materials between 5-10 µg. For cloning of DNA fragments into desired vectors, the insert and backbone DNAs were digested with the appropriate restriction enzymes for 3 hours or overnight at 37°C, or appropriate different temperature. DNA fragments were separated by gel electrophoresis and purified via QIAquick gel extraction kit according to the manufacturer's instructions.

5.2.1.4: Alkaline phosphatase treatment

Before ligating the digested and gel purified DNA fragments, Antarctic phosphatase buffer was added to a final conc. of 1x and the vector backbone was treated with approx. 5units of Antarctic Phosphatase for 15 min (blunt or 3' recessed ends) or 1 hour (5' recessed ends) at 37°C. The phosphatase was then inactivated at 65°C for 5 min.

5.2.1.5: Ligation

Ligation was performed using 1 Unit of T4 ligase in a 10 μ l reaction. Different ratios of vector:insert were set up and incubated overnight at 16°C. For cloning of RACE PCR fragments into vector backbones, the TOPO-TA cloning was done according to the manufacturer's instructions. Taq Polymerase generated PCR fragments contained single deoxyadenosine overhangs at the 3'-end (dA-3') while the linearized pCRII vector possessed an overhanging deoxythymidine residue (dT-3'). This allowed efficient annealing of the PCR fragment to the vector, catalyzed by Topoisomerase I, which was covalently bound to the vector. Blunt PCR fragments generated by Pfu, Phusion[™] or Herculase[™], the Blunt Zero TOPO kit was used. For subcloning of the PCR fragments into different expression vectors, appropriate restriction digests were performed and fragments were purified as described above.

5.2.1.6: Polymerase Chain Reaction (PCR)

Standard PCR was performed using either 2x PCR Premix (Fermentas), a mixture of Taq and Pfu polymerases (BD Advantage polymerase mix). High-fidelity PCR was performed using the Herculase II system. PCR was set up in a 25 or 50 μ l reaction as follows:

2x PCR premix	BD Advantage	Herculase II
2x PCR premix	10x BD Adv. PCR buffer	5x Herculase PCR buffer
10-100ng template DNA or cDNA	10-100ng template DNA or cDNA	10-100ng template DNA or cDNA
20pmol/ μ l 5'- and 3'- primers each	20pmol/ μ l 5'- and 3'- primers each	20pmol/ μ l 5'- and 3'- primers each
NA	200uM dNTPs (10mM dNTPs stock)	250uM dNTPs (10mM dNTPs stock)
PCR grade water	PCR grade water	PCR grade water

PCR protocols were customized according to template length, primer melting temperature and the manufacturer's instructions.

5.2.1.7: DNA Sequencing

PCR amplicons were either sequenced directly from the PCR reaction following ExoSAP-IT (USB, Cleveland, OH) treatment to degrade amplification primers, or were first extracted from TBE-agarose gels with the QIAquick Gel Extraction Kit (QIAGEN, Valencia, CA) and then submitted directly for sequencing. Occasionally, gel-extracted PCR products were TOPO-cloned into either pCR-II or pCR-ZERO BLUNT (Invitrogen), followed by transformation into TOP-10 chemically competent DH5a *E. coli*. After plating, colonies were screened for the presence of insert by colony PCR, and positive colonies were inoculated into overnight cultures, minipreped (QIAprep Spin Miniprep Kit, QIAGEN), and submitted for sequencing. All sequencing was performed by Sequencing Core Facilities either at the Vollum Institute or the OHSU Department of Molecular and Medical Immunology.

5.2.1.8: Site-directed mutagenesis (SDM): Quickchange II XL

To generate point mutations in a plasmid, PCRs were performed using the *PfuUltra* high-fidelity (HF) DNA polymerase (2.5U/ μ l), dNTP mix and 10x reaction buffer supplied by the manufacturer (Stratagene). Templates were used together with the mutagenesis primers listed in 5.1.3. Sample reactions were prepared with 20ng of dsDNA template. Extension time was 1min/kb. The resulting PCR products were digested with 1 μ l of DpnI restriction enzyme (10U/ μ l) for 1 hour at 37°C to digest the parental supercoiled dsDNA. This was followed by transformation of XL1-Blue Supercompetent cells/ OneShot Top 10 cells via chemical transformation (5.2.2.0), as per the manufacturer's instructions (Invitrogen), using SOC media.

5.2.1.9: Isolation of mRNA and Genomic DNA from larvae

mRNA was isolated using the AMBION RNAPurist kit according to the manufacturer's instructions. Specifically, the dry weight of the larval tissue was treated as 1mg of tissue per larva for the purpose of estimating the volume of lysis buffer required. The volume was then rounded up to the next 50ul, and no less than 250ul were used. The lysate was then triturated through a 27-gauge needle, and mRNA extraction proceeded according to the manufacturer's instructions.

mRNA was precipitated over night at -20°C in NH₄Cl, glycogen and ethanol as recommended. After washing with 70% ethanol, the mRNA was then resuspended in 10-20ul of THE_RNA storage solution.

For genomic DNA extraction, larvae were incubated at 50° C in lysis buffer (10 mM Tris, 1 mM EDTA) in an Eppendorf thermomixer at 500 rpm. Protein was pelleted at 13,000 x g at 4° C, and genomic DNA was phenol/chloroform extracted from the supernatant and resuspended in ddH₂O or Tris-EDTA (pH 8.0).

5.2.1.10: Reverse Transcription of mRNA for PCR

Reverse transcription of mRNA was performed according to the manufacturer's instructions using either the RT-for-PCR kit (BD/Takara) or the Superscript III kit (Invitrogen). 1-4ul of purified mRNA were used, and either poly(d)T, random hexamer or gene-specific primers were applied.

5.2.1.11: Rapid Amplification of cDNA Ends (RACE)

RACE was performed according to the manufacturer's instructions (BD/Takara). 5' and 3' raceable single-strand cDNA libraries were generated from purified mRNA. Transcripts of interest were amplified using touch-down PCR with a gene-specific primer and a universal primer provided by the kit. Optionally, a second round of PCR was performed using a nested gene-specific primer and a nested universal primer (provided by the kit). In some cases, PCR products were TOPO cloned for later processing and/or sequencing.

5.2.1.12: Quantitative Real-time PCR (qPCR)

For qPCR, the Platinum SYBR Green qPCR SuperMix UDG was used on a MX3000P thermocycler from Stratagene. Cycling parameters were 40x (95°C,30"- 60°C,30" 72°C,30"), reaction size was 25µl. A dilution series of template over 3 orders of magnitude was prepared, and each dilution tested in triplicates with each primer. mRNA was selectively isolated to high purity and treated with DNaseI (Turbo, AMBION) before oligo(dT) primed reverse transcription (RT, Superscript III). cDNA was treated with RNaseH after RT. No-RT and no template controls were performed, which did not yield product. No primer dimer was observed in the melting curve after qPCR. To obtain the data for total *synj1*, we used a primer pair in exon 29. *gapdh* was used as an internal standard, and we define wild-type levels as "1-fold expression". To detect *synj1-145*, we used an exon-spanning primer pair E29-E30 (forward) and E30-E31 (reverse). To detect *synj1-170*, we used an exon spanning primer E29-E31 (forward) and a reverse primer in exon 31.

To obtain the data for total *vglut3/vglut1*, we designed primers spanning the respective exon3/4 borders. To detect *vglut3 exon2*, primers spanned exon1/2 and sat down within exon2.

GAPDH - AY818346	FWD 5'- GTGTAGGCGTGGACTGTGGT – 3' REV 5'- TGGGAGTCAACCAGGACAAATA – 3'
SJ145exon Set 4	FWD 5'- AGC CTG GAC TGG CAT CTC CAA A – 3' REV 5'- TAA CCT GAG GAT TGC TCC TGC TGT – 3'
SJ170_only Set 2	FWD 5'- CCA ACA ACA CAG GGC CAA GAA CAT – 3' REV 5'- TGT TCT GGA AGA GGG ATT GAG GGT – 3'
SJ1 Set	FWD 5'- AAG GCC TCA GAT GAC ATC ACC CAT – 3' REV 5'- TGA GGC ATC AGA GGA GCA GGT AA – 3'
vg1_Nt Set 1	FWD 5'- CTT TAA AGC CCA GGC AGG GAA A – 3' REV 5'- TGA CAG CTC GAT CGT CTC TCC ATT – 3'
VG3N Set 8	FWD 5'- AAT TGG GAT CCA GAG ACA GTG GGA – 3' REV 5'- ATG GCT GCT CCA AAC ACC CTG TTA – 3'
VG3 E2 Set 2	FWD 5'- TGG CTC AAA TGT GAC CGA AGA GGA – 3' REV 5'- TCC ACT GAG CAT GGC GAT GAT GTA – 3'

5.2.1.13: Transformation of competent cells

For transformations of chemically competent cells (One shot Top 10 cells, Invitrogen), cells were thawed on ice and 5ul of the ligation mixture was added to 50ul of competent cells. After 30 min on ice, cells were heat-shocked at 42°C for 30s and chilled on ice for 2 min. Cells were then incubated in 250ul of SOC media for 1 hour at 37°C, 220rpm. Cells were finally plated on either LB Ampicillin/Carbenicillin or Kanamycin plates and incubated overnight at 37°C.

5.2.1.14: *In situ* hybridization

Digoxigenin-labeled riboprobes were generated with the DIG Labeling Kit (Roche) from fragments of *vglut1* (nt 1-692), *vglut2a* (nt 1-797) and *b/c* (nt 789-2352), and *vglut3* (nt 1653-2445) cDNA that had been cloned into pCR-II (Invitrogen). *In situ* hybridization was conducted as previously described (Sollner et al., 2004) with 200 ng of probe in 300ul of Hyb+. Larvae at 72 hours post fertilization (hpf) were imaged on a Zeiss Axio bright-field microscope using a 10X or 20X dry lens objective. Images were acquired via an AxioCam MRc5 color digital camera using Axiovision software and exported as TIFF files to Adobe Photoshop for analysis.

5.2.1.15: Transformation of spontaneous affective disorder

For emergency mood transformation, 1x mood transformation buffer was prepared freshly and applied as necessary. All components were kept on ice. 1 can of lime concentrate was placed in a blender, and approximately 4fl. oz. of 38% EtOH “tequila” soln. were added, along with 1/2 can of “triple sec” soln. and three glasses of ice. The buffer was then homogenized in the blender, and aliquoted into available containers. Container rims were optionally decorated with freshly cut 1/4 lime segments, and mood transformation buffer was finally drunk slowly while counting to ten and enjoying the view of Portland by night.

5.2.2: Methods in Histology

5.2.2.1: Generation of antibodies

Rabbit polyclonal antibodies were generated with the assistance of PTGLAB, Chicago (IL). The peptide sequences were listed in Table (5.1). Briefly, all peptides were expressed as fusion proteins with a known antigenic moiety, presumably Keyhole Limpet Hemocyanin, in bacterial culture. 2 rabbits were immunized with each fusion protein after isolation. Antibodies were affinity purified and tested against the antigen in both Western Blot and ELISA.

5.2.2.2: Immunofluorescence Microscopy

Larvae were anesthetized in 0.02% MESAB (Tricaine) and prefixed for ~10min @RT in 4% Formaldehyde/PBS on a rocking table or rotisserie. They were then transferred to 4C, and fixed for >24h. They were then washed twice in PBST (0.1%) for 5 min each, and permeabilized O/N @4C in 0.5-2% Triton-X100. They were again rinsed twice with PBST (0.1%) and blocked in 1xFSGB 1-2hrs @RT or O/N. Following the blocking, larvae were incubated for 3-4hrs @RT or over night @4C with primary antibody in FSGB, washed 6x 20min with PBST (0.1%) @RT, incubated with secondary antibody for 3-4hrs @RT in the dark and again washed 6x 20min with PBST (0.1%) @RT, before they were mounted and analyzed.

For mounting of larvae, 1-4% of low-melting agarose was used to immobilize and orientate larvae on a microscopy slide. For confocal imaging, a type 1.5 coverslip was placed over the larva and the edges were sealed with nailpolish or topcoat.

ProLong Antifade Kit (P-7481) (Molecular Probes) was employed to mount samples for longer storage. Both primary and secondary antibodies were diluted in FSGB between 1:100-1:1000, with the dilution depending on the affinity of the antibodies. In general, all secondary antibodies were used in 1:1000 dilutions.

Larvae were examined using a Zeiss AxioImager.M1-microscope equipped with a Zeiss AxioCam MRm camera, controlled by Zeiss AxioVision software.

Confocal micrographs were taken by an Olympus BX51-Microscope using an Olympus PlanApo 60 x Oil immersion objective. Images were analyzed using AxioVision software (for fluorescence micrographs) and ImageJ/ NIH Image software and the UCSD suite of plugins for compatibility with the Olympus Fluoview software for confocal micrographs.

5.2.2.3: Alternate Protocol for Immunostaining

After 2-4hrs of fixation at 4 degrees C a methanol dehydration series (25%, 50%, 75%,100%) and rehydration series were performed on larvae 3dpf or younger. Blocking and antibody incubation periods were as above (5.2.4.1).

5.2.2.4: Protocol for Immunostaining of Cryosections

Embryos were fixed in 4% PFA/ PBS as above. Embryos were cryosectioned embedded in sucrose/ OCT or fish gelatin, and placed on “Ultrastick” (Fisher) slides. Optionally, and to minimize sample loss by detachment, slides with sections were desiccated in an airtight container at -20°C for two weeks. Sections were circled with a PAP pen (hydrophobic marker) and re-hydrated/ washed 2x 5 min in 1x PBS at RT. They were then placed in a humidified chamber and soaked in FSGB for 1-2h at RT. Incubation with primary antibody diluted in FSGB was for 2-4hrs at RT or O/N at 4°C, followed by three 15 min washed with 1x PBS at RT. Secondary antibody was diluted in FSGB and put on the slides in the dark for 2-4hrs at RT or O/N at 4°C. Another three 15 min washes in 1x PBS at RT were followed by a rinse step with H₂O. Optionally, anti-fade reagent was applied, the sections were covered with large type 1.5 coverslips, sealed, and kept in the dark until ready to view.

5.2.2.5: Staining of Phosphoinositides Using Specific Antibodies

Due to their lipidic nature, phosphoinositide species are highly susceptible to detergents. To obtain successful labeling, PBST was replaced with PBS in all steps of the sectional labeling protocol. Cryosections were not chemically permeabilized. Sections were then treated as described in 5.2.2.4.

5.2.2.6: Electron Microscopy

Day 5 larvae were euthanized with MESAB and fixed overnight in freshly prepared 3% glutaraldehyde with 1.5% paraformaldehyde in 0.1 M phosphate buffer. After rinsing with 0.1M phosphate buffer, larvae were stained with 1% osmium in 0.1M phosphate buffer for 1 h, rinsed again and dehydrated in an ethanol series (3 x 10 min. washes each of 50%, 80%, 95% and 100% ethanol). The larvae were then washed 2 x 30 min. with propylene oxide and incubated serially in two propylene oxide:araldite mixtures (1:1 and 1:3) before being transferred into 100% araldite for overnight incubation. The following day, the larvae were transferred in araldite to a casting tray, and the araldite was polymerized at 60° C for 48 hours.

Transverse sections were taken through embedded larvae on a microtome with a glass knife. 5 micron sections were taken until just past the eye, then three micron sections were taken into the ear. When the otolith of the anterior macula was visible in one or both ears, the blocks were handed to Jackie DeGagne at the OHRC EM Core for thin sectioning on an RMC MT-7000 ultramicrotome. 60-80 nm thin sections were transferred to a grid for imaging on a Phillips CM100 Electron Microscope. HC ribbons in the ear and neuromasts were imaged at 21,000X – 39,000X magnification.

Images were acquired on an analog camera and negatives were scanned into Adobe Photoshop at 1200 dpi. Image levels were adjusted as necessary to reveal synaptic vesicles close to the ribbon bodies.

5.2.3: Methods in Animal Husbandry

5.2.3.1: Zebrafish Maintenance and Breeding

All *D. rerio* strains are kept on a 14 hr/10 hr light/dark cycle. To obtain clutches of *comet* or *asteroid* larvae, previously separated ID (heterozygous) males and females were placed in a 1L tank with a grating just above the bottom and left overnight. Mating generally begins within 30 minutes of lights on. Embryos were collected by transferring the pair to a holding tank, removing the grating, and pouring the system water with the embryos through a sieve. The retained embryos were washed into a petri dish with E3 embryo medium (5mM NaCl, 0.17 mM KCl, 0.33 mM CaCl₂, 0.33 mM MgSO₄, 10⁻⁵% methylene blue) and transferred to a 30° C incubator, where they were grown up for up to seven days with periodic refreshing of the medium. Generally, a one or two-week minimum between matings was observed.

To obtain embryos for microinjection (see below), pairs were set up overnight in a 2L tank with a divider between the male and female. The following morning, the male and female were combined on the upper side of the divider. Embryos were collected within 20 minutes of pairing.

5.2.3.2: Sorting of Larvae

Clutches from deafness mutant ID fish pairings were subject to three tests. On day 4 or 5, larvae were visually examined, and those that had aberrant posture (i.e. failure to orient their dorsal sides up) were separated from their siblings. These two pools were then assessed for deafness by tapping the sides of their petri dishes to elicit a startle response. Non-responders were transferred to a third petri dish, and the swim-trajectories of individual larvae were tested by touching their tails with a fine metal probe. Larvae that failed to orient themselves dorsal-up, showed no startle response, and had spiraling swim-trajectories were classified as *asteroid* mutants. For *comet* mutant larvae, the swirl test was performed instead of the tap test. E3 and larvae in a dish were swirled using a transfer pipet. Failure to actively orient against the circular water movement indicated a balance defect. All larvae that were malformed, or that met

just one or two of the above criteria, were discarded, and those that failed to meet all three criteria were retained as wild-type siblings.

5.2.3.3: Microinjection of DNA, RNA, Morpholinos

Injection needles were pulled from 1.2 mm thin wall glass pipettes (World Precision Instruments, Sarasota, FL) on a Narishige PC-10 pipette puller in double-pull mode (temp 1 = 90.1, temp 2 = 80.6). Prior to injection, embryos were collected into injection molds (2% agarose in E3) and oriented with one-cell embryo to the side. Needles were filled with 3-5 μ l of MO or mRNA, fitted to a PV820 pneumatic pump (World Precision Instruments) and controlled with a Narishige M152 micromanipulator.

Plasmid was injected in ddH₂O at 25-100ng/ μ l. mRNA was injected in ddH₂O at 25-200ng/ μ l. Morpholinos were injected at 250, 500 or 1000 μ M in 100 mM KCl. Phenol red was added to a final volume of 5% as an injection tracer. DNA was injected directly into the fertilized first cell, the embryo. MOs and mRNA were injected into the yolk sac of 1-cell stage embryos. Injection pressure and time was adjusted to create an injection bolus approximately 1/5 the volume of the cell, or 1/4 the diameter of the yolk sac, respectively. Larvae were raised in E3 embryo medium at 30° C until screening at day 3 or 4 for RNA, day 4 or 5 for morpholinos and DNA.

6 Literature

- Allwardt BA, Dowling JE (2001) The pineal gland in wild-type and two zebrafish mutants with retinal defects. *J Neurocytol* 30:493-501.
- Allwardt BA, Lall AB, Brockerhoff SE, Dowling JE (2001) Synapse formation is arrested in retinal photoreceptors of the zebrafish nrc mutant. *J Neurosci* 21:2330-2342.
- Anggono V, Smillie KJ, Graham ME, Valova VA, Cousin MA, Robinson PJ (2006) Syndapin I is the phosphorylation-regulated dynamin I partner in synaptic vesicle endocytosis. *Nat Neurosci* 9:752-760.
- Aravanis AM, Pyle JL, Tsien RW (2003) Single synaptic vesicles fusing transiently and successively without loss of identity. *Nature* 423:643-647.
- Assad JA, Shepherd GM, Corey DP (1991) Tip-link integrity and mechanical transduction in vertebrate hair cells. *Neuron* 7:985-994.
- Augustin I, Rosenmund C, Sudhof TC, Brose N (1999) Munc13-1 is essential for fusion competence of glutamatergic synaptic vesicles. *Nature* 400:457-461.
- Bai J, Wang CT, Richards DA, Jackson MB, Chapman ER (2004) Fusion pore dynamics are regulated by synaptotagmin-t-SNARE interactions. *Neuron* 41:929-942.
- Bai L, Xu H, Collins JF, Ghishan FK (2001) Molecular and functional analysis of a novel neuronal vesicular glutamate transporter. *J Biol Chem* 276:36764-36769.
- Bellocchio EE, Reimer RJ, Fremeau RT, Jr., Edwards RH (2000) Uptake of glutamate into synaptic vesicles by an inorganic phosphate transporter. *Science* 289:957-960.
- Bellocchio EE, Hu H, Pohorille A, Chan J, Pickel VM, Edwards RH (1998) The localization of the brain-specific inorganic phosphate transporter suggests a specific presynaptic role in glutamatergic transmission. *J Neurosci* 18:8648-8659.
- Bensen ES, Costaguta G, Payne GS (2000) Synthetic genetic interactions with temperature-sensitive clathrin in *Saccharomyces cerevisiae*. Roles for synaptojanin-like Inp53p and dynamin-related Vps1p in clathrin-dependent protein sorting at the trans-Golgi network. *Genetics* 154:83-97.
- Beurg M, Evans MG, Hackney CM, Fettiplace R (2006) A large-conductance calcium-selective mechanotransducer channel in mammalian cochlear hair cells. *J Neurosci* 26:10992-11000.
- Beutner D, Voets T, Neher E, Moser T (2001) Calcium dependence of exocytosis and endocytosis at the cochlear inner hair cell afferent synapse. *Neuron* 29:681-690.

- Blero D, Payraastre B, Schurmans S, Erneux C (2007) Phosphoinositide phosphatases in a network of signalling reactions. *Pflugers Arch* 455:31-44.
- Brandt A, Khimich D, Moser T (2005) Few CaV1.3 channels regulate the exocytosis of a synaptic vesicle at the hair cell ribbon synapse. *J Neurosci* 25:11577-11585.
- Burger PM, Mehl E, Cameron PL, Maycox PR, Baumert M, Lottspeich F, De Camilli P, Jahn R (1989) Synaptic vesicles immunisolated from rat cerebral cortex contain high levels of glutamate. *Neuron* 3:715-720.
- Ceccarelli B, Hurlbut WP, Mauro A (1973) Turnover of transmitter and synaptic vesicles at the frog neuromuscular junction. *J Cell Biol* 57:499-524.
- Chang YT (2007) Small-molecule switch for zebrafish gene expression. *Nat Chem Biol* 3:135-136.
- Chen Y, Deng L, Maeno-Hikichi Y, Lai M, Chang S, Chen G, Zhang JF (2003) Formation of an endophilin-Ca²⁺ channel complex is critical for clathrin-mediated synaptic vesicle endocytosis. *Cell* 115:37-48.
- Chuang YY, Tran NL, Rusk N, Nakada M, Berens ME, Symons M (2004) Role of synaptotjanin 2 in glioma cell migration and invasion. *Cancer Res* 64:8271-8275.
- Chung EK, Chen LW, Chan YS, Yung KK (2006) Up-regulation in expression of vesicular glutamate transporter 3 in substantia nigra but not in striatum of 6-hydroxydopamine-lesioned rats. *Neurosignals* 15:238-248.
- Clayton EL, Evans GJ, Cousin MA (2007) Activity-dependent control of bulk endocytosis by protein dephosphorylation in central nerve terminals. *J Physiol*.
- Cleves AE, Novick PJ, Bankaitis VA (1989) Mutations in the SAC1 gene suppress defects in yeast Golgi and yeast actin function. *J Cell Biol* 109:2939-2950.
- Cockcroft S, De Matteis MA (2001) Inositol lipids as spatial regulators of membrane traffic. *J Membr Biol* 180:187-194.
- Cohen NL (1995) Medical and surgical perspectives: issues in treatment and management of severe and profound hearing impairment. *Ann Otol Rhinol Laryngol Suppl* 166:149-150.
- Corey DP (2006) What is the hair cell transduction channel? *J Physiol* 576:23-28.
- Corey DP, Hudspeth AJ (1979) Ionic basis of the receptor potential in a vertebrate hair cell. *Nature* 281:675-677.
- Corey DP, Hudspeth AJ (1983) Kinetics of the receptor current in bullfrog saccular hair cells. *J Neurosci* 3:962-976.

- Cousin MA, Robinson PJ (2001) The dephosphins: dephosphorylation by calcineurin triggers synaptic vesicle endocytosis. *Trends Neurosci* 24:659-665.
- Cremona O, De Camilli P (2001) Phosphoinositides in membrane traffic at the synapse. *J Cell Sci* 114:1041-1052.
- Cremona O, Di Paolo G, Wenk MR, Luthi A, Kim WT, Takei K, Daniell L, Nemoto Y, Shears SB, Flavell RA, McCormick DA, De Camilli P (1999) Essential role of phosphoinositide metabolism in synaptic vesicle recycling. *Cell* 99:179-188.
- Daniels RW, Collins CA, Chen K, Gelfand MV, Featherstone DE, DiAntonio A (2006) A single vesicular glutamate transporter is sufficient to fill a synaptic vesicle. *Neuron* 49:11-16.
- De Gois S, Jeanclos E, Morris M, Grewal S, Varoqui H, Erickson JD (2006) Identification of endophilins 1 and 3 as selective binding partners for VGLUT1 and their co-localization in neocortical glutamatergic synapses: implications for vesicular glutamate transporter trafficking and excitatory vesicle formation. *Cell Mol Neurobiol* 26:679-693.
- de Heuvel E, Bell AW, Ramjaun AR, Wong K, Sossin WS, McPherson PS (1997) Identification of the major synaptotagmin-binding proteins in brain. *J Biol Chem* 272:8710-8716.
- De Matteis MA, Godi A (2004) PI-loting membrane traffic. *Nat Cell Biol* 6:487-492.
- Deng J, Zhang FX, Pang YW, Li JL, Li YQ (2006) Vesicular glutamate transporter-immunoreactivities in the vestibular nuclear complex of rat. *Neurosci Bull* 22:204-208.
- Di Paolo G, De Camilli P (2006) Phosphoinositides in cell regulation and membrane dynamics. *Nature* 443:651-657.
- Di Paolo G, Moskowitz HS, Gipson K, Wenk MR, Voronov S, Obayashi M, Flavell R, Fitzsimonds RM, Ryan TA, De Camilli P (2004) Impaired PtdIns(4,5)P₂ synthesis in nerve terminals produces defects in synaptic vesicle trafficking. *Nature* 431:415-422.
- Dick O, tom Dieck S, Altmann WD, Ammermuller J, Weiler R, Garner CC, Gundelfinger ED, Brandstätter JH (2003) The presynaptic active zone protein bassoon is essential for photoreceptor ribbon synapse formation in the retina. *Neuron* 37:775-786.
- Dickman DK, Horne JA, Meinertzhagen IA, Schwarz TL (2005) A slowed classical pathway rather than kiss-and-run mediates endocytosis at synapses lacking synaptotagmin and endophilin. *Cell* 123:521-533.
- Dickman DK, Lu Z, Meinertzhagen IA, Schwarz TL (2006) Altered synaptic development and active zone spacing in endocytosis mutants. *Curr Biol* 16:591-598.

- Domin J, Gaidarov I, Smith ME, Keen JH, Waterfield MD (2000) The class II phosphoinositide 3-kinase PI3K-C2alpha is concentrated in the trans-Golgi network and present in clathrin-coated vesicles. *J Biol Chem* 275:11943-11950.
- Duguid IC, Smart TG (2004) Retrograde activation of presynaptic NMDA receptors enhances GABA release at cerebellar interneuron-Purkinje cell synapses. *Nat Neurosci* 7:525-533.
- Eastwood SL, Harrison PJ (2005) Decreased expression of vesicular glutamate transporter 1 and complexin II mRNAs in schizophrenia: further evidence for a synaptic pathology affecting glutamate neurons. *Schizophr Res* 73:159-172.
- Edmonds B, Reyes R, Schwaller B, Roberts WM (2000) Calretinin modifies presynaptic calcium signaling in frog saccular hair cells. *Nat Neurosci* 3:786-790.
- Edmonds BW, Gregory FD, Schweizer FE (2004) Evidence that fast exocytosis can be predominantly mediated by vesicles not docked at active zones in frog saccular hair cells. *J Physiol* 560:439-450.
- Evans GJ, Cousin MA (2007a) Simultaneous monitoring of three key neuronal functions in primary neuronal cultures. *J Neurosci Methods* 160:197-205.
- Evans GJ, Cousin MA (2007b) Activity-dependent control of slow synaptic vesicle endocytosis by cyclin-dependent kinase 5. *J Neurosci* 27:401-411.
- Eybalin M, Caicedo A, Renard N, Ruel J, Puel JL (2004) Transient Ca²⁺-permeable AMPA receptors in postnatal rat primary auditory neurons. *Eur J Neurosci* 20:2981-2989.
- Fenster SD, Chung WJ, Zhai R, Cases-Langhoff C, Voss B, Garner AM, Kaempf U, Kindler S, Gundelfinger ED, Garner CC (2000) Piccolo, a presynaptic zinc finger protein structurally related to bassoon. *Neuron* 25:203-214.
- Ferguson SM, Brasnjo G, Hayashi M, Wolfel M, Collesi C, Giovedi S, Raimondi A, Gong LW, Ariel P, Paradise S, O'Toole E, Flavell R, Cremona O, Miesenbock G, Ryan TA, De Camilli P (2007) A selective activity-dependent requirement for dynamin 1 in synaptic vesicle endocytosis. *Science* 316:570-574.
- Fernandez-Alfonso T, Kwan R, Ryan TA (2006) Synaptic vesicles interchange their membrane proteins with a large surface reservoir during recycling. *Neuron* 51:179-186.
- Fiorentini C, Falzano L, Fabbri A, Stringaro A, Logozzi M, Travaglione S, Contamin S, Arancia G, Malorni W, Fais S (2001) Activation of rho GTPases by cytotoxic necrotizing factor 1 induces macropinocytosis and scavenging activity in epithelial cells. *Mol Biol Cell* 12:2061-2073.

- Freneau RT, Jr., Voglmaier S, Seal RP, Edwards RH (2004a) VGLUTs define subsets of excitatory neurons and suggest novel roles for glutamate. *Trends Neurosci* 27:98-103.
- Freneau RT, Jr., Kam K, Qureshi T, Johnson J, Copenhagen DR, Storm-Mathisen J, Chaudhry FA, Nicoll RA, Edwards RH (2004b) Vesicular glutamate transporters 1 and 2 target to functionally distinct synaptic release sites. *Science* 304:1815-1819.
- Freneau RT, Jr., Troyer MD, Pahner I, Nygaard GO, Tran CH, Reimer RJ, Bellocchio EE, Fortin D, Storm-Mathisen J, Edwards RH (2001) The expression of vesicular glutamate transporters defines two classes of excitatory synapse. *Neuron* 31:247-260.
- Freneau RT, Jr., Burman J, Qureshi T, Tran CH, Proctor J, Johnson J, Zhang H, Sulzer D, Copenhagen DR, Storm-Mathisen J, Reimer RJ, Chaudhry FA, Edwards RH (2002) The identification of vesicular glutamate transporter 3 suggests novel modes of signaling by glutamate. *Proc Natl Acad Sci U S A* 99:14488-14493.
- Furness DN, Lawton DM (2003) Comparative distribution of glutamate transporters and receptors in relation to afferent innervation density in the mammalian cochlea. *J Neurosci* 23:11296-11304.
- Gabellec MM, Panzanelli P, Sassoe-Pognetto M, Lledo PM (2007) Synapse-specific localization of vesicular glutamate transporters in the rat olfactory bulb. *Eur J Neurosci* 25:1373-1383.
- Gad H, Low P, Zotova E, Brodin L, Shupliakov O (1998) Dissociation between Ca²⁺-triggered synaptic vesicle exocytosis and clathrin-mediated endocytosis at a central synapse. *Neuron* 21:607-616.
- Gad H, Ringstad N, Low P, Kjaerulff O, Gustafsson J, Wenk M, Di Paolo G, Nemoto Y, Crun J, Ellisman MH, De Camilli P, Shupliakov O, Brodin L (2000) Fission and uncoating of synaptic clathrin-coated vesicles are perturbed by disruption of interactions with the SH3 domain of endophilin. *Neuron* 27:301-312.
- Gaidarov I, Keen JH (1999) Phosphoinositide-AP-2 interactions required for targeting to plasma membrane clathrin-coated pits. *J Cell Biol* 146:755-764.
- Gale JE, Marcotti W, Kennedy HJ, Kros CJ, Richardson GP (2001) FM1-43 dye behaves as a permeant blocker of the hair-cell mechanotransducer channel. *J Neurosci* 21:7013-7025.
- Girard M, Allaire PD, McPherson PS, Blondeau F (2005) Non-stoichiometric relationship between clathrin heavy and light chains revealed by quantitative comparative proteomics of clathrin-coated vesicles from brain and liver. *Mol Cell Proteomics* 4:1145-1154.
- Glowatzki E, Fuchs PA (2002) Transmitter release at the hair cell ribbon synapse. *Nat Neurosci* 5:147-154.

- Granseth B, Odermatt B, Royle SJ, Lagnado L (2006) Clathrin-mediated endocytosis is the dominant mechanism of vesicle retrieval at hippocampal synapses. *Neuron* 51:773-786.
- Gras C, Vinatier J, Amilhon B, Guerci A, Christov C, Ravassard P, Giros B, El Mestikawy S (2005) Developmentally regulated expression of VGLUT3 during early post-natal life. *Neuropharmacology* 49:901-911.
- Gras C, Herzog E, Bellenchi GC, Bernard V, Ravassard P, Pohl M, Gasnier B, Giros B, El Mestikawy S (2002) A third vesicular glutamate transporter expressed by cholinergic and serotonergic neurons. *J Neurosci* 22:5442-5451.
- Griesinger CB, Richards CD, Ashmore JF (2002) Fm1-43 reveals membrane recycling in adult inner hair cells of the mammalian cochlea. *J Neurosci* 22:3939-3952.
- Griesinger CB, Richards CD, Ashmore JF (2004) Apical endocytosis in outer hair cells of the mammalian cochlea. *Eur J Neurosci* 20:41-50.
- Griesinger CB, Richards CD, Ashmore JF (2005) Fast vesicle replenishment allows indefatigable signalling at the first auditory synapse. *Nature* 435:212-215.
- Hackney CM, Mahendrasingam S, Penn A, Fettiplace R (2005) The concentrations of calcium buffering proteins in mammalian cochlear hair cells. *J Neurosci* 25:7867-7875.
- Harata NC, Choi S, Pyle JL, Aravanis AM, Tsien RW (2006) Frequency-dependent kinetics and prevalence of kiss-and-run and reuse at hippocampal synapses studied with novel quenching methods. *Neuron* 49:243-256.
- Harris TW, Hartweg E, Horvitz HR, Jorgensen EM (2000) Mutations in synaptojanin disrupt synaptic vesicle recycling. *J Cell Biol* 150:589-600.
- Harteringer J, Jahn R (1993) An anion binding site that regulates the glutamate transporter of synaptic vesicles. *J Biol Chem* 268:23122-23127.
- Hawthorne JN, Pickard MR (1979) Phospholipids in synaptic function. *J Neurochem* 32:5-14.
- Hayashi M, Otsuka M, Morimoto R, Hirota S, Yatsushiro S, Takeda J, Yamamoto A, Moriyama Y (2001) Differentiation-associated Na⁺-dependent inorganic phosphate cotransporter (DNPI) is a vesicular glutamate transporter in endocrine glutamatergic systems. *J Biol Chem* 276:43400-43406.
- He L, Wu LG (2007) The debate on the kiss-and-run fusion at synapses. *Trends Neurosci* 30:447-455.
- Heller S, Bell AM, Denis CS, Choe Y, Hudspeth AJ (2002) Parvalbumin 3 is an abundant Ca²⁺ buffer in hair cells. *J Assoc Res Otolaryngol* 3:488-498.

- Herzog E, Gilchrist J, Gras C, Muzerelle A, Ravassard P, Giros B, Gaspar P, El Mestikawy S (2004) Localization of VGLUT3, the vesicular glutamate transporter type 3, in the rat brain. *Neuroscience* 123:983-1002.
- Herzog E, Bellenchi GC, Gras C, Bernard V, Ravassard P, Bedet C, Gasnier B, Giros B, El Mestikawy S (2001) The existence of a second vesicular glutamate transporter specifies subpopulations of glutamatergic neurons. *J Neurosci* 21:RC181.
- Heuser JE, Reese TS (1973) Evidence for recycling of synaptic vesicle membrane during transmitter release at the frog neuromuscular junction. *J Cell Biol* 57:315-344.
- Hirono M, Denis CS, Richardson GP, Gillespie PG (2004) Hair cells require phosphatidylinositol 4,5-bisphosphate for mechanical transduction and adaptation. *Neuron* 44:309-320.
- Honing S, Ricotta D, Krauss M, Spate K, Spolaore B, Motley A, Robinson M, Robinson C, Haucke V, Owen DJ (2005) Phosphatidylinositol-(4,5)-bisphosphate regulates sorting signal recognition by the clathrin-associated adaptor complex AP2. *Mol Cell* 18:519-531.
- Hudspeth AJ (1989) How the ear's works work. *Nature* 341:397-404.
- Hughes WE, Cooke FT, Parker PJ (2000) Sac phosphatase domain proteins. *Biochem J* 350 Pt 2:337-352.
- Jia JY, Lamer S, Schumann M, Schmidt MR, Krause E, Haucke V (2006) Quantitative proteomics analysis of detergent-resistant membranes from chemical synapses: evidence for cholesterol as spatial organizer of synaptic vesicle cycling. *Mol Cell Proteomics* 5:2060-2071.
- Jockusch WJ, Praefcke GJ, McMahon HT, Lagnado L (2005) Clathrin-dependent and clathrin-independent retrieval of synaptic vesicles in retinal bipolar cells. *Neuron* 46:869-878.
- Johannes L, Lamaze C (2002) Clathrin-dependent or not: is it still the question? *Traffic* 3:443-451.
- Johnson SL, Marcotti W, Kros CJ (2005) Increase in efficiency and reduction in Ca²⁺ dependence of exocytosis during development of mouse inner hair cells. *J Physiol* 563:177-191.
- Jost M, Simpson F, Kavran JM, Lemmon MA, Schmid SL (1998) Phosphatidylinositol-4,5-bisphosphate is required for endocytic coated vesicle formation. *Curr Biol* 8:1399-1402.
- Jung N, Haucke V (2007) Clathrin-mediated endocytosis at synapses. *Traffic* 8:1129-1136.
- Kaksonen M, Toret CP, Drubin DG (2006) Harnessing actin dynamics for clathrin-mediated endocytosis. *Nat Rev Mol Cell Biol* 7:404-414.

- Kappler JA, Starr CJ, Chan DK, Kollmar R, Hudspeth AJ (2004) A nonsense mutation in the gene encoding a zebrafish myosin VI isoform causes defects in hair-cell mechanotransduction. *Proc Natl Acad Sci U S A* 101:13056-13061.
- Karasek M, Cozzi B (1990) "Synaptic" ribbons in the pineal gland of the horse. *J Pineal Res* 8:355-358.
- Kartenbeck J, Stukenbrok H, Helenius A (1989) Endocytosis of simian virus 40 into the endoplasmic reticulum. *J Cell Biol* 109:2721-2729.
- Kashani A, Lepicard E, Poirel O, Videau C, David JP, Fallet-Bianco C, Simon A, Delacourte A, Giros B, Epelbaum J, Betancur C, El Mestikawy S (2007) Loss of VGLUT1 and VGLUT2 in the prefrontal cortex is correlated with cognitive decline in Alzheimer disease. *Neurobiol Aging*.
- Kazmierczak P, Sakaguchi H, Tokita J, Wilson-Kubalek EM, Milligan RA, Muller U, Kachar B (2007) Cadherin 23 and protocadherin 15 interact to form tip-link filaments in sensory hair cells. *Nature* 449:87-91.
- Keen EC, Hudspeth AJ (2006) Transfer characteristics of the hair cell's afferent synapse. *Proc Natl Acad Sci U S A* 103:5537-5542.
- Kessels MM, Qualmann B (2002) Syndapins integrate N-WASP in receptor-mediated endocytosis. *Embo J* 21:6083-6094.
- Khimich D, Nouvian R, Pujol R, Tom Dieck S, Egnér A, Gundelfinger ED, Moser T (2005) Hair cell synaptic ribbons are essential for synchronous auditory signalling. *Nature* 434:889-894.
- Khvotchev M, Sudhof TC (1998a) Developmentally regulated alternative splicing in a novel synaptotagmin. *J Biol Chem* 273:2306-2311.
- Khvotchev M, Sudhof TC (1998b) Newly synthesized phosphatidylinositol phosphates are required for synaptic norepinephrine but not glutamate or gamma-aminobutyric acid (GABA) release. *J Biol Chem* 273:21451-21454.
- Kirkham M, Parton RG (2005) Clathrin-independent endocytosis: new insights into caveolae and non-caveolar lipid raft carriers. *Biochim Biophys Acta* 1746:349-363.
- Kros CJ (2007) How to build an inner hair cell: challenges for regeneration. *Hear Res* 227:3-10.
- Le PU, Guay G, Altschuler Y, Nabi IR (2002) Caveolin-1 is a negative regulator of caveolae-mediated endocytosis to the endoplasmic reticulum. *J Biol Chem* 277:3371-3379.
- Lee DW, Zhao X, Zhang F, Eisenberg E, Greene LE (2005) Depletion of GAK/auxilin 2 inhibits receptor-mediated endocytosis and recruitment of both clathrin and clathrin adaptors. *J Cell Sci* 118:4311-4321.
- Lee RY, Sawin ER, Chalfie M, Horvitz HR, Avery L (1999) EAT-4, a homolog of a mammalian sodium-dependent inorganic phosphate cotransporter, is

- necessary for glutamatergic neurotransmission in *Caenorhabditis elegans*. *J Neurosci* 19:159-167.
- Lee SY, Wenk MR, Kim Y, Nairn AC, De Camilli P (2004) Regulation of synaptotagmin 1 by cyclin-dependent kinase 5 at synapses. *Proc Natl Acad Sci U S A* 101:546-551.
- Leenders AG, Scholten G, de Lange RP, Lopes da Silva FH, Ghijsen WE (2002) Sequential changes in synaptic vesicle pools and endosome-like organelles during depolarization near the active zone of central nerve terminals. *Neuroscience* 109:195-206.
- LeMasurier M, Gillespie PG (2005) Hair-cell mechanotransduction and cochlear amplification. *Neuron* 48:403-415.
- Lenzi D, Crum J, Ellisman MH, Roberts WM (2002) Depolarization redistributes synaptic membrane and creates a gradient of vesicles on the synaptic body at a ribbon synapse. *Neuron* 36:649-659.
- Lenzi D, Runyeon JW, Crum J, Ellisman MH, Roberts WM (1999) Synaptic vesicle populations in saccular hair cells reconstructed by electron tomography. *J Neurosci* 19:119-132.
- Liguz-Leczna M, Skangiel-Kramska J (2007) Vesicular glutamate transporters (VGLUTs): the three musketeers of glutamatergic system. *Acta Neurobiol Exp (Wars)* 67:207-218.
- Liu JP, Sim AT, Robinson PJ (1994) Calcineurin inhibition of dynamin I GTPase activity coupled to nerve terminal depolarization. *Science* 265:970-973.
- Liu SH, Marks MS, Brodsky FM (1998) A dominant-negative clathrin mutant differentially affects trafficking of molecules with distinct sorting motifs in the class II major histocompatibility complex (MHC) pathway. *J Cell Biol* 140:1023-1037.
- Llobet A, Cooke A, Lagnado L (2003) Exocytosis at the ribbon synapse of retinal bipolar cells studied in patches of presynaptic membrane. *J Neurosci* 23:2706-2714.
- LoGiudice L, Matthews G (2007) Endocytosis at ribbon synapses. *Traffic* 8:1123-1128.
- Lumpkin EA, Marquis RE, Hudspeth AJ (1997) The selectivity of the hair cell's mechano-electrical-transduction channel promotes Ca^{2+} flux at low Ca^{2+} concentrations. *Proc Natl Acad Sci U S A* 94:10997-11002.
- Malecz N, McCabe PC, Spaargaren C, Qiu R, Chuang Y, Symons M (2000) Synaptotagmin 2, a novel Rac1 effector that regulates clathrin-mediated endocytosis. *Curr Biol* 10:1383-1386.
- Mammano F, Bortolozzi M, Ortolano S, Anselmi F (2007) Ca^{2+} signaling in the inner ear. *Physiology (Bethesda)* 22:131-144.

- Mansergh F, Orton NC, Vessey JP, Lalonde MR, Stell WK, Tremblay F, Barnes S, Rancourt DE, Bech-Hansen NT (2005) Mutation of the calcium channel gene *Cacna1f* disrupts calcium signaling, synaptic transmission and cellular organization in mouse retina. *Hum Mol Genet* 14:3035-3046.
- Marazita ML, Ploughman LM, Rawlings B, Remington E, Arnos KS, Nance WE (1993) Genetic epidemiological studies of early-onset deafness in the U.S. school-age population. *Am J Med Genet* 46:486-491.
- Martin PE, Blundell G, Ahmad S, Errington RJ, Evans WH (2001) Multiple pathways in the trafficking and assembly of connexin 26, 32 and 43 into gap junction intercellular communication channels. *J Cell Sci* 114:3845-3855.
- Martinez-Dunst C, Michaels RL, Fuchs PA (1997) Release sites and calcium channels in hair cells of the chick's cochlea. *J Neurosci* 17:9133-9144.
- Massol RH, Boll W, Griffin AM, Kirchhausen T (2006) A burst of auxilin recruitment determines the onset of clathrin-coated vesicle uncoating. *Proc Natl Acad Sci U S A* 103:10265-10270.
- Matos MF, Rizo J, Sudhof TC (2000) The relation of protein binding to function: what is the significance of munc18 and synaptotagmin binding to syntaxin 1, and where are the corresponding binding sites? *Eur J Cell Biol* 79:377-382.
- Matsubara A, Laake JH, Davanger S, Usami S, Ottersen OP (1996) Organization of AMPA receptor subunits at a glutamate synapse: a quantitative immunogold analysis of hair cell synapses in the rat organ of Corti. *J Neurosci* 16:4457-4467.
- McPherson PS, Garcia EP, Slepnev VI, David C, Zhang X, Grabs D, Sossin WS, Bauerfeind R, Nemoto Y, De Camilli P (1996) A presynaptic inositol-5-phosphatase. *Nature* 379:353-357.
- Meinertzhagen IA, Govind CK, Stewart BA, Carter JM, Atwood HL (1998) Regulated spacing of synapses and presynaptic active zones at larval neuromuscular junctions in different genotypes of the flies *Drosophila* and *Sarcophaga*. *J Comp Neurol* 393:482-492.
- Merrifield CJ, Perrais D, Zenisek D (2005) Coupling between clathrin-coated-pit invagination, cortactin recruitment, and membrane scission observed in live cells. *Cell* 121:593-606.
- Merrifield CJ, Feldman ME, Wan L, Almers W (2002) Imaging actin and dynamin recruitment during invagination of single clathrin-coated pits. *Nat Cell Biol* 4:691-698.
- Meyers JR, MacDonald RB, Duggan A, Lenzi D, Standaert DG, Corwin JT, Corey DP (2003) Lighting up the senses: FM1-43 loading of sensory cells through nonselective ion channels. *J Neurosci* 23:4054-4065.

- Montesinos ML, Castellano-Munoz M, Garcia-Junco-Clemente P, Fernandez-Chacon R (2005) Recycling and EH domain proteins at the synapse. *Brain Res Brain Res Rev* 49:416-428.
- Moser T, Beutner D (2000) Kinetics of exocytosis and endocytosis at the cochlear inner hair cell afferent synapse of the mouse. *Proc Natl Acad Sci U S A* 97:883-888.
- Moser T, Neef A, Khimich D (2006) Mechanisms underlying the temporal precision of sound coding at the inner hair cell ribbon synapse. *J Physiol* 576:55-62.
- Mueller VJ, Wienisch M, Nehring RB, Klingauf J (2004) Monitoring clathrin-mediated endocytosis during synaptic activity. *J Neurosci* 24:2004-2012.
- Murthy VN, Stevens CF (1998) Synaptic vesicles retain their identity through the endocytic cycle. *Nature* 392:497-501.
- Murthy VN, De Camilli P (2003) Cell biology of the presynaptic terminal. *Annu Rev Neurosci* 26:701-728.
- Nakatsu F, Okada M, Mori F, Kumazawa N, Iwasa H, Zhu G, Kasagi Y, Kamiya H, Harada A, Nishimura K, Takeuchi A, Miyazaki T, Watanabe M, Yuasa S, Manabe T, Wakabayashi K, Kaneko S, Saito T, Ohno H (2004) Defective function of GABA-containing synaptic vesicles in mice lacking the AP-3B clathrin adaptor. *J Cell Biol* 167:293-302.
- Nemoto Y, Wenk MR, Watanabe M, Daniell L, Murakami T, Ringstad N, Yamada H, Takei K, De Camilli P (2001) Identification and characterization of a synaptojanin 2 splice isoform predominantly expressed in nerve terminals. *J Biol Chem* 276:41133-41142.
- Newton AJ, Kirchhausen T, Murthy VN (2006) Inhibition of dynamin completely blocks compensatory synaptic vesicle endocytosis. *Proc Natl Acad Sci U S A* 103:17955-17960.
- Ni B, Rosteck PR, Jr., Nadi NS, Paul SM (1994) Cloning and expression of a cDNA encoding a brain-specific Na(+)-dependent inorganic phosphate cotransporter. *Proc Natl Acad Sci U S A* 91:5607-5611.
- Nicolson T (2005) The genetics of hearing and balance in zebrafish. *Annu Rev Genet* 39:9-22.
- Nouvian R, Beutner D, Parsons TD, Moser T (2006) Structure and function of the hair cell ribbon synapse. *J Membr Biol* 209:153-165.
- Odorizzi G, Babst M, Emr SD (2000) Phosphoinositide signaling and the regulation of membrane trafficking in yeast. *Trends Biochem Sci* 25:229-235.
- Oh P, McIntosh DP, Schnitzer JE (1998) Dynamin at the neck of caveolae mediates their budding to form transport vesicles by GTP-driven fission from the plasma membrane of endothelium. *J Cell Biol* 141:101-114.

- Paillart C, Li J, Matthews G, Sterling P (2003) Endocytosis and vesicle recycling at a ribbon synapse. *J Neurosci* 23:4092-4099.
- Parsons TD, Sterling P (2003) Synaptic ribbon. Conveyor belt or safety belt? *Neuron* 37:379-382.
- Pelkmans L, Puntener D, Helenius A (2002) Local actin polymerization and dynamin recruitment in SV40-induced internalization of caveolae. *Science* 296:535-539.
- Perera RM, Zoncu R, Lucast L, De Camilli P, Toomre D (2006) Two synaptojanin 1 isoforms are recruited to clathrin-coated pits at different stages. *Proc Natl Acad Sci U S A* 103:19332-19337.
- Platzer J, Engel J, Schrott-Fischer A, Stephan K, Bova S, Chen H, Zheng H, Striessnig J (2000) Congenital deafness and sinoatrial node dysfunction in mice lacking class D L-type Ca²⁺ channels. *Cell* 102:89-97.
- Prescott ED, Zenisek D (2005) Recent progress towards understanding the synaptic ribbon. *Curr Opin Neurobiol* 15:431-436.
- Ramjaun AR, McPherson PS (1996) Tissue-specific alternative splicing generates two synaptojanin isoforms with differential membrane binding properties. *J Biol Chem* 271:24856-24861.
- Richards DA, Guatimosim C, Betz WJ (2000) Two endocytic recycling routes selectively fill two vesicle pools in frog motor nerve terminals. *Neuron* 27:551-559.
- Richards DA, Rizzoli SO, Betz WJ (2004) Effects of wortmannin and latrunculin A on slow endocytosis at the frog neuromuscular junction. *J Physiol* 557:77-91.
- Roberts WM, Jacobs RA, Hudspeth AJ (1990) Colocalization of ion channels involved in frequency selectivity and synaptic transmission at presynaptic active zones of hair cells. *J Neurosci* 10:3664-3684.
- Rohatgi R, Ma L, Miki H, Lopez M, Kirchhausen T, Takenawa T, Kirschner MW (1999) The interaction between N-WASP and the Arp2/3 complex links Cdc42-dependent signals to actin assembly. *Cell* 97:221-231.
- Rothberg KG, Heuser JE, Donzell WC, Ying YS, Glenney JR, Anderson RG (1992) Caveolin, a protein component of caveolae membrane coats. *Cell* 68:673-682.
- Roux I, Safieddine S, Nouvian R, Grati M, Simmler MC, Bahloul A, Perfettini I, Le Gall M, Rostaing P, Hamard G, Triller A, Avan P, Moser T, Petit C (2006) Otoferlin, defective in a human deafness form, is essential for exocytosis at the auditory ribbon synapse. *Cell* 127:277-289.
- Royle SJ, Lagnado L (2003) Endocytosis at the synaptic terminal. *J Physiol* 553:345-355.
- Rybak LP, Ramkumar V (2007) Ototoxicity. *Kidney Int* 72:931-935.

- Safieddine S, Wenthold RJ (1999) SNARE complex at the ribbon synapses of cochlear hair cells: analysis of synaptic vesicle- and synaptic membrane-associated proteins. *Eur J Neurosci* 11:803-812.
- Sauvonnet N, Dujeancourt A, Dautry-Varsat A (2005) Cortactin and dynamin are required for the clathrin-independent endocytosis of gamma cytokine receptor. *J Cell Biol* 168:155-163.
- Schafer MK, Varoqui H, Defamie N, Weihe E, Erickson JD (2002) Molecular cloning and functional identification of mouse vesicular glutamate transporter 3 and its expression in subsets of novel excitatory neurons. *J Biol Chem* 277:50734-50748.
- Schafer SP, Dittrich PS, Petrov EP, Schwille P (2006) Single molecule fluorescence imaging of the photoinduced conversion and bleaching behavior of the fluorescent protein Kaede. *Microsc Res Tech* 69:210-219.
- Schiavo G, Gu QM, Prestwich GD, Sollner TH, Rothman JE (1996) Calcium-dependent switching of the specificity of phosphoinositide binding to synaptotagmin. *Proc Natl Acad Sci U S A* 93:13327-13332.
- Schmitz F, Konigstorfer A, Sudhof TC (2000) RIBEYE, a component of synaptic ribbons: a protein's journey through evolution provides insight into synaptic ribbon function. *Neuron* 28:857-872.
- Schnee ME, Lawton DM, Furness DN, Benke TA, Ricci AJ (2005) Auditory hair cell-afferent fiber synapses are specialized to operate at their best frequencies. *Neuron* 47:243-254.
- Schuske K, Jorgensen EM (2004) Neuroscience. Vesicular glutamate transporter--shooting blanks. *Science* 304:1750-1752.
- Schuske KR, Richmond JE, Matthies DS, Davis WS, Runz S, Rube DA, van der Blik AM, Jorgensen EM (2003) Endophilin is required for synaptic vesicle endocytosis by localizing synaptojanin. *Neuron* 40:749-762.
- Seal RP, Edwards RH (2006a) Functional implications of neurotransmitter co-release: glutamate and GABA share the load. *Curr Opin Pharmacol* 6:114-119.
- Seal RP, Edwards RH (2006b) The diverse roles of vesicular glutamate transporter 3. *Handb Exp Pharmacol*:137-150.
- Seiler C, Nicolson T (1999) Defective calmodulin-dependent rapid apical endocytosis in zebrafish sensory hair cell mutants. *J Neurobiol* 41:424-434.
- Shin JB, Streijger F, Beynon A, Peters T, Gadzala L, McMillen D, Bystrom C, Van der Zee CE, Wallimann T, Gillespie PG (2007) Hair bundles are specialized for ATP delivery via creatine kinase. *Neuron* 53:371-386.
- Shkel AM, Zeng FG (2006) An electronic prosthesis mimicking the dynamic vestibular function. *Audiol Neurootol* 11:113-122.

- Sidi S, Friedrich RW, Nicolson T (2003) NompC TRP channel required for vertebrate sensory hair cell mechanotransduction. *Science* 301:96-99.
- Sidi S, Busch-Nentwich E, Friedrich R, Schoenberger U, Nicolson T (2004) gemini encodes a zebrafish L-type calcium channel that localizes at sensory hair cell ribbon synapses. *J Neurosci* 24:4213-4223.
- Simonsen A, Wurmser AE, Emr SD, Stenmark H (2001) The role of phosphoinositides in membrane transport. *Curr Opin Cell Biol* 13:485-492.
- Singer JH, Lassoova L, Vardi N, Diamond JS (2004) Coordinated multivesicular release at a mammalian ribbon synapse. *Nat Neurosci* 7:826-833.
- Smear MC, Tao HW, Staub W, Orger MB, Gosse NJ, Liu Y, Takahashi K, Poo MM, Baier H (2007) Vesicular glutamate transport at a central synapse limits the acuity of visual perception in zebrafish. *Neuron* 53:65-77.
- Sollner C, Rauch GJ, Siemens J, Geisler R, Schuster SC, Muller U, Nicolson T (2004) Mutations in cadherin 23 affect tip links in zebrafish sensory hair cells. *Nature* 428:955-959.
- Stauffer EA, Holt JR (2007) Sensory Transduction and Adaptation in Inner and Outer Hair Cells of the Mouse Auditory System. *J Neurophysiol*.
- Stauffer EA, Scarborough JD, Hirono M, Miller ED, Shah K, Mercer JA, Holt JR, Gillespie PG (2005) Fast adaptation in vestibular hair cells requires myosin-1c activity. *Neuron* 47:541-553.
- Stefan CJ, Audhya A, Emr SD (2002) The yeast synaptojanin-like proteins control the cellular distribution of phosphatidylinositol (4,5)-bisphosphate. *Mol Biol Cell* 13:542-557.
- Sudhof TC (2000) The synaptic vesicle cycle revisited. *Neuron* 28:317-320.
- Sudhof TC (2004) The synaptic vesicle cycle. *Annu Rev Neurosci* 27:509-547.
- Takamori S (2006) VGLUTs: 'exciting' times for glutamatergic research? *Neurosci Res* 55:343-351.
- Takamori S, Rhee JS, Rosenmund C, Jahn R (2000) Identification of a vesicular glutamate transporter that defines a glutamatergic phenotype in neurons. *Nature* 407:189-194.
- Takamori S, Rhee JS, Rosenmund C, Jahn R (2001) Identification of differentiation-associated brain-specific phosphate transporter as a second vesicular glutamate transporter (VGLUT2). *J Neurosci* 21:RC182.
- Takamori S, Malherbe P, Broger C, Jahn R (2002) Molecular cloning and functional characterization of human vesicular glutamate transporter 3. *EMBO Rep* 3:798-803.
- Takamori S, Holt M, Stenius K, Lemke EA, Gronborg M, Riedel D, Urlaub H, Schenck S, Brugger B, Ringler P, Muller SA, Rammner B, Gräter F, Hub JS, De Groot BL, Mieskes G, Moriyama Y, Klingauf J, Grubmuller H,

- Heuser J, Wieland F, Jahn R (2006) Molecular anatomy of a trafficking organelle. *Cell* 127:831-846.
- Takei K, Mundigl O, Daniell L, De Camilli P (1996) The synaptic vesicle cycle: a single vesicle budding step involving clathrin and dynamin. *J Cell Biol* 133:1237-1250.
- Teng H, Lin MY, Wilkinson RS (2007) Macroendocytosis and endosome processing in snake motor boutons. *J Physiol* 582:243-262.
- Thomsen P, Roepstorff K, Stahlhut M, van Deurs B (2002) Caveolae are highly immobile plasma membrane microdomains, which are not involved in constitutive endocytic trafficking. *Mol Biol Cell* 13:238-250.
- Toker A (2002) Phosphoinositides and signal transduction. *Cell Mol Life Sci* 59:761-779.
- tom Dieck S, Altmann WD, Kessels MM, Qualmann B, Regus H, Brauner D, Fejtova A, Bracko O, Gundelfinger ED, Brandstatter JH (2005) Molecular dissection of the photoreceptor ribbon synapse: physical interaction of Bassoon and RIBEYE is essential for the assembly of the ribbon complex. *J Cell Biol* 168:825-836.
- Tomizawa K, Ohta J, Matsushita M, Moriwaki A, Li ST, Takei K, Matsui H (2002) Cdk5/p35 regulates neurotransmitter release through phosphorylation and downregulation of P/Q-type voltage-dependent calcium channel activity. *J Neurosci* 22:2590-2597.
- Tomizawa K, Sunada S, Lu YF, Oda Y, Kinuta M, Ohshima T, Saito T, Wei FY, Matsushita M, Li ST, Tsutsui K, Hisanaga S, Mikoshiba K, Takei K, Matsui H (2003) Cophosphorylation of amphiphysin I and dynamin I by Cdk5 regulates clathrin-mediated endocytosis of synaptic vesicles. *J Cell Biol* 163:813-824.
- Tran D, Carpentier JL, Sawano F, Gorden P, Orci L (1987) Ligands internalized through coated or noncoated invaginations follow a common intracellular pathway. *Proc Natl Acad Sci U S A* 84:7957-7961.
- Tucker WC, Chapman ER (2002) Role of synaptotagmin in Ca²⁺-triggered exocytosis. *Biochem J* 366:1-13.
- Vallis Y, Wigge P, Marks B, Evans PR, McMahon HT (1999) Importance of the pleckstrin homology domain of dynamin in clathrin-mediated endocytosis. *Curr Biol* 9:257-260.
- Van Camp G, Willems PJ, Smith RJ (1997) Nonsyndromic hearing impairment: unparalleled heterogeneity. *Am J Hum Genet* 60:758-764.
- Van Epps HA, Hayashi M, Lucast L, Stearns GW, Hurley JB, De Camilli P, Brockerhoff SE (2004) The zebrafish nrc mutant reveals a role for the polyphosphoinositide phosphatase synaptojanin 1 in cone photoreceptor ribbon anchoring. *J Neurosci* 24:8641-8650.

- Verstreken P, Koh TW, Schulze KL, Zhai RG, Hiesinger PR, Zhou Y, Mehta SQ, Cao Y, Roos J, Bellen HJ (2003) Synaptojanin is recruited by endophilin to promote synaptic vesicle uncoating. *Neuron* 40:733-748.
- Voglmaier SM, Kam K, Yang H, Fortin DL, Hua Z, Nicoll RA, Edwards RH (2006) Distinct endocytic pathways control the rate and extent of synaptic vesicle protein recycling. *Neuron* 51:71-84.
- Vollrath MA, Kwan KY, Corey DP (2007) The micromachinery of mechanotransduction in hair cells. *Annu Rev Neurosci* 30:339-365.
- Von Kriegstein K, Schmitz F, Link E, Sudhof TC (1999) Distribution of synaptic vesicle proteins in the mammalian retina identifies obligatory and facultative components of ribbon synapses. *Eur J Neurosci* 11:1335-1348.
- Wall C, 3rd, Merfeld DM, Rauch SD, Black FO (2002) Vestibular prostheses: the engineering and biomedical issues. *J Vestib Res* 12:95-113.
- Waltzman SB (2006) Cochlear implants: current status. *Expert Rev Med Devices* 3:647-655.
- Wan L, Almers W, Chen W (2005) Two ribeye genes in teleosts: the role of Ribeye in ribbon formation and bipolar cell development. *J Neurosci* 25:941-949.
- Wang Y, Okamoto M, Schmitz F, Hofmann K, Sudhof TC (1997) Rim is a putative Rab3 effector in regulating synaptic-vesicle fusion. *Nature* 388:593-598.
- Wang Y, Pang YW, Dong YL, Zhang FX, Li JL, Li YQ (2007) Localization of vesicular glutamate transporters in the peripheral vestibular system of rat. *Neurosci Bull* 23:175-179.
- Weick JP, Groth RD, Isaksen AL, Mermelstein PG (2003) Interactions with PDZ proteins are required for L-type calcium channels to activate cAMP response element-binding protein-dependent gene expression. *J Neurosci* 23:3446-3456.
- Wojcik SM, Rhee JS, Herzog E, Sigler A, Jahn R, Takamori S, Brose N, Rosenmund C (2004) An essential role for vesicular glutamate transporter 1 (VGLUT1) in postnatal development and control of quantal size. *Proc Natl Acad Sci U S A* 101:7158-7163.
- Woscholski R, Finan PM, Radley E, Parker PJ (1998) Identification and characterisation of a novel splice variant of synaptojanin1. *FEBS Lett* 432:5-8.
- Wu LG (2004) Kinetic regulation of vesicle endocytosis at synapses. *Trends Neurosci* 27:548-554.
- Yamada E (1955) The fine structure of the renal glomerulus of the mouse. *J Biophys Biochem Cytol* 1:551-566.

- Zenisek D, Steyer JA, Feldman ME, Almers W (2002) A membrane marker leaves synaptic vesicles in milliseconds after exocytosis in retinal bipolar cells. *Neuron* 35:1085-1097.
- Zhao X, Greener T, Al-Hasani H, Cushman SW, Eisenberg E, Greene LE (2001) Expression of auxilin or AP180 inhibits endocytosis by mislocalizing clathrin: evidence for formation of nascent pits containing AP1 or AP2 but not clathrin. *J Cell Sci* 114:353-365.
- Zoncu R, Perera RM, Sebastian R, Nakatsu F, Chen H, Balla T, Ayala G, Toomre D, De Camilli PV (2007) Loss of endocytic clathrin-coated pits upon acute depletion of phosphatidylinositol 4,5-bisphosphate. *Proc Natl Acad Sci U S A* 104:3793-3798.